Models for circumstellar nebulae around red and blue supergiants

Sabina Chiţă

ISBN 978-90-393-5249-6

Cover image: Sher 25 nebula, as observed by Hubble Space Telescope, collated with the model of emission density from circumstellar material around a blue supergiant as presented in chapter 3 of this thesis. Design: Frans Snik

Models for circumstellar nebulae around red and blue supergiants

Modellen van nevels rond rode en blauwe superreuze
(met een samenvatting in het Nederlands)

Proefschrift

ter verkrijging van de graad van doctor aan de Universiteit Utrecht op gezag van de rector magnificus, prof. dr. G. J. van der Zwaan, ingevolge het besluit van het college voor promoties in het openbaar te verdedigen op donderdag 6 oktober 2011 des middags te 2.30 uur

door

Sabina Mădălina Chiţă

geboren op 26 februari 1980 te Brăila, Roemenië

Promotoren: Prof. dr. N. Langer
Prof. dr. A. Achterberg

pentru mami şi tati

Contents

Chapter 1

Introduction

The quest for knowledge

Human beings have wondered about the mysteries of the sky for centuries and struggled to understand its secrets. The study of astronomy is a genuine extension of human curiosity. Understanding the true, wonderful nature of the universe lies not only in observing stars and galaxies, but also in considering the physical processes that cause the stars to exist.

Archeoastronomy, or the study of the astronomy of past cultures, relied on the alignment of ancient structures toward celestial objects. Mathematical models of Nature, first proposed by the ancient Greeks such as Pythagoras, led to the Copernican revolution. Our perception of the universe has changed dramatically since the physical causes of observable phenomena started to be considered and understood. The application of physics to astronomy has proved to be very successful in explaining a wide range of observations: strange and exotic objects and events such as pulsating stars, supernovae, black holes and quasars.

The rapid development of astronomy over the past decades occurred because of the equally large improvement of the tools we use to study the universe: telescopes and computers. With modern telescopes, both on the ground and in space, we are able to see X-rays, ultraviolet light (UV), infrared radiation (IR) and radio signals, while computers have provided us with the capability to check complicated mathematical models that use fundamental physical principles. Understanding these physical processes is the first step to reveal the secrets encrypted in the stars and thus the formation and evolution of the universe.

The influence of stars on their environment

Astronomical objects such as stars, stellar clusters, nebulae, galaxies, clusters of galaxies and more exotic objects like pulsating stars, black holes and quasars are all surrounded by interstellar gas. This interstellar gas consists roughly of two states: a cold state, where most of the hydrogen consists of neutral atoms (H I), and a hot phase where hydrogen is either partially or fully ionized: the so-called H II regions. The H II regions, also known as diffuse nebulae, can be observed in our galaxy as well in the nearby galaxies.

H II regions play a crucial part in the star formation history and the evolution of chemical elements in our galaxy and other galaxies. Star formation starts in giant molecular clouds where the density is high, and the temperature is low. Only after the stars ignite their nuclear fusion do they provide the UV photons that ionizes the hydrogen. H II regions indicate sites of

star formation and arise at locations where a large number of stars have been created recently. Some of these young stars are the most massive and hot stars, which use their nuclear energy quickly. These can be single stars, but are often grouped in clusters that provide more photons capable of ionizing the H II regions. The hot ionized gas of the H II region, or diffuse nebula, can expand into the cold surrounding neutral gas, decreasing the density of the nebula and increasing the volume of ionized gas.

During their lives, stars interact with the surrounding interstellar medium through their ionizing radiation and through the mass, momentum and energy carried by their winds. The mass lost by the star is returned into the interstellar medium. Because of the nuclear processes that occur in the interior of stars, this material is very often chemically enriched.

Dynamical interaction between stellar winds and their surroundings produce wind bubbles. The winds of massive stars release large amounts of energy. Moreover, massive stars are often grouped in stellar clusters, so the energy of their ejected winds can accumulate. Galaxies contain many of such large mass aggregates of stars. Here dynamical processes take place, such as binary formation and disruption, stellar collisions and mergers, supernova explosions and gamma-ray bursts.

If a star ejects consecutive winds at different velocities and with different densities, the wind-wind interaction creates a circumstellar nebula with a complex structure. These are isolated nebulae typically indicating that the star which created them is a fairly old object. Many circumstellar nebulae are observed in the Galaxy and in nearby systems such as the Magellanic clouds. Their luminosity is smaller than that of H II regions as they are powered by a single and older star.

Massive stars end their lives as supernovae. The material ejected in stars catastrophic supernova explosions, comes back to the interstellar medium, contributing to the birth of new stars. Thin layers or filaments of gas surrounding the supernova, called supernova remnants can be observed. Most of their radiation energy is powered by the thermal energy generated in shocks when the gas filaments move around and collide with the ambient gas or the interstellar medium.

Thesis achievements

This thesis constitutes the first generic study of the circumstellar material for typical supernova progenitors: stars that are born with a mass more than eight times that of our Sun. The work presented here concentrates on modeling the nebulae around single, massive stars, from their birth until their supernova explosion. From our circumstellar models we were able to predict the mass, the temperature, the geometry and abundance of the chemical elements present in the nebula.

The life of stars - a short overview

Formation

Stars form out of gas found in molecular clouds. These clouds occupy a small fraction of the volume of the interstellar medium. The mass of a molecular cloud can reach 10^4 $M_\odot$ and the temperature can be as low as 30 K. Overly dense regions within the giant molecular clouds form a clumpy pattern. A molecular cloud is surrounded by a layer of atomic gas that shields the molecules inside the cloud from the interstellar UV radiation field. Such clouds can contract, fragment and these fragments collapse further into proto-stars, ultimately allowing nuclear fusion to take place and forming a hot core. If the core initial mass is larger than 0.1 $M_\odot$, its temperature of can rise to 10^7 K. This newly born star can live from less than a million years to a billion of years, depending on its initial mass and composition, constantly transforming itself as it evolves.

Classification and evolution

Stars spend most of their life in the Main Sequence (MS). In this stage of their evolution the source of energy production is the fusion of hydrogen into helium in their core. This energy escapes from the star in the form of radiation and, to a minor fraction, in the form of stellar wind. Depending on the initial mass, stars have different properties during their MS stage. If the main sequence stars are like our Sun, they are yellow, warm (6000 K) and they live for about 10 billion years. Stars that are less massive than our Sun, are cool, red and can live longer, while stars more massive can be blue, hot ($\geq$ 25000 K) and live only for a few million years. During the MS stage, the stars temperature and the luminosity remain almost constant. The stars are classified in spectral classes, from O and B (the most massive and hot stars), to A, F, G, K and M (the least massive and cold stars).

Once the hydrogen in the core is exhausted at the end of the MS, the luminosity and temperature can change dramatically. The central temperature increases and the star starts to fuse helium. The future of the central star is now determined by its mass at birth. If its initial mass was less than 8 $M_\odot$, the core will contract after helium core burning into a small compact star called a white dwarf, and it will shed its outer layers as a planetary nebula. Heavier stars can become red supergiants (RSG) or luminous blue variables (LBV) depending on the original mass of the central star. RSGs are cold stars with a very large diameter. LBVs are extremely bright blue supergiant stars. Stars with masses between 8 to 20 $M_\odot$ evolve to the RSG stage and can become blue supergiants (BSG) making a so-called blue-loop (see Fig. 1.1) before returning for a second time to the RSG stage. However, if the star has around 20 to 30 $M_\odot$, the end of its evolution is a RSG phase. Massive stars with a mass of about 30 to 50 $M_\odot$ can become Wolf-Rayet (WR) stars (e.g. Schaller et al. [1992]) and loose their mass in the form of stellar wind at an amazingly high rate (about 10^{-5} $M_\odot$ yr^{-1}), while stars with a mass higher than about 50 $M_\odot$ become LBVs. Most massive stars continue through all nuclear burning stages until the formation of an iron-nickel core. Fusion of iron into even heavier nuclei would cost rather than produce energy. With the energy source exhausted, the core loses equilibrium and collapses as pressure forces can no longer balance gravity. These

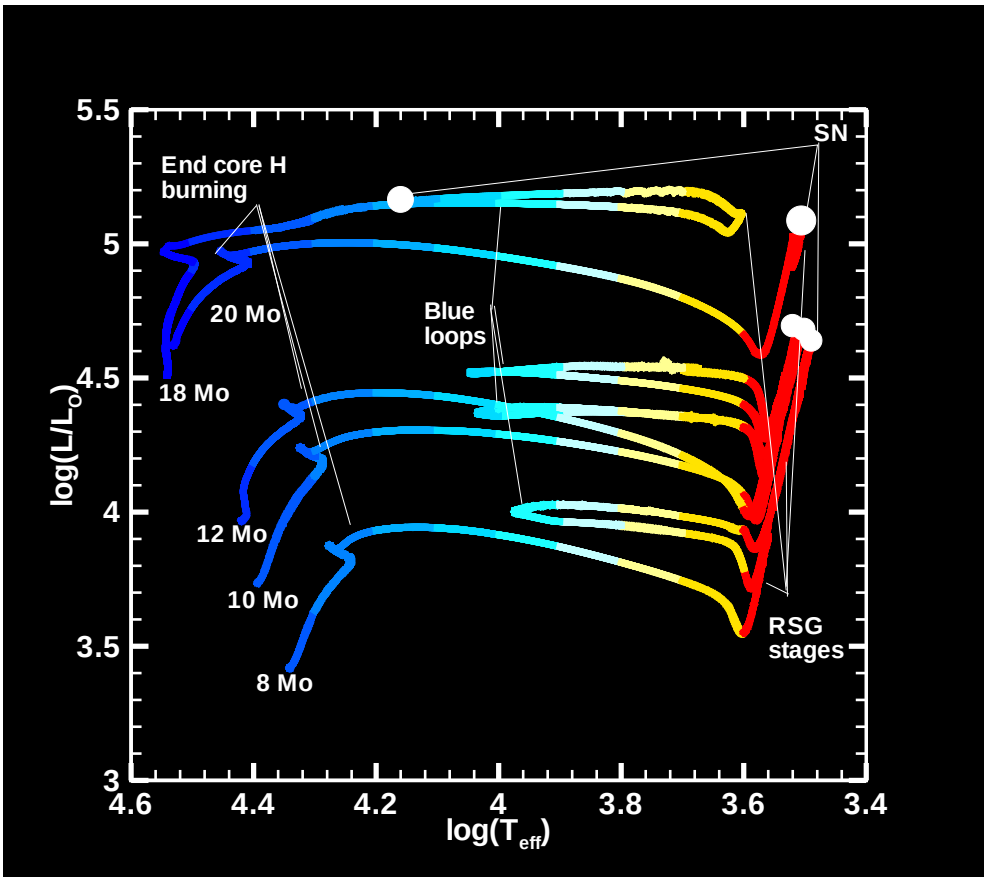

Figure 1.1: Evolutionary tracks of our adopted stellar evolution models in the Hertzprung-Russell diagram, from the zero age main sequence to the pre-supernova stage.

stars end their lives as a neutron star or a black hole (e.g. Eldridge et al. [2004]). The layers outside the core are ejected due to supernova explosion that results as the core collapses.

Stars often rotate. Sufficiently rapid rotation can change the course of stellar evolution. A rotating star will typically develop a larger helium core, becoming more luminous than a non-rotating star with same mass. If the rapidly rotating star explodes as supernova, the explosion leads to a Gamma Ray Burst event (e.g. Rigon [2003]). These events release extreme amounts of energy ($E \geq 10^{51}$ erg) in just a few seconds. Gamma Ray Bursts can also occur in certain types of close binaries where both components are compact objects like neutron stars or black holes (see Woosley et al. [1993] and MacFadyen et al. [1999]). When a star resides in a binary system, its evolution can differ signifcantly from a single star. In close binaries mass can be transferred from the more massive star to the less massive star. As a result, the evolution of both stars is changed and their luminosities and surface temperature

are altered.

Stellar winds

Stars, independently of their mass during the MS phase and their maturing stages, shed mass in the form of a stellar wind. When observing stellar winds, two important parameters become crucial: the mass loss rate, the amount of mass lost by the star per unit time, and the velocity of the stellar wind far away from the star (terminal wind velocity). The different possible stages of evolution are characterized by different mass loss rates and terminal wind velocities. For example, in the case of stars with masses larger than 30 $M_{\odot}$, the mass loss rate is tremendously large, leading to an accelerated evolution. Stars with a lower mass on the other hand enjoy an effective mass loss only at the end of their evolution. The repercussion of mass loss on stellar evolution has been described earlier by e.g. Iben & Renzini [1983] and Chiosi & Maeder [1986].

Numerous ways exist to detect and measure mass loss from the stars. Employing observation methods based on spectral lines, e.g. P-Cygni profiles (a combination of emission and absorption lines) for hot stars from UV and optical emission lines and for cool stars from molecular lines, we can get information about velocity or column density. The amount of gas or dust in a cool star can be estimated from its IR continuum radiation. Both methods combined, line profiling and continuum measurement, can be used to determine the wind parameters (for a complete description we refer to Lamers & Cassinelli [1999]).

Rotating stars commonly concentrate their winds into regions around the equatorial plane. Two archetype theories try to explain the inhomogeneity of the wind density. The first is the rotation induced bi-stability Lamers & Pauldrach [1991], which states that the equatorial mass flux is larger than that at the poles. Also the speed at which the wind material breaks away from the pole is magnificently larger compared to the equatorial domain. The second theory (Bjorkman & Casinelli [1993]) assumes that the wind is compressed in the equatorial plane by using a flow that collimates towards the equatorial plane. This culminates in having a decreased wind density toward the pole while having an increased wind density toward the equator all independent of the mass loss rate of the star (see *Chapter 3, 4* for more details).

The dynamical shaping of circumstellar nebulae

The main sequence bubble

During their life, most stars lose mass by ejecting winds into the interstellar medium (ISM). This stream of material leaves the surface of the star and attains supersonic speed at some distance from the star. When it encounters the ISM it creates a shock. At this point the wind starts to sweep up gas material from the ISM into a shell. During the MS stage, this spherical shell moves away from central star into the ISM, forming a bubble, a region with almost constant density and thermal pressure. Moving outward from the star (see Fig. 1.2), the morphology of the main sequence bubble can be divided into several parts. The first part is the free-streaming stellar wind that has a constant velocity and a density decreasing with the radius squared. The next part of the circumstellar bubble contains shocked wind material.

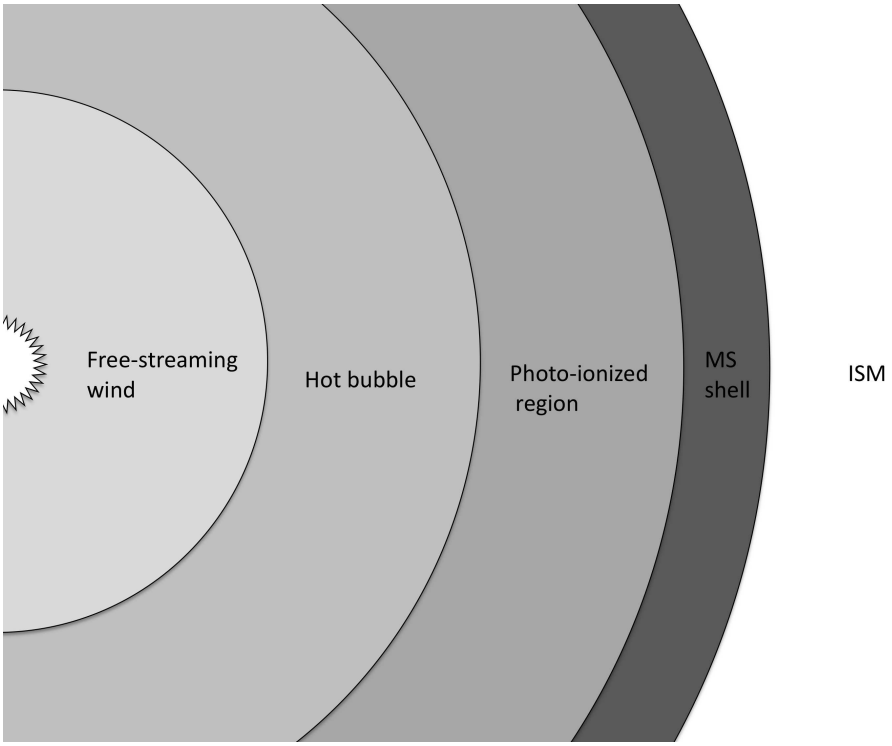

Figure 1.2: Schematic representation of the main sequence bubble.

At the outer edge of the hot bubble, one encounters the moving shell of shocked interstellar material. This shell has been swept up by the stellar wind and is driven outward by the high thermal pressure of the hot bubble (Weaver et al. [1977]).

Massive stars also emit high-energy photons, creating a photo-ionized H II region. A star cannot ionize an indefinitely large amount of surrounding material and due to recombination, occurring constantly within the gas, photons are continuously absorbed. The maximum radius at which the star can ionize the gas is called Strömgren radius: it defines the outer edge of the so-called Strömgren sphere. If the Strömgren sphere extends beyond the wind bubble, the wind sweeps up photo-ionized gas rather than cold interstellar medium. If the wind is strong, (as is the case for stars that become LBVs), the thermal pressure of the H II region can be insufficient to stop the fast moving shell. If the wind is not strong, the velocity of the shell can drop below the external sound speed. Once it becomes subsonic the shell can dissipate. The shocked wind material and the ionized ISM are separated by a contact discontinuity. The morphology of the main sequence bubble is now structured as a region with an inner part formed by the shocked wind material, while the outer part consists of photo-ionized ISM.

Post main sequence events

Stars with masses between 8...20 $M_\odot$ become red or blue supergiants after the main sequence, depending on several parameters. It has been shown by Heger & Langer [2000b] that at the end of MS (core H burning), the rotating stars will slow down from their rotation and evolve from the MS to the RSG stage. Rotating stars that are in a RSG phase (or in a blue loop) develop a core helium burning stage. The RSG stage is characterized by a strong loss of mass and angular momentum due to the stellar wind. Langer [1991b] demonstrated that due to rotation the helium core will mix with the H burning shell and will make the star to experience a blue loop. He also showed that small changes in mass loss can affect the star's evolution and the transition between the blue and red supergiant stage. Stellar mass loss and rotational velocity are interdependent as mass loss is enlarged by the rotational velocity, but mass loss also diminishes the rotational velocity during the evolution (see Langer [1998]).

Heger & Langer [1998] showed that if stars have masses $\leq 12\,M_\odot$ then they may experience a blue loop. BSGs created in this way can rotate close to their critical rotation rate. Mass loss increases as the star approaches the so-called Ω limit (see *Chapter 4* for more details). During the blue-loop period the stars will spin up and lose angular momentum. The fast rotation can occur since the angular momentum is concentrated in a small mass fraction near the surface of the star. As a result of the mass loss, the rapidly rotating layers get soon lost and the star slows down quickly (see Heger & Langer [1998]). After the blue loop the RSGs are rotating slower compared to RSGs that do not evolve into the BSG stage.

While for MS stars the effect of mass loss is somewhat small (for example, circumstellar material is generally not seen around MS stars), stars in the RSG and or BSG stages have rather high mass loss rates. Although the winds of MS stars have been pretty well understood (de Koter [2008]), what dominates the mass loss mechanism for RSGs is not yet identified. A possible explanation of the observed mass loss rates for massive asymptotic giant branch stars (AGBs) and RSGs has been put forward by van Loon et al. [2005] (for more details see *Chapter 2*). Nevertheless, the driving mechanism of RSG stars mass loss is still disputed. For hot stars like BSGs, the mass loss rates are correlated with the luminosity, while terminal velocities are a few times the escape velocity and the dominant mass loss mechanism for hot stars is photon absorption in spectral lines (Lamers & Cassinelli [1999]).

The rotation of the central star can make a RSG become a BSG. Some RSGs will make a blue loop and go through intermediate stages, while other will end their life as Type II supernova. Rotation affects first the MS stage: because of mixing, fresh fuel is brought up to the core, slowing down its decrease in mass during the MS evolution. This effect produces a more massive helium core at the end of the H burning phase and this favors the transition toward the lower temperatures, respectively toward the RSG stage. Another effect of rotation is to increase the stellar surface abundances (Heger & Langer [2000b]), while mixing transforms the RSG into a BSG.

Fingerprints left by the evolution of the donor star

As mentioned before, at the end of the MS, a massive star can become a RSG, a BSG, or an LBV. When the star leaves the MS not only the stellar interior changes, but also the wind

parameters: the mass loss rate increases while the wind velocity decreases. This process influences the resulting circumstellar nebula. A new shell of post main sequence wind material forms as a consequence of the variation of the wind parameters. The number of high-energy photons can decrease once the surface temperature drops and thus the region outside the shocked wind material will no longer be photo-ionized. The thermal pressure drops and the shell eventually starts to dissipate. The region of shocked wind material starts to drive a new shell into the old H II region.

Once the central star goes through the different stages of stellar evolution, the circumstellar nebula will contain information about the stars past evolution. Also the chemical abundances identified in the constituent nebular material can tell us about the past evolutionary phases of the central star. Circumstellar nebulae constitute the environment of the massive star at the moment of their supernova explosion. The structure (mass, size) of circumstellar nebulae will affect the evolution of the supernova remnant that remains after the parent star has exploded.

Observing the circumstellar medium around Red and Blue Supergiants

Nebulae consisting of interstellar material are very distinct from circumstellar nebulae containing material previously present in the central star. A direct detection of circumstellar nebula is often difficult since most of the times the circumstellar nebulae are situated around very luminous stars. But also a detectable circumstellar shell requires to be comprised by very high density material, much denser than the stellar wind expelled itself. The observations of such interesting objects as circumstellar nebulae can determine usually several physical parameters such as: the mass, the composition, the geometry of the nebula, the expansion time and the kinetic energy of the stellar wind.

In the visible, starlight is scattered by the dust and fundamental emission lines can be observed. Polarimetry and coronagraphy can be used in addition to dim the direct light coming from the central star. Also for visible wavelengths narrow band and long-slit spectroscopy (or Integral Field spectroscopy) are used to detect emission lines. In near-IR compared to visible the light is less polarized, so coronagraphy and Adaptive Optics can be used for nebula imaging. For mid- and far-IR thermal IR radiation from dust can be detected with instruments like Herschel and sub mm ALMA. Dust in a shell can make up quite a large portion of the total mass of the nebula. Radio interferometers using continuum free free radiation observe the structure and expansion of shells. While nebulae around LBVs and WR stars can be seen at radio wavelengths, circumstellar material is very hard to catch in X-rays since only very strong shocks can be far off from the central star and bright enough to be identified (see Smith [2010] for a review of observing techniques).

Modeling the circumstellar medium around Red Supergiants

A large number of nebulae have been previously found around WR and LBV stars. Many models of circumstellar material around massive stars focused on stars more massive than about 30 $M_{\odot}$. Making the assumption that during different phases of the stellar evolution the winds are isotropic, Weaver et al. [1977] and García-Segura et al. [1995a] have developed

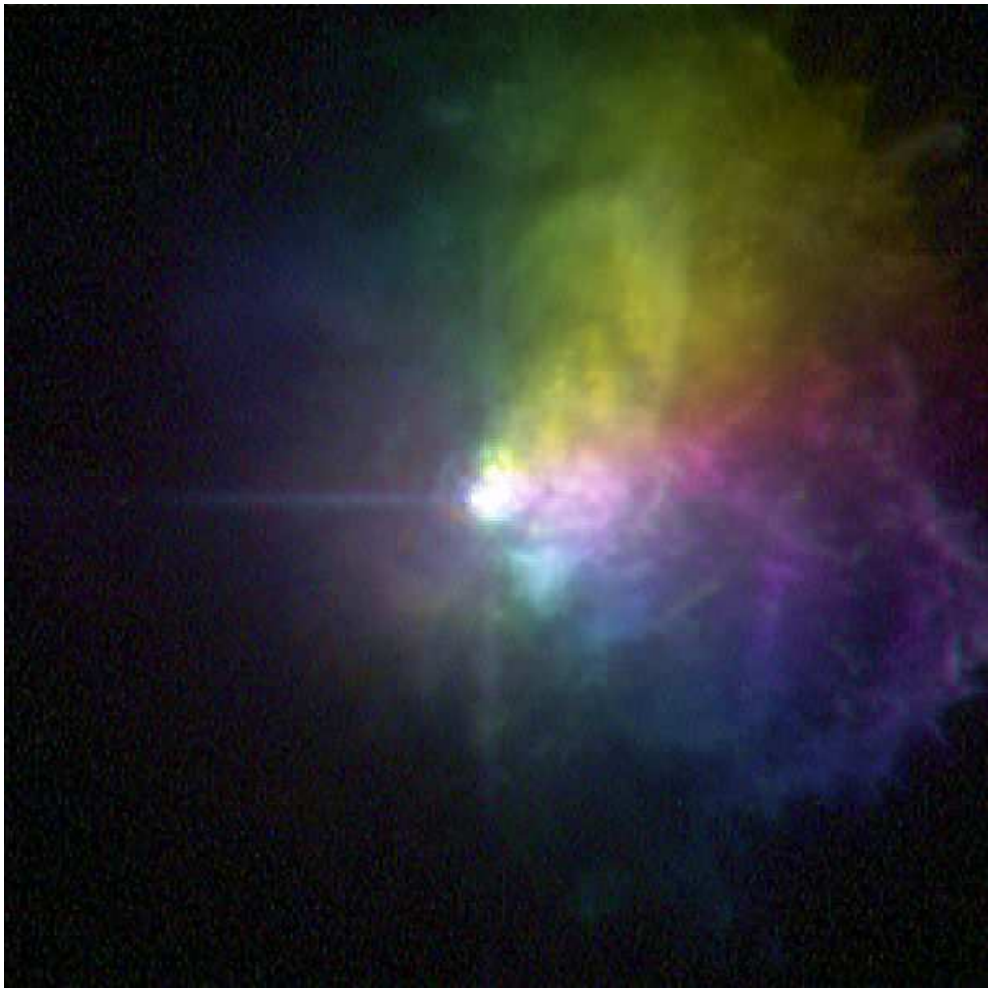

Figure 1.3: This Hubble picture shows the ejection of huge amounts of gas by VY Canis Majoris during one of its outbursts. Credit: NASA, ESA, and R. Humphreys (University of Minnesota)

analytic descriptions of the circumstellar medium. These interpretations take account of an interaction between a constant wind and the ISM and for the interaction between two winds. For more complicated cases of time dependent winds one needs to use a numerical approach based on multi-dimensional hydrodynamical models. A number of models have basically confirmed the analytic results, but uncovered a complex world of hydrodynamical instabilities present in the various shells and bubbles (e.g. Bringhenti & D'Ercole [1995a,b], García-Segura et al. [1995b, 1996a,b], van Marle et al. [2006], Dwarkadas [2007]).

The red supergiant shells or the nebulae around the RSG stars have been so far only indirectly observed. One of the aims of this thesis is to predict their properties based on

multi-dimensional modeling, allowing for a comparison between observations and theory. In *Chapter 2* we discuss several properties of RSG shells formed around stars with a mass in the range of 8...20 $M_{\odot}$. A RSG shell could be found if for example the central RSG star had substantial changes in the mass loss behavior on a short timescale. Or if the RSG stars are found in a relatively high pressure environment created maybe by an O star or by other massive stars nearby. We know that if the environment pressure is high enough, a RSG shell can form (e.g. García-Segura et al. [1995b, 1996a,b], van Marle et al. [2006]).

Nebular features have been recently found for the Mira system by Martin et al. [2007]. The observations show a comet-like tail from the AGB star Mira A stretching out (Wareing et al. [2007]). A transitional object that deviates from simple spherical symmetry is HD 179821, indicating multiple gas shells and circumstellar dust (Reddy & Hrivnak [1999], Jura et al. [2001], Patel et al. [2008]). There has been evidence of very strong enhanced episodes of mass loss in the case of IRC+10420 (Humphreys et al. [1997]) and for VY CMa (Smith et al. [2001, 2009]), showing a circumstellar environment with filaments, arclike structures and bright clumps (Fig. 1.3). Another interesting example is the case of α Ori or Betelgeuse, the brightest and the closest RSG to us, situated at 197 ± 45 pc (Harper et al. [2008]) whose circumstellar medium properties have been discussed by Noriega-Crespo et al. [1997] and Smith et al. [2009]. Obviously we cannot directly compare our RSG nebulae models with the shell around α Ori, but the observations show that if the outside medium has a confining pressure, the slow, dense RSG wind material can gather into a shell.

Modeling the circumstellar medium around Blue Supergiants

When a star becomes a RSG, the ejected wind stalls at the point where the thermal pressure in the hot bubble formed by the earlier MS wind equals the ram pressure of the RSG wind (e.g. García-Segura et al. [1996b]). If afterward the star evolves into a BSG, the wind velocity increases and the preceding wind material is swept up into an expanding shell. Massive stars are often rotating rapidly such that their winds may by highly anisotropic, and this can give rise to structured, rotationally symmetric circumstellar shells and nebula (e.g. Langer et al. [1999], Chiţă et al. [2008]). A region of hot dense gas can also form during the collision between the RSG shell and the BSG shell. In *Chapter 3* we show that this gas dominates the emission from the circumstellar medium.

Earlier models of BSG nebulae have concentrated either on stars above ~ 30 $M_{\odot}$ (e.g. Perez-Rendon et al. [2009]), that can become WR stars or LBVs (Martin et al. [1995], García-Segura et al. [1996a], Meyer et al. [1997] and Woosley et al. [1997]), either on exclusive cases, like the triple ring system around Supernova 1987A (Burrows et al. [1995] and Crotts & Heathcote [2000]) suggesting that binary phenomena are held accountable for the complex triple-ring structures (e.g. Podsiadlowski et al. [1991], Blondin & Lundqvist [1993], Lloyd et al. [1995] and Podsiadlowski et al. [2005]). With this thesis study, and more specifically in *Chapter 4,* we give a generic approach for models of circumstellar nebulae around stars in the mass range of 10...20 $M_{\odot}$ that have been evolved into BSG from RSGs. A few general characteristics of these types of BSG nebulae like the emission geometry and the expansion velocities result from our models.

It is not clear if any nebulae have been observed around BSGs that have been transfigured

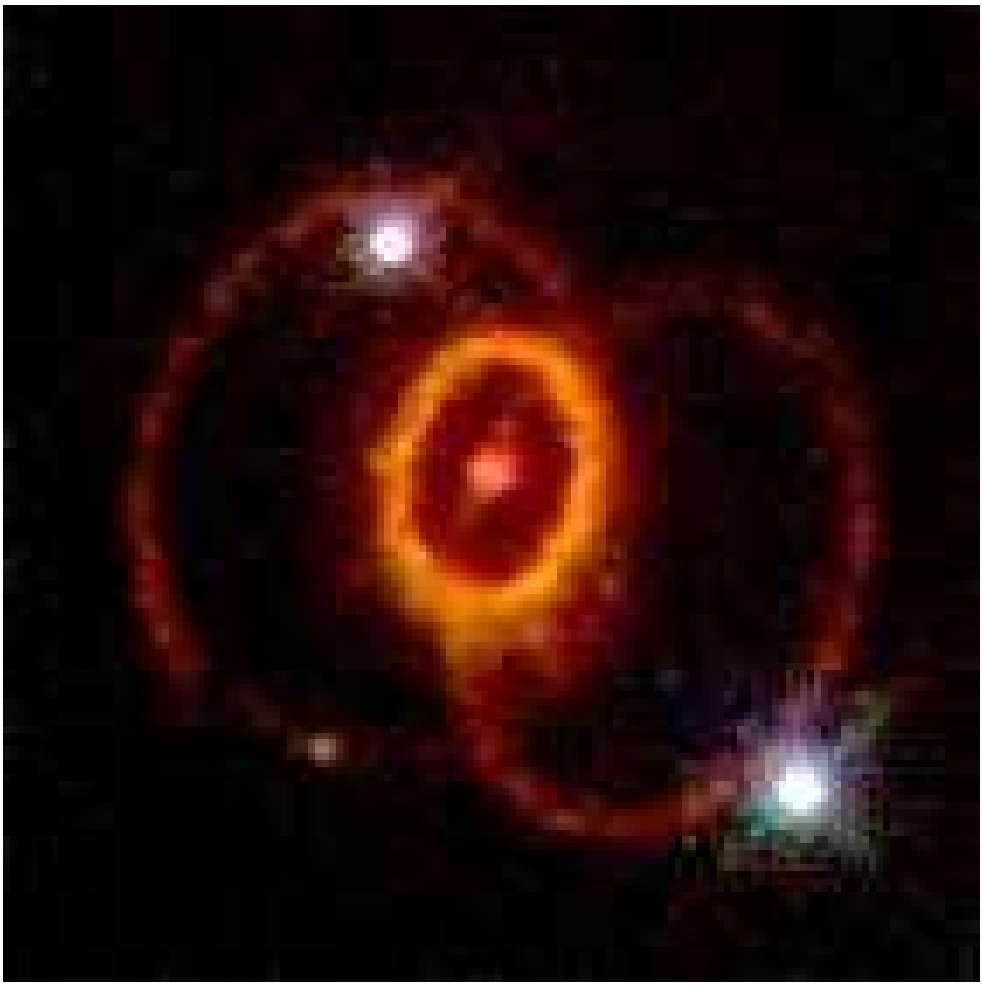

Figure 1.4: This Hubble picture shows the three rings of gas of Supernova 1987A, a star which exploded in February 1987. The small bright ring lies in a plane containing the supernova, the two larger rings lie in front and behind it. Credit: Dr. Christopher Burrows, ESA/STScI and NASA

from RSGs. A few examples exist where nebulae around BSGs (other than LBVs) have been found. The rings found around SN 1987A (see Fig. 1.4), which occurred from an exploding BSG in the Large Magellanic Cloud, are a good example. The SN 1987A nebula was only discovered because photoionisation from the supernova increased the brightness of the nebula. In *Chapter 5* we attempt to model the SN 1987A nebula based on the assumption that the progenitor star was a fast spinning BSG just recovering from the RSG stage. Similar nebulae have been found around HD 168625 (the so-called ”twin” of the progenitor of SN 1987A) and SBW 1 (e.g. Smith et al. [2007b]), and around the Galactic B supergiant Sher 25 (Brand-

ner et al. [1997]), which shows a central ring and two polar caps (see cover image). Although a few general characteristics of observed BSG nebulae are similar to our models, we cannot fit our results to any object in particular.

Specifics of the ZEUS code

We use the ZEUS 3D code developed by Stone et al. [1992] and Clark [1996] to model the circumstellar medium evolution. This three dimensional, ideal (non-resistive, non-viscous, adiabatic), non-relativistic, magnetohydrodynamical, Eulerian explicit code solves the coupled partial differential equations of (magneto)hydrodynamics as a function of time and space on a fully staggered grid. These are the governing equations for an ideal fluid without viscosity or radiative losses, assuming no magnetic fields:

The continuity equation, describing the mass density changes as a result of the flow

$$\frac{\partial \rho}{\partial t} + \nabla \cdot (\rho \mathbf{v}) = 0, \tag{1.1}$$

the momentum conservation, quantifying the change in momentum in a volume

$$\frac{\partial \mathbf{S}}{\partial t} + \nabla \cdot (\mathbf{S}\mathbf{v}) + \nabla P = 0, \tag{1.2}$$

the energy equation, showing the change in internal energy of the gas

$$\frac{\partial e}{\partial t} + \nabla \cdot (e\mathbf{v}) + P\nabla \cdot \mathbf{v} = 0. \tag{1.3}$$

Here ρ is the mass density, $\mathbf{v}$ is the velocity field, P (the thermal pressure)=(γ-1)e, $\mathbf{S}$=$\rho\mathbf{v}$ is the momentum density, e is the internal energy density of the gas per unit volume and γ the adiabatic gas index, which equals γ= 5/3 for an ideal, mono-atomic gas.

Radiative energy losses are included in the code by changing equation 1.3 into:

$$\frac{\partial e}{\partial t} + \mathrm{n_e}\,\mathrm{n_H}\Lambda(\mathrm{T}) + \nabla(\mathrm{e}\mathbf{v}) + \mathrm{P}\nabla\mathbf{v} = 0. \tag{1.4}$$

The Λ is a cooling function (MacDonald et al. [1981]) which we used for the first part of our results. The $\mathrm{n_e}$ an $\mathrm{n_H}$ are the number density for free electrons and total hydrogen particles. The last consists of ionized and neutral particles and we have assumed that the gas consists only of hydrogen to be able to calculate these number densities. The cooling function describes the amount of energy lost through radiation as function of temperature and ionization fraction. Our code does not keep track of the abundances, thus we can only use the temperature to determine the value of the cooling function. This cooling curve is a combination of multiple cooling functions from various atoms in different stages of ionization and is extrapolated below 10^4 K. For temperatures above 10^8 K only electron Bremsstrahlung (free-free radiation) is considered as cooling mechanism. Cooling is set to 0 for $T < 100$ K which means that below 100 K only adiabatic expansion cools the gas.

Because of the uncertainties in the cooling rate for temperatures below 10^4 K of MacDonald et al. [1981], we have implemented a different plasma cooling function (Smith et al.

[2008]). This cooling curve starts from temperatures of 10 K. If we compare the two cooling functions we see that cooling in MacDonald et al. [1981] is overestimated for temperatures between 10^3 and 10^4 K. For temperatures between 100 and 10^3 K the cooling of the gas is underestimated.

The effect of photoionization has been included in our code by García-Segura et al. [1999] and is determined by calculating the Strömgren radius along each radial line from the star across the grid. The matter outside this radius is considered neutral while the matter inside this radius is considered ionized. The stellar evolution models that we use as our input do not give the number of ionizing photons. Previously this number was calculated according to the black-body radiation. We implemented a new way of calculating the number of ionizing photons. We compute this number according to the stellar effective temperature and surface gravities. The corresponding spectral energy distributions (SEDs) are found by interpolation from a grid of SEDs calculated by Lefever et al. [2007]. This grid has been computed for OB stars with solar metallicity using the FASTWIND non-LTE code (Puls et al. [2005]).

Computations use detailed time-dependent input from stellar evolution calculations based on models computed by Heger & Langer [2000b] and Heger et al. [2000a]. The simulations are performed by filling a spherical grid with ISM material, which has a density of 20 cm^{-3}. At the center of this grid we have a source of mass, momentum and energy that corresponds to the stellar wind. The code is not capable of resolving the star or the inner (sub-sonic) part of the wind. The wind flows into the constant-density interstellar medium. Wind parameters vary over time, following the stellar evolution. We first compute the evolution of the CSM for all our models in 1D for the entire evolution of the star, from the main sequence to the pre-supernova stage. The 1D model is then mapped onto a 2D grid for the final stages of the evolution. The mapping method employed in this thesis was applied earlier by García-Segura et al. [1996,a,b] and by van Marle et al. [2005, 2007, 2008].

Although ZEUS-3D is fully three-dimensional it only works efficiently (given current limitations on computer power) in one or two dimensions. High-resolution runs are needed to resolve dynamical instabilities. Because of the high cost in CPU time and memory inevitable when working in three dimensions, we assume axis symmetry and perform the 2-D simulations. Although the instabilities are 3-D, the 2-D models can give us a useful first description of them and whatever is unstable in 2-D is certainly 3-D unstable. The axisymmetry and the choice of grid resolution determines the numerical viscosity. The numerical diffusion can profoundly affect the development of dynamical instabilities. To separate numerical effects from physical behavior we use different grid resolutions. Structures on scales less than the grid size will be suppressed but this is acceptable as the observations we want to compare them with have limited resolution.

Thesis content

This thesis constitutes the first generic study of the structure of the circumstellar environment for typical supernovae progenitors. As such, it presents models of the circumstellar medium around stars with masses between 8 and 20 $M_\odot$ and there are a few reasons why we consider this interesting and important:

- Surprisingly a circumstellar nebula has been observed around Betelgeuse, a RSG star that has not been evolved from a WR or a LBV phase
- A short-lived, luminous and highly structured nebula can form around rapidly rotating BSG immediately after the RSG stage, entirely due to wind-wind interactions
- The expelled stellar wind material returns back into the interstellar medium after it has been chemically enriched due to star's inner nuclear processes

Gazing at the sky in the interest of uncovering these unique objects we will have to search for RSG shells that form at a distance from central the star varying between 1 to 4 pc or between 3.26 to 13.04 ly. Containing a large portion from the total mass lost in the course of the RSG stage, the shell masses will span between 0.005, 0.001 and 1.55 $M_\odot$. The luminosity of the shells equals about 0.2 $L_\odot$, while they will typically have temperatures of several 10^4 K. The bow shock detected around Betelgeuse shows that the RSG wind can pile up against the ram pressure from the ISM interaction. As the density of the RSG shells is a few times lower than ISM density, uncovering a bow shock gives us the possibility of an indirect observation of RSG shells. We also consider BSG nebulae. They are generally dimmer, compared for example to planetary nebulae, since their mass is around 0.01 $M_\odot$. Due to the collision between the BSG and RSG shells, the nebulae have luminosities up to 1 $L_\odot$ for 10^4 yr. Wind-wind encounters, or BSG wind sweeping up RSG wind, produces a nebula relatively close to the star: 0.9...2.3 pc with a spherical shape (if the central star is a slow rotator) and a bipolar architecture (if the central star is a rapid rotator). Nevertheless, if most stars in the considered mass range of 10...20 $M_\odot$ would have undergone a blue loop, only a small proportion are expected to have observable BSG nebulae.

The thesis layout is as follows :

- **Chapter 2:**

In Chapter 2, we model the circumstellar medium of stars with initial masses of 8, 12, and 20 $M_\odot$, over their entire life, focusing on the RSG stages of these stars (see Fig. 1.1). During the post-main-sequence stages, stars can evolve through several blue and red supergiant stages depending on their initial mass, composition and rotation rate. The models considered in this Chapter have long-lasting RSG stages starting after the MS. In this phase, they develop shells of RSG wind material at the location where the free streaming RSG wind is stalled by the thermal pressure of the hot MS bubble, close to the central star. The RSG shells develop violent Rayleigh-Taylor instabilities, which occur at the contact discontinuity between the RSG shell and the hot shocked MS wind material. Once these instabilities grow non-linear,

the RSG shell becomes highly structured as clumps form, and shell material mixes with material in the hot bubble. Later on they evolve to the BSG stage, during which the RSG shells are completely destroyed. These models return to the RSG stage at core helium exhaustion, and build new RSG shells, which are more massive than those formed earlier. RSG shells are essential for our understanding of bipolar emission nebulae around BSGs.

- **Chapter 3:**

Results for a rapidly rotating $12\,M_\odot$ single star are presented here. On a time scale of a few 10^4 yr, a BSG hour-glas shaped nebula expands into the sphere defined by the RSG shell. The faster polar parts of the hour glass hit the inner edge of the RSG shell first. The collision creates a pair of hot and dense polar caps. As time passes, the collision zone moves to lower latitudes of the RSG shell and becomes more confined in latitude. At the same time, the interaction of the BSG wind with the equatorial disk defines a second, ring shaped collision zone in the equatorial plane. These structures are reminiscent of the observed nebulae around the blue supergiant Sher 25 (see cover image).

- **Chapter 4:**

Here we present calculations are shown that predict the properties of the circumstellar medium for rapidly rotating and slowly rotating blue supergiants. The interaction of their winds with the outside medium is followed through all stages of stellar evolution, from main sequence to the pre-supernova stage for stellar models with masses in the range of 10, 12 and 18 $M_\odot$ (see Fig. 1.1). Our stars spend most of their life time in the main sequence stage. In their post-main-sequence phases, the stars with 10 and 12 $M_\odot$ undergo a blue-loop following a first red supergiant stage. Before they explode as supernovae, the stars go back for a second time to the red supergiant stage. We also analyze an 18 $M_\odot$ model with an evolution presumably resembling that of the progenitor of SN 1987A, which explodes as a blue supergiant after evolving through a short red supergiant stage. In case of a rapidly rotating central star, the collision of an hour-glass shaped shell with a stationary red supergiant shell forms a highly structured rotationally symmetric nebula. In contrast: if the star rotates slowly, a spherical nebula may form.

- **Chapter 5:**

We present preliminary results of our investigation of possible ways for the formation of the outer rings observed around SN 1987A nebula (see Fig. 1.4) through wind-wind interaction in this chapter. At the end of the main sequence stage, our star model goes through a first blue supergiant post-main sequence stage. Towards the end of core helium burning, it becomes a red supergiant. Before exploding as a supernova, the progenitor enters a second blue supergiant phase. During this phase the star reaches critical rotation. For both test models, the wind ejected during the first blue supergiant stage is aspherical and sets material into the hot bubble. During the previous red supergiant stage, the slow red supergiant wind is accumulated in a shell around the central star. Due to the non-spherical wind of the first BSG phase, this shell is broken into two parts, with a high density ring-shaped intersection at mid-latitudes, which has some similarity to the outer circumstellar rings of SN 1987A.

Chapter 2

The circumstellar medium of massive stars. I. Models for red supergiants

based on S. M. Chiţă, N. Langer, B. van Veelen, A. J. van Marle, G. García-Segura 2010, submitted to A&A

Abstract

Massive stars emit strong winds throughout their evolution, and thereby shape the circumstellar medium around them. This leaves observable signatures throughout the life of a massive star, and at the time it explodes as a supernova. We model the circumstellar medium of stars with initial masses of 8, 12, and 20 $M_\odot$, over their entire life. In this Paper, we focus on the red supergiant (RSG) stages of these models. Stellar evolution models provide us with the time dependent stellar wind and ionization parameters as input for our 1D and 2D hydrodynamic simulations of the circumstellar medium. The post-main-sequence phases are modeled in 2D.

All three considered stellar models have long-lasting RSG stages starting after core hydrogen exhaustion. In this phase, they develop shells of RSG wind material at the location where the free streaming RSG wind is stalled by the thermal pressure of the hot main sequence bubble at a distance of about 1...4 pc from the star. These RSG shells develop violent Rayleigh-Taylor instabilities, and shed clumps of RSG wind material into the main sequence bubble, rendering the shell masses (0.005 $M_\odot$, 0.01 $M_\odot$ and 1.55 $M_\odot$) well below the total mass lost in the RSG stage (0.12 $M_\odot$, 0.35 $M_\odot$ and 4.14 $M_\odot$, for the 8, 12, and 20 $M_\odot$ sequences). Our 8 and 12 $M_\odot$ sequences evolve to the blue supergiant stage during core helium burning, during which the RSG shells are completely destroyed. These models return to the RSG stage at core helium exhaustion, and build new RSG shells which are more massive than those formed earlier. Our models predict that red supergiants should be surrounded by wind shells with parsec scale radii. While their densities are expected to be below typical ISM densities, the recent detection of a parsec size wind bow shock around Betelgeuse indicates that they may well be observable. RSG shells are also essential to understand bipolar emission nebulae around blue supergiants. For low and high mass RSGs, their shells may also affect the late stages of the supernova evolution.

Introduction

Massive stars eject large amounts of mass during their life time and undergo a complex evolution through the Hertzsprung-Russell diagram (HRD). Depending on their initial mass, composition and rotation rate, the post-main-sequence evolution before the supernova explosion, may involve several blue and red supergiant stages. The wind interaction that follows from the stellar evolution dictates their nebular variety.

Motivated by the nebulae found around a large fraction of Wolf-Rayet stars and Luminous Blue Variables, previous models of the circumstellar medium around massive stars have focused on stars more massive than about 30 $M_\odot$. Assuming that the stellar winds in the different stages of stellar evolution are isotropic, analytic descriptions have been developed by Weaver et al. [1977] and García-Segura et al. [1995a]. Multi-dimensional hydrodynamical models have basically confirmed the analytic results, but revealed a multitude of hydrodynamical instabilities present in the various shells and bubbles (e.g. Bringhenti & D'Ercole [1995a,b], García-Segura et al. [1995b, 1996a,b], Dwarkadas [2007]).

In the present Paper, we investigate the circumstellar medium around stars which end their lifes as red supergiants (RSGs). While stars in the corresponding mass range (about 8 $M_\odot$ – 20 $M_\odot$) do not lose as much mass as their more massive counterparts, there are three reasons why the circumstellar medium of RSGs is interesting. First, circumstellar nebulae have been found around stars without a Wolf-Rayet or LBV phase (e.g. Noriega-Crespo et al. [1997], Ueta et al. [2008], Smith et al. [2009]). Secondly, Chiţă et al. [2008] (hereafter Paper I) showed that highly structured, luminous nebulae around blue supergiants (BSGs) are expected if a red supergiant shell has been formed in a previous evolutionary stage. And third, if RSGs are surrounded by a circumstellar shell at the time the star explodes, then this shell may provide an observational signature in the display of the corresponding Type II supernova.

The hydrodynamic calculations in the present Paper used detailed time dependent input from stellar evolution calculations, based on models computed by Heger & Langer [2000b], Heger et al. [2000a]. We investigate the evolution of the circumstellar medium of an 8 $M_\odot$ and a 12 $M_\odot$ model which both evolve into red supergiants after their main-sequence stage, then evolve back to become blue supergiants, and return to the red supergiant branch to explode as supernova. We further explore a 20 $M_\odot$ model, which turns into a red supergiant after its main-sequence evolution and remains a RSG throughout its further life. Here, we only investigate the circumstellar medium during the red supergiant stages of these models. The corresponding blue supergiant circumstellar medium structures are discussed in Chiţă et al. [2010b] (hereafter Paper III).

In Sect. 2, we give a short introduction into the stellar evolution models which we adopted for our calculations. In Sect. 3 we present our computational method, while results of our circumstellar hydrodynamic calculations are presented in Sect. 4 and Sect. 5. We compare our results with observations in Sect. 6, and we give our main conclusions in Sect. 7.

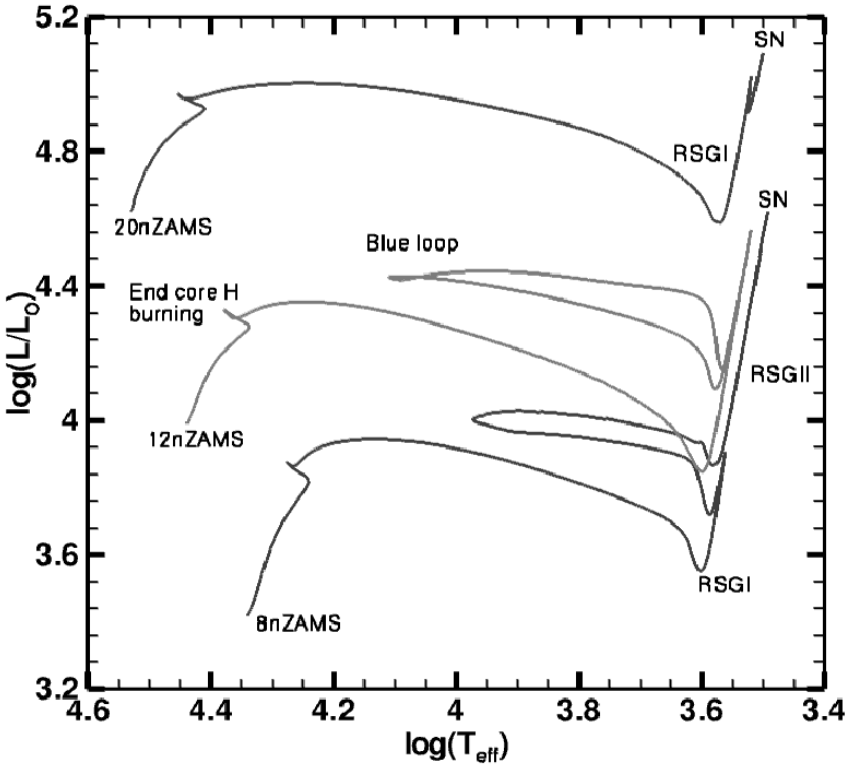

Figure 2.1: Evolutionary tracks of our adopted stellar evolution models in the Hertzprung-Russell diagram, from the zero age main sequence to the pre-supernova stage for Models 8n, 12n 20n.

Stellar evolution models

The evolution of massive stars from the zero-age main sequence (ZAMS) until the pre-supernova stage has been computed previously by Heger & Langer [2000b], Heger et al. [2000a]. These models have been computed using an implicit hydrodynamic scheme containing OPAL opacities, detailed nuclear networks, mass loss according to Nieuwenhuijzen et al. [1990], the physics of rotation for the stellar interior, and rotationally modulated stellar winds, as described in Heger et al. [2000a]. We use their results given for stars of 8, 12 and 20 $M_\odot$, specifically their Model E08 (hereafter Model 8n) with an initial rotational velocity of 205 $km\,s^{-1}$, Model G12B (hereafter Model 12n), with an ZAMS rotational velocity of 99 $km\,s^{-1}$, and Model E20B (hereafter Model 20n) with 201 $km\,s^{-1}$ as initial rotational velocity. In Fig. 2.1 we show the evolutionary tracks of the selected models in Hertzsprung-

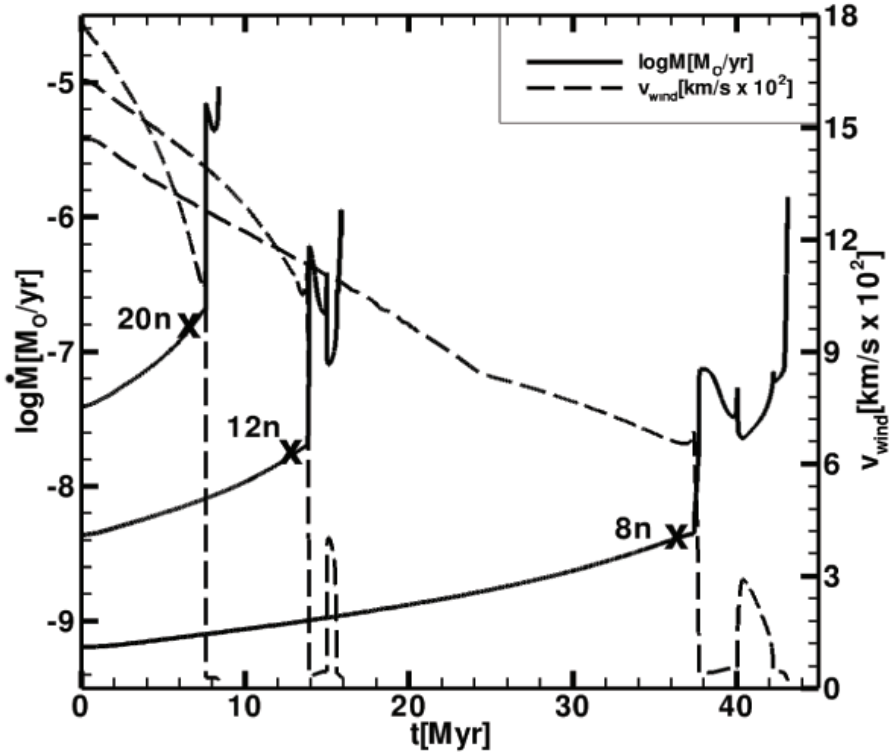

Figure 2.2: Mass-loss rate (solid line) and the terminal wind velocity (dashed line) as function of time for our employed models 8n, 12n and 20n. The symbols represent the starting points for our 2D simulations.

Russell diagram (HRD), and identify their various evolutionary phases.

The selected stellar evolution models spend most of their life in the MS stage (cf. Table 2.1) and then move to the RSG regime . Models 8n and 12n remain there for 2.31 Myrs and 1.07 Myr, respectively, which represents roughly half of the core-He burning life time. Then, both models undergo a so called blue loop, i.e. they evolve from the RSG to the BSG stage, where they spend most of the remaining core helium burning time, before they return to the red supergiant branch. Model 20n, after spending 7.61 Myr on the MS, moves to the RSG regime where it stays for 0.78 Myr before it explodes as supernova.

From the output of the stellar evolution models (Fig. 2.2), we compute the time-dependent mass loss rate, terminal wind velocity and ionizing fluxes (cf. Section 3). In this Paper we do not consider any wind anisotropy which might be caused by the rotation of the star, since

Table 2.1: The approximate duration of each evolutionary phase (Δt), the ejected mass (ΔM), momentum (Δp), and kinetic energy (ΔE) during this phases. The evolutionary phase is identified in the second column: main sequence phase (MS), first red supergiant phase (RSG I), blue supergiant stage (BSG), second red supergiant stage (RSG II).

Model	Phase	Δt	ΔM	Δp	ΔE
		Myr	$M_\odot$	10^{38} g cm s^{-1}	10^{45} erg
8n	MS	37.69	0.06	109	510
	RSG I	2.31	0.12	11	3
	BSG I	2.23	0.07	28	31
	RSG II	0.85	0.09	68	2
12n	MS	13.90	0.13	325	2156
	RSG I	1.07	0.35	27	5
	BSG I	0.65	0.07	42	73
	RSG II	0.26	0.13	9	2
20n	MS	7.61	0.66	1800	12705
	RSG I	0.78	4.14	229	32

their effects on the circumstellar medium in the red supergiant stage is negligible. During the main sequence phase, the star's rotation will not produce any significant asphericities in the swept-up interstellar medium, since this shell is driven by the pressure of the hot bubble produced by the shocked main sequence wind. During the red supergiant phase, the ratio between the centrifugal force and the gravity at the surface is smaller than about 0.2 so this will not influence the structure of the nebula. The approach of critical rotation can strongly affect the wind geometry at the onset of the BSG stage, which we will discuss in Paper III.

Numerical method

We use the ZEUS 3D code developed by Stone et al. [1992] and Clark [1996] to simulate the evolution of the circumstellar matter (CSM). This is a three dimensional, ideal (non-resistive, non-viscous, adiabatic), non-relativistic, magnetohydrodynamical, Eulerian explicit code which solves the coupled partial differential equations as function of time and space on a fully staggered grid. Radiatively optically-thin cooling is used by solving the energy equation implicitly according to Mac Low et al. [1989]. Originally the plasma cooling curve employed in the code was the one given in MacDonald et al. [1981] (hereafter MB), but we have implemented the plasma cooling curve of Smith et al. [2008] (hereafter SM).

We first compute the evolution of the CSM for all our models in 1D for the entire stellar evolution, from the main sequence to the pre-supernova stage. We choose a grid with 1000 grid points over a radius of 45 pc, and an interstellar medium density of 20 cm^{-3}. As mentioned in García-Segura et al. [1996a,b] and Dwarkadas [2007], the main sequence wind is steady and it creates a stable MS bubble. We map the 1D model onto a 2D spherical grid at the end of main sequence to compute its further evolution. The mapping method was applied before by García-Segura et al. [1996,a,b], van Marle et al. [2005, 2007] and Papers I, III. The

Table 2.2: Various quantities for the MS stage as calculated from our models, Model 8n, 20n, 12n and 12n-MB: time averaged wind mechanical luminosity $L_{\rm wind}$, analytical radius of the outer shock R_2, hydrodynamical radius at the end of MS phase $R_{\rm TAMS}$.

Model	$\tau_{\rm ZAMS}$	$L_{\rm wind}$	R_2	$R_{\rm TAMS}$
	Myr	$L_\odot$	pc	pc
8n	37.7	0.11	28.9	-
12n-MB	13.9	1.29	26	25
12n	13.9	1.29	26	24
20n	7.61	13.8	29.2	32

2D grid has an inflow inner boundary condition applied at 0.025 pc, and the outer boundary is at 45 pc. The radial component of the grid is resolved with 500 grid points, where 400 grid points are used for the inner 10 pc, and 100 grid points for the outer 35 pc; while the angular component of 90 degrees is resolved with 200 grid points for the alt-azimuthal coordinate.

For our hydrodynamical calculations we use the time dependent mass loss rate which follows directly from the stellar evolution model. The terminal wind velocity is calculated from the stellar escape velocity according to the star surface temperature scaling proposed by Eldridge et al. [2006]. We account for the effect of photoionization by calculating the Strömgren radius along each radial grid line and considering the matter within this radius to be ionized and the matter outside this radius as neutral. This method was used before by Bodenheimer, Tenorio-Tagle & Yorke [1979], García-Segura et al. [1996, 1999], van Marle et al. [2005, 2007, 2008] and Papers I, III.

We compute the number of ionizing photons according to the effective temperatures and surface gravities from the stellar evolution model by interpolating in a grid of model atmospheres for massive OB stars of solar metallicity. This grid was computed with the FASTWIND non-LTE code (Puls et al. [2005]) and was described in detail by Lefever et al. [2007] and used in Papers I, III.

1D results

As we have described in the previous section, different stellar wind properties correspond to distinct phases of the stellar evolution. A large amount of time is spent in the MS stage (cf. Table 2.2), and during this phase the wind mass loss slowly increases, while the wind velocity decreases (Fig. 2.2).

From the analytic approximation of a MS bubble given by Weaver et al. [1977], we summarize the solution to their Eq. (21) as:

$$R_2 = \left(\frac{250}{308\pi}\right)^{1/5} L_{\rm wind}^{1/5}\, \rho_0^{-1/5}\, t^{3/5} \tag{2.1}$$

were $L_{\rm wind}$ is the mechanical wind luminosity (which is assumed to be time-independent in Weaver et al. [Weaver et al. 1977], t the time, R_2 is the outer shock radius and ρ_0 the ISM density.

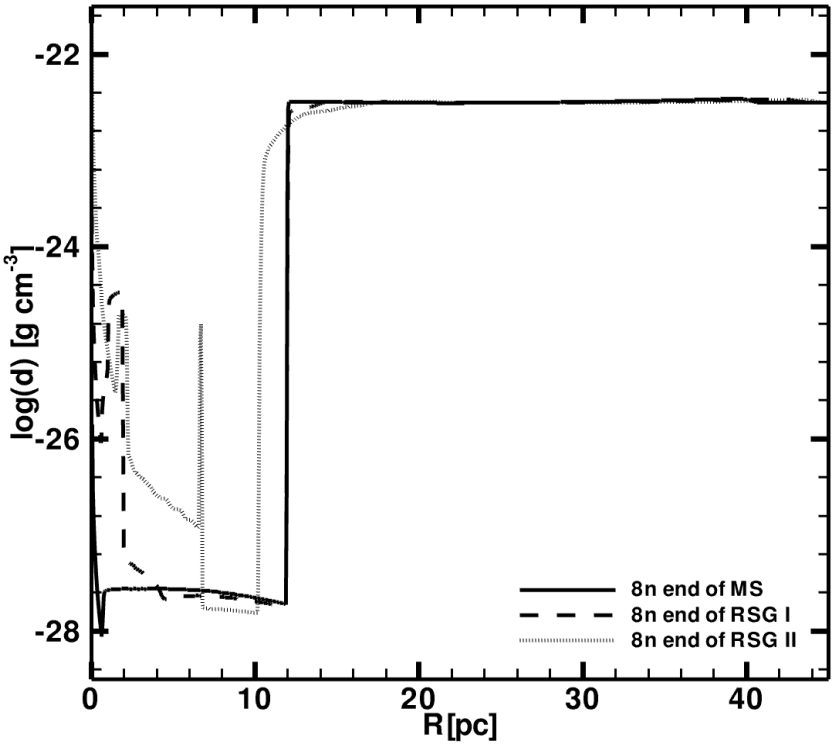

Figure 2.3: The density distribution of the circumstellar medium around Model 8n, as function of radius from the central star for three time snapshots of our 1D simulation: the end of the main sequence phase (solid line) — which is used to start the 2D simulation; cf. Fig. 2.2 —, the end of first red supergiant stage (dashed line), and the pre-supernova stage (dotted line). While the hot MS bubble extends to about 10 pc, the remnant of the collision between the blue and red supergiant shells is found at about 6 pc, and the final red supergiant shell has a radius of about 2 pc.

In Table 2.2, the values of the outer shock radius from our 1D models at the end of the main sequence phase are compared with those obtained from Eq. (2.1), using our values for the density of the ISM of $\rho_0 = 10^{-22.5}\,\mathrm{g\,cm^{-3}}$, and a time-averaged mechanical wind luminosity. We find reasonable agreement for Models 12n (independent of which cooling curve was employed) and 20n.

The main sequence shell of Model 8n has been smeared out into the ISM, such that no forward shock exists when the star finishes core hydrogen burning (see Fig. 2.3), although the analytical model predicts an outer shock radius of roughly 29 pc. For our hydrodynamical

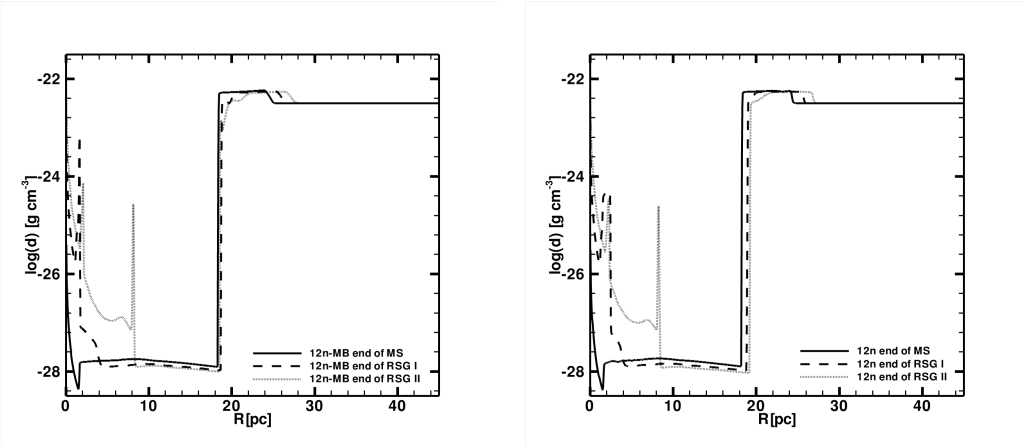

Figure 2.4: The density of the circumstellar medium for Model 12n, for three moments in time of our 1D simulation. The left panel shows results obtained with MB cooling curve, and the right panel shows results obtained with SM cooling curve. In both panels the end of main sequence is represented by the solid line, the end of first red supergiant stage by the dashed line, and with the dotted line we represented the pre-supernova stage. The main sequence shell in both cases has kept its location over the entire evolution at 18 pc and the remnant of the collision between the blue and red supergiant shells (see text for details) is situated in both cases at 8 pc. The second, pre-SN red supergiant shell forms in both cases at about 2 pc.

model with a long main sequence phase, the main sequence shell is expanding into the ISM more rapidly than the discontinuity between the the shell and the hot bubble moves forward. The motion of this discontinuity is subsonic compared to the sound speed in the shell, which means that the internal gas pressure in the shell starts to spread out the shell, while the thermal pressure in the shell pushes back against the hot bubble. Basically the bubble reaches pressure equilibrium with the interstellar medium (García-Segura et al. [1996]).

For Model 12n, the hydrodynamic model predicts an outer shock radius of 24...25 pc (depending on the employed cooling curve; cf. Fig. 2.4), while the analytic value is slightly larger (26 pc). As mentioned by García-Segura et al. [1996b], the radius of the MS bubbles from the numerical computations, when including radiative energy losses, will be smaller then the estimate given by Weaver et al. [1977] for the adiabatic bubbles.

The main sequence shell of Model 20n has a smaller analytical value (29 pc), compared to the hydrodynamical outer shock radius of 32 pc. Although in our model, at the end of core hydrogen burning, there is no pronounced photoionized region (see Fig. 2.5), during the MS, the high temperature free streaming wind inserts extra energy in the form of heated gas making the main sequence shell to move forward.

Our 1D simulations include the entire stellar wind evolution following the various stellar stages. In the red supergiant phase the wind terminal velocity is small, while the mass loss rate increases, as seen in Fig. 2.2 and in Table 2.2. During this stage, the wind speed is about

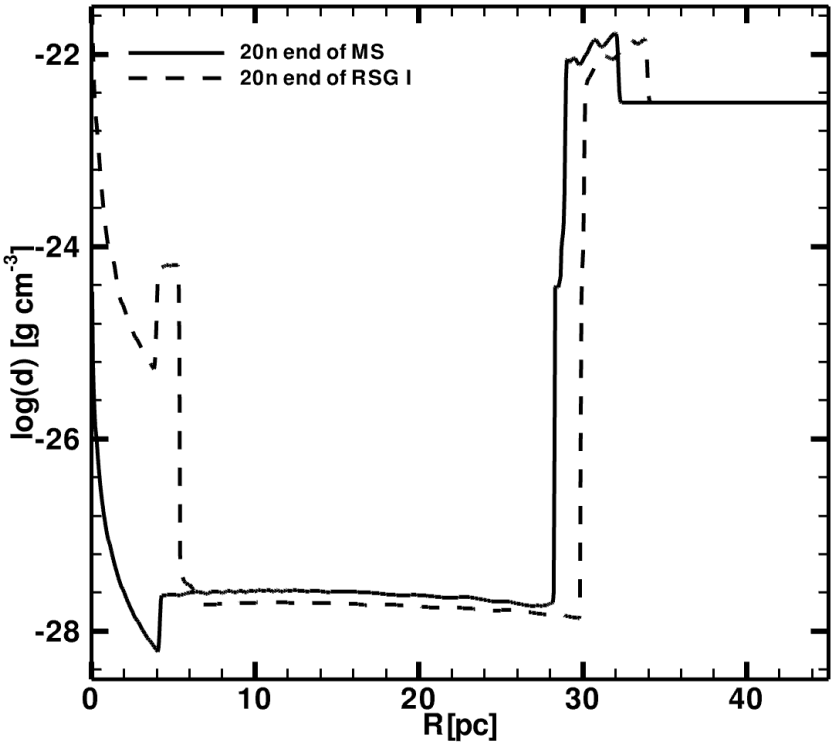

Figure 2.5: The density of the circumstellar medium for Model 20n, at the end of the main sequence evolution (solid line) and the pre-supernova stage (dashed line). A main sequence shell is formed at 28 pc and a red supergiant shell at 4 pc.

$v_{wind} \simeq 47$ km s^{-1} for Model 8n, $v_{wind} \simeq 40$ km s^{-1} for Model 12n, and $v_{wind} \simeq 28$ km s^{-1} for Model 20n. As shown by García-Segura et al. [1996b], in the transition between the MS stage and the RSG stage, the ram pressure of the wind drops and the wind termination shock moves inward. In the quest to reach equilibrium, it oscillates, and once the balance between the thermal pressure of the hot bubble and the RSG wind ram pressure is achieved, the RSG shell starts to form. The RSG wind material starts to pile up against this shock and adds mass to the thin RSG shell. In our models, the radii of these RSG shells are 2 pc (Models 8n and 12n; Figs 2.3 and 2.4) and 4 pc (Model 20n, Fig. 2.5).

The BSG phase characteristic only to Models 8n and 12n, ejects a high mass loss and high speed wind into the pre-existing RSG wind. As consequence a new shell forms by sweeping RSG wind material. This shell collides with the RSG shell and results in a high density

peak located at $\sim$ 6 pc in Fig. 2.3 and at $\sim$ 8 pc in Fig. 2.4 in the pre-supernova stage. This collision is completely unstable when computed in 2D, with the result that the material corresponding to this density peak is distributed throughout the main sequence bubble (see Paper III).

The second RSG stage with an increase in mass loss and decrease of wind velocity brings up a final increase of CSM density and a second RSG shell seen for Model 8n at 2 pc (Fig. 2.3) and at 2 pc Fig. 2.4 for Model 12n. For the latter case, we have also performed 1D and 2D simulation with MB cooling curve as shown in Fig. 2.4 left panel, and with SM cooling curve (Fig. 2.4, right panel).

In the 1D results, hydrodynamic instabilities of the various shells can not be obtained, so a more detailed description is presented in the next sections.

2D results

Our 2D simulation for all models start during but towards the end of main sequence evolution of the central star. In Fig. 2.2, which shows the mass loss rate of the stellar models as function of time, where the transition from the main sequence to the post-main sequence evolution is well marked by the first sharp rise of the mass loss rate, we mark the onset of the 2D calculations for the various models by a symbol. The corresponding 1D density structures are shown in Figs. 2.3, 2.4, and 2.5 by the solid line. We do not apply artificial noise to trigger instabilities.

Model 8n

At the time when we start our numerical calculations in 2D, Model 8n has a CSM formed by a hot bubble with a radius of 12 pc whose MS shell has merged with the ISM. The evolution of the first RSG shell is displayed in Fig. 2.6, which shows only the inner 8 pc of our 45 pc grid. The next collection of time snapshots in Fig. 2.7, taken after the BSG stage, shows the formation and evolution of the second RSG shell up to the pre-supernova stage.

The RSG shells of our 8 $M_\odot$ model show violent Rayleigh-Taylor instabilities, both, during the first and during the second RSG stage. The distinct Rayleigh-Taylor fingers are most pronounced during the formation phase of the RSG shell. During later phases, the Rayleigh-Taylor fingers expand outwards, eventually breaking out from the shell such that individual high density clumps are shed off the shell at random locations. Before the onset of the blue supergiant stage, these clumps can travel out to distances of about 4 pc (Fig. 2.6).

While at the beginning of the RSG stage the hot bubble has a high pressure, later after the injection of mass coming from the RSG wind in the form of clumps, the average density increases, and as a consequence the MS bubble starts to cool and loose pressure. Combined with the long duration of RSG stage, the MS shell, containing clumpy remnants of the collision between the RSG shell and the BSG shell (see Fig. 2.3), pushes inwards. This effect is noticeable at the top of the lower right image of Fig. 2.6. The later evolution of the MS shell is shown in Fig. 2.7.

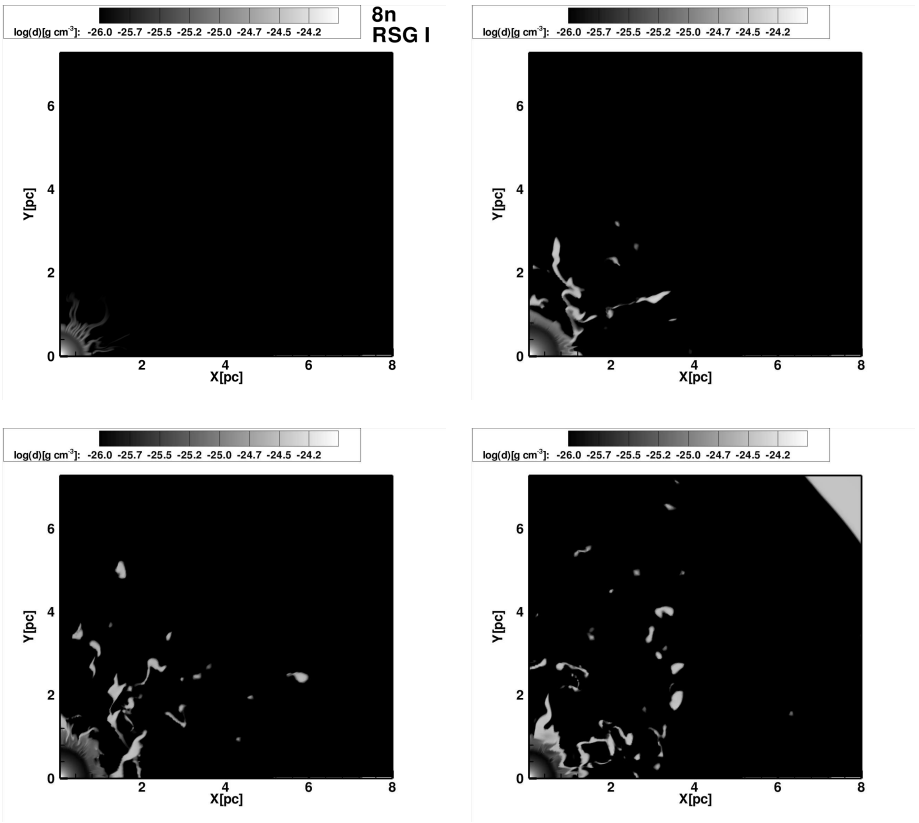

Figure 2.6: Snapshots of the density distribution of the circumstellar medium for the inner 8 pc part of our 45 pc grid, during the first red supergiant stage of Model 8n. The upper left panel is taken 0.6 Myr after the start of the 2D simulation, and shows the onset of the formation of the red supergiant shell, which shows prominent Rayleigh-Taylor instabilities. This shell is located at 1 pc in the upper right panel taken at 1.2 Myr; it sheds dense clumps into the hot main sequence bubble. The lower left panel is taken 1.8 Myr after the start of the 2D simulation. The lower right panel (at 2.3 Myr) shows the structure of the first red supergiant shell before the onset of the blue supergiant wind. The outer MS shell has pushed inwards and starts to be visible in the upper corner of the lower right panel.

As a result of the pressure in the hot bubble, a second RSG shell forms after the termination of the blue loop of the central star, which develops again Rayleigh-Taylor instabilities. While fragile at first, the second RSG shell becomes more pronounced due to the sharp increase in the mass loss rate during the last few 10^5 *yr* in the life of the star, as it climbs up the Hayashi line in the HR-diagram (Fig. 2.1) before producing a Type II supernova. In Fig. 2.7, the lower right image captures the ”pre-supernova” shell at 2 pc. The detailed characteristics of the RSG shells are presented in the next section.

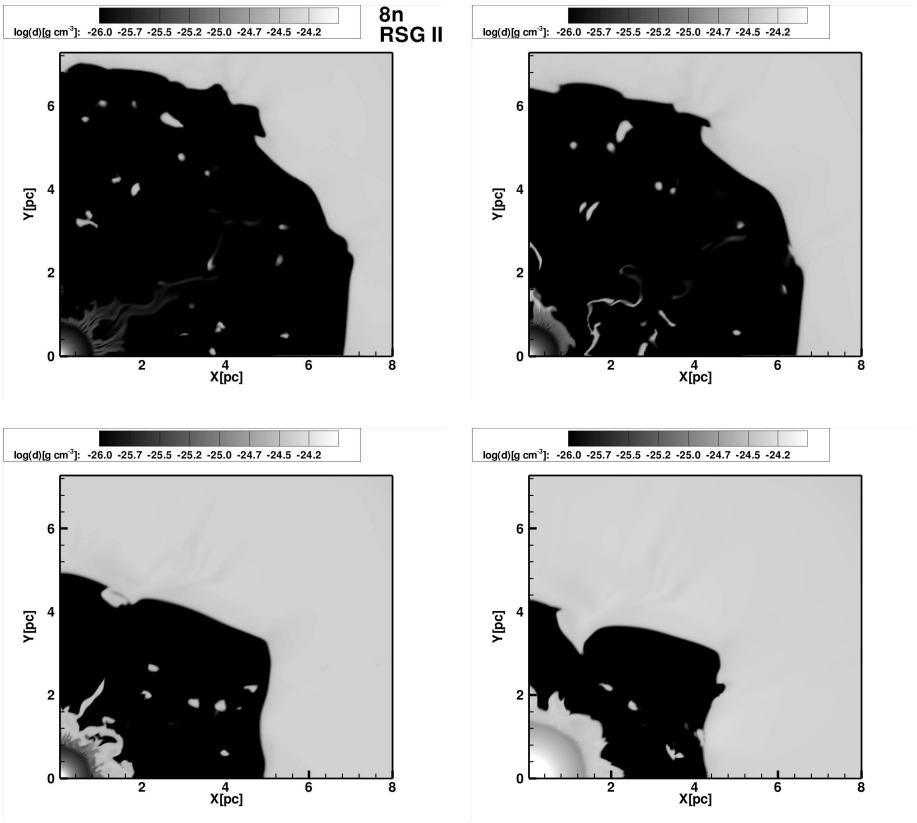

Figure 2.7: The logarithm of the density of the circumstellar medium of Model 8n during the second red supergiant stage, at four different times. The upper left panel shows the formation of the second red supergiant shell after the end of the BSG stage, about 4.5 Myr after the start of the 2D run. The further panels are taken 4.67 Myr, 5.17 Myr, and 5.36 Myr after the start of the 2D calculation. The lower right panel corresponds to the pre-supernova stage.

Model 12n

We have calculated 2D simulations of this model for three separate cases: a) we used the same physics and assumptions as in Models 8n and 20n (Model 12n), b) same as a), except that the 2D calculations used the MB cooling curve (Model 12n-MB), and c) same as a) except that we started the 2D simulations after the onset of the RSG stage (Model 12n-RSG). Models 12n-MB and 12n-RSG are discussed in the next subsection.

The 2D results of Model 12n for the first RSG stage are shown in Fig. 2.8. A RSG shell forms a a radius of about 1 pc, and develops Rayleigh-Taylor instabilities (cf. Fig. 2.8 in the upper right image), which continue to grow into Rayleigh-Taylor fingers as the shell is evolving (cf. Fig. 2.8 in the lower left and right image). As for Model 8n, the instability

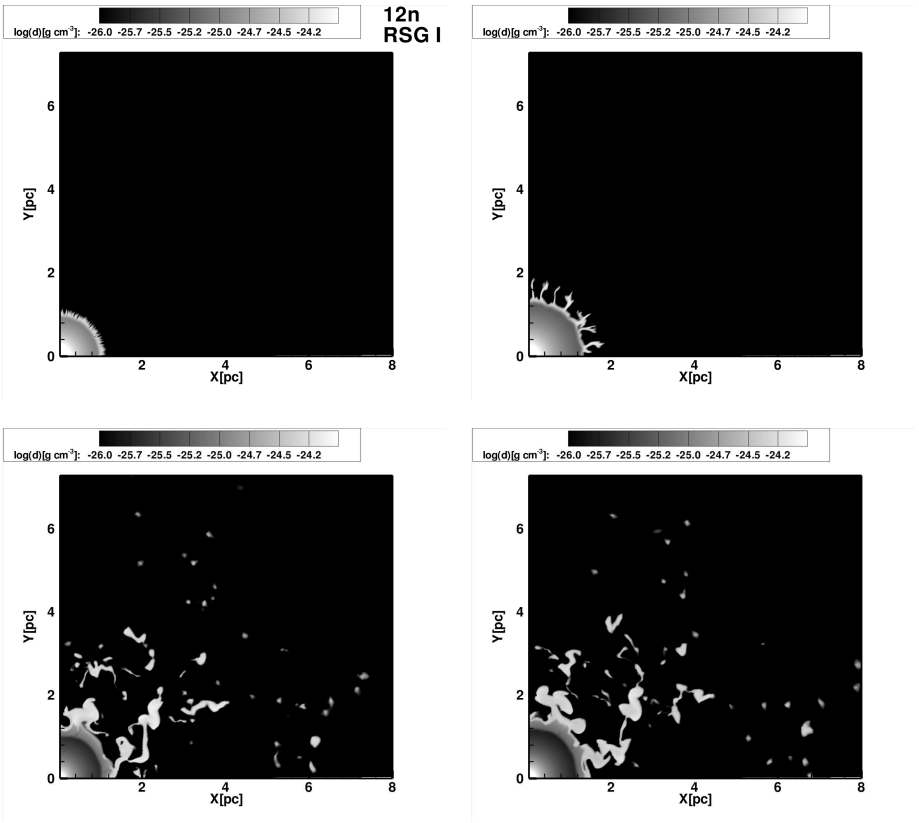

Figure 2.8: Same as Fig. 2.6, for the first red supergiant stage of Model 12n. A red supergiant shell formes at 1 pc, seen in the upper left panel, 0.14 Myrs after the start of the 2D simulations. Rayleigh-Taylor instabilities start to develop and grow in time as seen in the upper right panel taken 0.181 Myr after the onset of the 2D run. The lower left panel, at 0.98 Myr, shows the clump shedding phase of the RSG shell. The lower right panel, at 1.11 Myr, shows the situation before the beginning of the BSG stage.

becomes more violent with time and develops into a clump-shedding stage (lower panels of Fig. 2.8).

After the BSG stage the first RSG shell has been completely wiped out by the fast BSG wind (which has a velocity of about 400 km s^{-1}), whose remnants are distributed throughout the hot bubble. The second RSG shell forms at a distance of about 1 pc from the central star. Rayleigh-Taylor instabilities develop during the first RSG phase. However, due to the short duration of the second RSG phase, the RSG shell does not reach the clump-shedding phase (Fig. 2.9). Therefore, in this case, most of the mass lost during the final RSG phase is still close to or inside the RSG shell by the time the star explodes as a supernova.

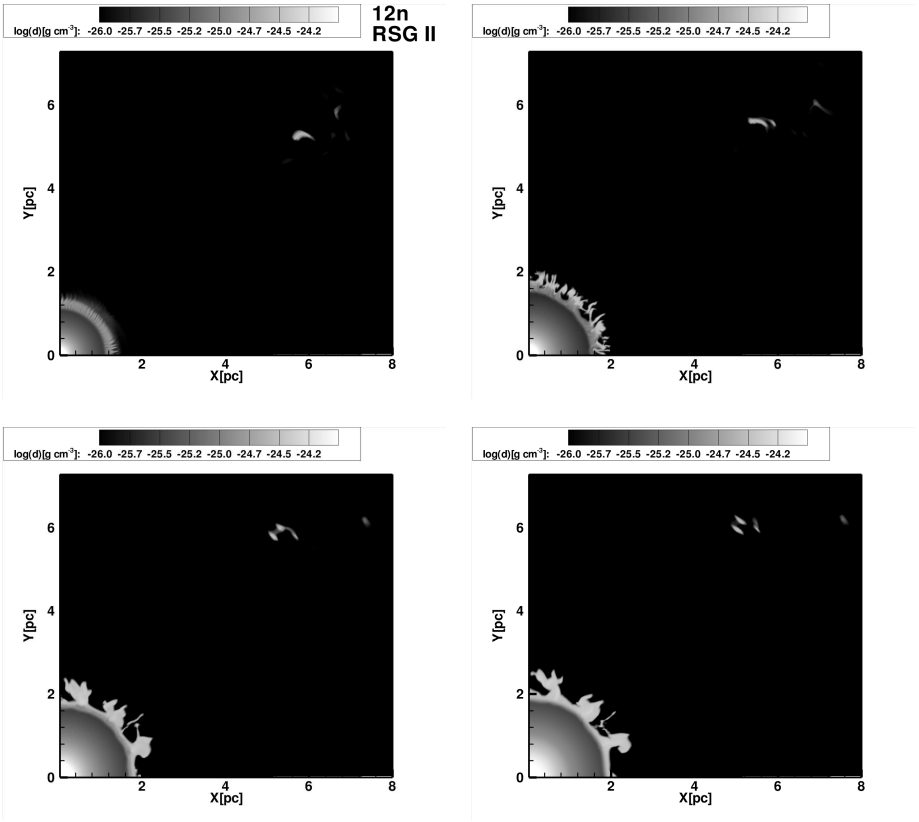

Figure 2.9: Same as Fig. 2.8, but for the second red supergiant stage. The upper left panel is taken 1.71 Myr after the onset of the 2D simulation. Also in this case, the RSG shell is unstable and develops Rayleigh-Taylor instabilities, which have grown in upper right panel at 1.79 Myr. The lower left and right panels show the second RSG shell at 1.87 Myr and 1.98 Myr, the latter corresponding to the pre-supernova stage. This shell does not form any clumps into the hot bubble before the star explodes as supernova.

Model 20n

Model 20n leaves the main sequence after about 7.6 Myr. Shortly before this, we map the 1D result on a 2D grid and simulate the further evolution. During the RSG stage, for over 0.78 Myrs, the terminal wind velocity decreases while the wind mass-loss increases. In Fig. 2.10 we see four time snapshots the inner part of our calculations (8 pc), where the main sequence bubble extends to about 28 pc.

Similar in structure to the previous models, and situated initially at almost 2 pc, a RSG shell forms. Like in the 8 $M_\odot$ and 12 $M_\odot$ cases, the shell becomes Raleigh-Taylor unstable, and the instability becomes more violent with time. The RSG shell settles at a radius of about

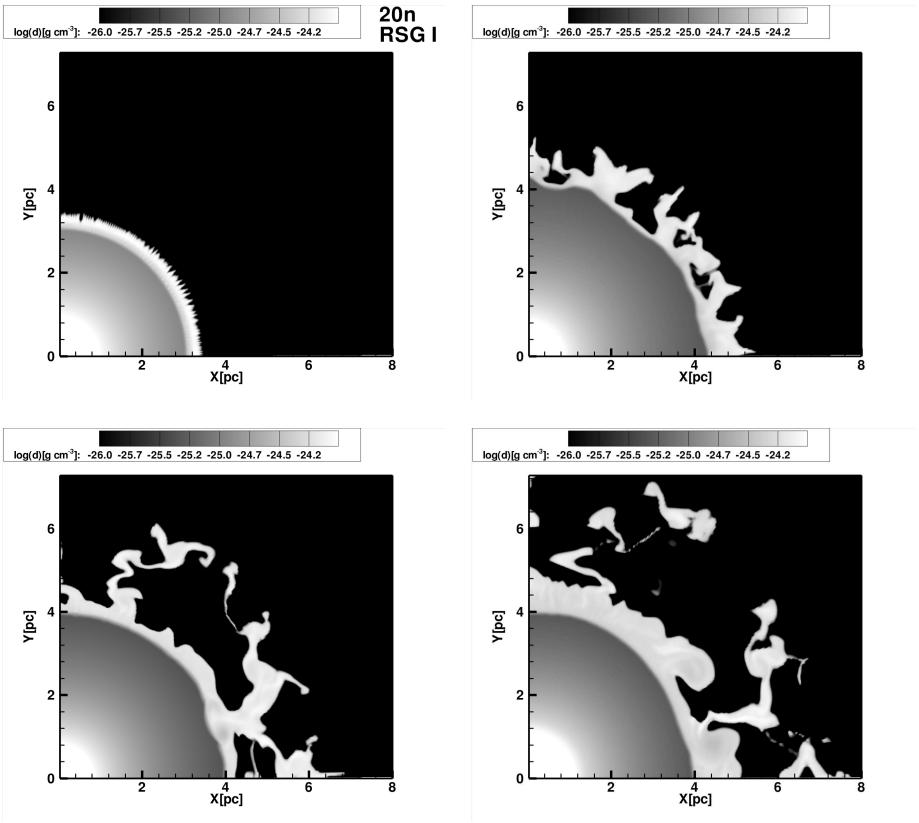

Figure 2.10: Same as Fig. 2.8 but for Model 20n. The upper left snapshot is taken 0.2 Myrs after the beginning of the 2D calculations and shows the early stage of the red supergiant shell at ($\simeq$ 3.5 pc). Rayleigh-Taylor instabilities grow with time as seen in the upper right panel taken at 0.4 Myr. The lower left (at 0.6 Myr) and right (0.8 Myr after the onset of the 2D calculation, corresponding to the pre-supernova stage) panel show the further evolution of the RSG shell.

4 pc for most of the RSG phase. However, unlike in the lower mass cases, the pre-supernova stage is reached soon after the clump-shedding stage has been reached. Consequently, our 20 $M_\odot$ mass model is still surrounded by a massive shell by the time it reaches the supernova stage.

RSG shell instabilities

García-Segura et al. [1996b], modeling the circumstellar medium evolution for a 35 $M_\odot$ star, assumed that their RSG shell was stable. Their 2D computation started only during the RSG stage shortly before the onset of the Wolf-Rayet stage of the corresponding stellar model.

A very different RSG shell structure, based on the same 35 $M_\odot$ model, is shown in Dwarkadas [2007]. In this case, the entire evolution from the beginning of the star's life was computed in 2D. The interior of MS bubble is found to be turbulent, and different then the spherical cavity assumed to be isotropic in García-Segura et al. [1996b]. The RSG shell, formed after the end of MS stage, is found to be Rayleigh-Taylor unstable, although no perturbations were added in the initial conditions of their hydrodynamical simulations.

For our Model 8n, 20n, 12n and 12n-MB, when the high thermal pressure of the hot bubble reaches the high density and low velocity RSG wind, the RSG shell becomes Rayleigh-Taylor unstable. These finger-like instabilities continue to grow until they break into clumps which are shaded into the hot bubble.

For Model 12n-RSG, the RSG shell is stable for a period of 0.376 Myrs as seen in the upper left image of Fig. 2.16. After 0.190 Myrs, the shell which has been stable against the hot bubble medium, starts becoming unstable at the outer edge region. We attribute these instabilities of the inner edge of the thick complex RSG shell structure to the lower temperature of the RSG wind which is streaming with $\rho \sim r^{-2}$ against the higher RSG shell temperature. In the same time, Rayleigh-Taylor instabilities start to develop at the outer edge of the RSG shell. The upper right image and lower left and right images of Fig. 2.16 show the continuous development of the instabilities through the evolution of the RSG shell over a period of 0.9 Myrs until the BSG stage. After the collision with the BSG shell, remnants are seen in the hot bubble medium. The second RSG shell (cf. Fig. 2.17) forms at the point where the ram pressure of the RSG wind equals the thermal pressure of the hot bubble. This shell is unstable with a structure more similar to the second RSG shell of the previous cases. The lower left panel shows the pre-supernova shell at 2.5 pc.

It might be that the instabilities that show up in the RSG shell structure are an effect of the ram pressure versus the thermal pressure. They could occur in the RSG shell as the shell is moving inwards and consecutively outwards, pushed in by the thermal pressure of the hot bubble and pushed out by the RSG wind ram pressure.

Characteristics of the RSG nebulae

Our models show that during the long-lasting RSG phases RSG shells form at a distance from the star where the RSG wind ram pressure — which drops with $1/r^2$ — balances the thermal pressure of the hot main sequence bubble. Once formed, the shell is almost stationary, which is expected since the wind properties during the RSG phase do not change much. For the first RSG stage of Models 8n and 12n, the shells are found at a distance of about 1 pc and 1.5 pc, respectively, while during their final RSG stage, at the time of the supernova, they are slightly further out (1.8 pc and 2 pc). Their thickness is of the order of 0.3 pc, but it is non-uniform due to the strong instabilities. The RSG shell of our 20 $M_\odot$ model develops at a distance of about 4 pc from the central star.

Our 8, 12, and 20 $M_\odot$ model stars lose 0.12 $M_\odot$, 0.35 $M_\odot$ and 4.14 $M_\odot$ during their first RSG stage. In Table 2.3 we have computed which fraction of this ends up in the RSG shell, and how much mass is found in the other two components, the free-streaming RSG wind, and the clumps which are lost from the RSG shell into the hot bubble. Remarkably, the shells around the 8 and 12 $M_\odot$ stars comprise only about 4 % of the total mass lost, while about

Table 2.3: Mass, radius, total ejected mass in the RSG stage $\Delta M_{\rm RSG}$, temperature of the RSG nebula $logT_2$, total luminosity as integrated over a sphere calculated for the red supergiant nebula for Models 8n, 12n, and 20n. The RSG nebula has been approximately divided in 3 main regions: the free streaming wind (1), the RSG shell (2) and the clumps (3). Each of these regions spread over an area (ΔR_1, ΔR_2, ΔR_3) and have a mass (ΔM_1, ΔM_2, ΔM_3). For calculating the mass of these three regions, the density has been integrated over the radius and angle from the last panels of Fig. 2.6, 2.7, 2.8, 2.9 and 2.10. The temperature has been taken as maximum from the nebula region.

Model RSG I	8n	12n	20n	Model RSG II	8n	12n
ΔM_1 ($M_\odot$)	0.001	0.06	0.82	ΔM_1 ($M_\odot$)	0.006	0.05
ΔM_2 ($M_\odot$)	0.005	0.01	1.55	ΔM_2 ($M_\odot$)	0.10	0.03
ΔM_3 ($M_\odot$)	0.10	0.28	1.82	ΔM_3 ($M_\odot$)	0.003	0.06
$\Delta M_{\rm RSG}$ ($M_\odot$)	0.12	0.35	4.14	$\Delta M_{\rm RSG}$ ($M_\odot$)	0.09	0.13
$logT_2$ (K)	4.7	4.8	4.2	$logT_2$ (K)	4.3	4.3
ΔR_1 (pc)	0...0.7	0...1.2	0...4	ΔR_1 (pc)	0...1	0...1.9
ΔR_2 (pc)	0.7...1.1	1.2...1.5	4...5	ΔR_2 (pc)	1...2	1.9...2.1
ΔR_3 (pc)	1.1...6.0	1.5...6.0	5...8	ΔR_3 (pc)	2...3	2.1...3
$L_{\rm 2total}$ (10^{32} erg s^{-1})	0.03	0.26	0.14	$L_{\rm 2total}$ (10^{32} erg s^{-1})	0.01	0.16
$L_{\rm 3total}$ (10^{32} erg s^{-1})	1.11	0.7	7.6	$L_{\rm 3total}$ (10^{32} erg s^{-1})	0.18	0.58

80 % of the mass has been split in the form of clumps into the hot bubble. In their second and final RSG stage, which is shorter and, especially for the 8 $M_\odot$ model, more extreme, the RSG shells contain close to 100 % (for the 8 $M_\odot$ model) and about 23 % (for the 12 $M_\odot$ model) of the total mass lost. This compares to a fraction of about 37 % of the mass retained in the RSG shell of the 20 $M_\odot$ model. In Paper III we analyze the model 10n only for the BSG stage. The properties of the RSG shell, from the point of view of instabilities and mass, are very similar to model 8n and 12n. We would like to mention that during the first and second RSG stage, model 10n accumulates 0.006 $M_\odot$ and 0.05 $M_\odot$ respectively.

We conclude that the fraction of the mass of the RSG shell to the total lost mass is large for massive RSGs. For the 20 $M_\odot$ model, the time scale of the development of the instability of the shell is comparable to the total duration of the RSG stage (780 000 yr); i.e. the first clumps are shed close to the end of the evolution. By contrast, the first 8 $M_\odot$ RSG shell starts shedding clumps after only about 10 % of the duration of the RSG stage have passed. The fraction of the RSG shell mass could have been even larger if the radius of the RSG shell ($\sim$ 4 pc) was smaller, which — together with the short RSG life time — implies that 20 % of the lost mass is still in the free streaming RSG wind by the time the star explodes.

Our results indicate that the fraction of the mass of the RSG shell to the total lost mass is also large for the final stage of RSGs of the lowest mass. This is due to the large increase in the mass loss rate in the very final phase of the life of the RSG (Fig. 2.2), which is a consequence of the final ascent of the red supergiant branch which is more pronounced for lower mass red supergiants. It implies two things. First, much of the mass lost during this (second) RSG phase is blown out very late and thus can not be fragmented any more into the hot bubble. Second, the RSG wind ram pressure increases (despite a slight drop in the wind

velocity), which moves the location of the RSG shell outward such that it sweeps up most of the previously split material, and even some clumps ejected during the first RSG stage.

Due to the shock heating of the RSG wind, the RSG shells of our models have temperatures in the range of several 10^4 K (cf. Table 2.3) and do not cool substantially during the evolution. Fig. 2.12 (left panels) shows the temperature structure of the RSG shell of Model 12n at the end of the first RSG stage, and at the time of the supernova. The right side of Fig. 2.12 shows the corresponding emissivity maps according to the employed cooling curve. It can be seen that the shell itself, as well as the stripped-off clumps, remain at a temperature of the order of 10^4 K, but that gas is eroded of the clumps and mixed into the hot bubble, whereby it is heated to temperatures above 10^5 K. (See appendix for corresponding plots for Models 8n and 20n.)

Table 2.3 shows that the total luminosity emitted by the RSG shells (corresponding to the lower right panels of Figs.2.6, 2.7, 2.8, 2.9 and 2.10) is rather small , i.e. of the order of 0.01 $L_\odot$ or less, which is a few percent of the mechanical luminosity of the RSG winds. More radiation comes from the gas which is eroded off the clumps: For Model 20n, the predicted emission is about 0.2 $L_\odot$.

Discussion

Model uncertainties

The wind mass-loss and wind velocity are important ingredients in the distribution of the circumstellar material around stars. While the winds of main sequence stars are rather well understood and allow accurate quantitative predictions (de Koter [2008]), the dominant mass-loss mechanism for red supergiant stars is not yet identified. The nature of the dominant mass-loss mechanism for stars like red supergiants and massive asymptotic giant branch stars is not clear. Radiation pressure is a possible mechanism but also it might be that the stars are cool enough to have dust-driven winds. The stellar evolution models, which we used for our hydro-calculations, include the empirical mass-loss rate of Nieuwenhuijzen et al. [1990]. Another approach of observed mass-loss rates for massive asymptotic giant branch stars and red supergiants has been recently discussed in van van Loon et al. [2005]. However the uncertainties in the mass loss of RSG stars are still under debate.

The cooling curves implemented consecutively in the code influence the 1D and 2D results. When comparing the MB cooling curve with SM there are several differences. The first difference is the lower limit of the temperature. The MB cooling curve has a lower limit of 100 K, while the SM cooling curve is calculated starting from 10 K. The second, and most important difference, is the fact that between 100 and 10 000 K, the values of the MB cooling curve are extrapolations, while for the SM cooling curve they are the outcome of the detailed models of Smith et al. [2008]. The values for the MB cooling curve between 100 and 10 000 K are calculated by setting λ (cooling function) = 0 at T = 100 K and performing a linear interpolation between this point and the value for λ at T=10 000K. When compared to the SM cooling curve this means that between approximately 1000 and 10 000 K the MB cooling curve overestimates the cooling. Between 100 and 1000 K the MB cooling curve underes-

timates the cooling. For model 12n-MB (Figs. 2.14 and 2.15) the effect of the MB cooling curve is seen in the high density clumps. These features are more compact than the clumps as seen in Fig. 2.8 and 2.9. However the RSG shell distance from the central star is relatively similar for both RSG stages.

The set-up for the outside medium is done by considering a steady environment with a constant density of 20 cm^{-3}. Our models spend most of their life time in the MS stage during which the hot bubble, created during this stage, measures a distance of a few tens of parsecs (12, 20 and 28 pc for Model 8n, 12n and 20n respectively). As described in Sect. 4 and 5, the long-lasting MS stage and the weak wind for Model 8n slows down the MS shell to about the sound speed and to spread out into ISM. By the time the first RSG wind stalls to form a shell, the pressure in the MS hot bubble is equal to the ISM pressure. The hot gas in the Model 12n and 20n has a higher pressure than the ISM and also the MS life time for these models is about half shorter than for Model 8n. We mentioned that previous authors Dwarkadas [2007], found the hot bubble not isotropic but turbulent with density inhomogeneities due to the constant variation of the wind parameters. This medium has implications in the development of the first RSG shell also in our cases. For Models 8n and 12n, when the second RSG wind forms a shell, the hot bubble medium is found again to have fluctuations in density and pressure due to a previous BSG stage. The pressure of the ISM can determine how far the first RSG shell will form in the pressurized hot bubble. If the ISM pressure is high, the hot bubble pressure will be high and so the RSG shell will form close to the central star and vice-versa.

Comparison with observations

Red supergiant shells are not a common observational feature, and one may wonder if they exist in nature at all. It is a major aim of this Paper to predict their properties, so a comparison between theory and observations is possible. As discussed above, our calculations are highly idealized, and whether one expects to find a RSG shell associated with a particular red supergiant depends strongly on its environment. On the other hand, at least the more massive RSGs are rather short lived, and at least a fraction of them can be expected to be found in a high pressure environment, either created by its O star progenitor, or by other massive stars nearby — and a high pressure environment is the only required condition to form a RSG shell.

We have seen that the RSG shells in particular around the lower mass RSGs are expected to be Rayleigh-Taylor unstable. As a consequence, the mass which is accumulated in the RSG shell is largely reduced, which diminishes the chance to observe the shell. The stripped-off clumps, on the other hand, get eroded and can, according to our models, emit considerable amounts of radiation. However, they are geometrically indistinctive, and may be hard to identify in an average situation. Observations for the circumstellar material around IRC+10420 (Humphreys et al. [1997]) and for VY CMa (Smith et al. [2001, 2009]), show a circumstellar environment with filaments, arclike structures and bright clumps. The evidence of these clumped features implies that probably one single mass-loss event occurred (Smith et al. [2001]), but it is still unclear if clumping could be the result of a variation in time of the mass-loss.

The brightest and the closest RSG to us situated at 197 ± 45 pc (Harper et al. [2008]),

is α Ori, or Betelgeuse, and its circumstellar medium properties have been discussed by Noriega-Crespo et al. [1997] and Smith et al. [2009]. Having a mass between $15-20$ $M_\odot$, Betelgeuse is emitting a dusty wind with a mass-loss rate of about $\dot{M} \simeq 2-4\times10^{-6}$ $M_\odot\,yr^{-1}$ and an wind velocity of 17 $km\,s^{-1}$ (Harper et al. [2006]), which is clumpy or inhomogeneous out to scales of about 0.05 pc (Smith et al. [2009]).

Of high relevance to our models is the recent discovery of an ISM-wind bow shock around α Ori, (Noriega-Crespo et al. [1997], Ueta et al. [2008]), which identifies this red supergiant as a runaway star with a velocity relative to its local ISM of 30 $km\,s^{-1}$ (e.g. Ueta et al. [2008]). The interaction of the ISM with the wind of α Ori give rise to a shell in the direction of the motion of the star with in the rest frame of the ISM, at a distance of about 0.5 pc. Noriega-Crespo et al. [1997] estimate the mass of the shell to about $0.14\,M_\odot$, which corresponds to the accumulated mass lost by the star over about 10^5 yr. Ueta et al. [2008] derive a dust temperature for different parts of the shell to be in the range 42...11 K. A further observed associated bar-shaped feature has no explanation so far.

While we can obviously not directly compare our models with the bow shock shell around α Ori, the observations clearly show that in the presence of an outside pressure — here in the form of the ram pressure from the ISM interaction — the RSG wind is piled up in a shell. The observed shell mass indicates a short RSG life time of α Ori of about 10^5 yr (where at the same time, the RSG life time is a lower limit). Alternatively, the shell mass corresponds to the stationary solution for the bow shock, where mass flows in continuously from the star, while mass is continuously leaving the shell downstream, thereby producing a trailing tail. Such a feature has recently been found for the Mira system by Martin et al. [2007], showing a comet-like tail from the AGB star Mira A stretching out 4 pc, interpreted as a ram-pressure stripped tail from the bow shock produced by a space motion of 130 $km\,s^{-1}$ (Wareing et al. [2007]). A transitional object showing a geometry of the circumstellar material that deviates from the spherical symmetry, with multiple gas shells and circumstellar dust lying within 0.008 pc, is HD 179821 (Reddy & Hrivnak [1999], Jura et al. [2001], Patel et al. [2008]). The temperature of the circumstellar dust shell is 130 K (Hrivnak et al. [1989], van der Veen et al. [1989]) with no warm dust component. Assuming that the central star lies within 6 kpc, Kastner & Weintraub [1995] calculated a dynamical lifetime of 5000 yr for the circumstellar envelope with ≈ 5 $M_\odot$ of gas and dust.

Summary and conclusions

We have described in this Paper the evolution of the circumstellar material around stars with initial masses of 8, 12 $M_\odot$ and 20 $M_\odot$. All three models show that distinct stellar stages with time dependent wind mass loss and terminal wind velocity, have an impact on the nebular properties. In the long lasting RSG phases wind material stalls where the ram pressure of the RSG wind equals the thermal pressure of the hot bubble. The RSG shells develop violent Rayleigh-Taylor instabilities, which occur at the contact discontinuity between the RSG shell and the hot shocked main sequence wind material. Once these instabilities evolve in time, the structure of the RSG shell begins to break out and clumpy structures start to float and mix around inside the hot bubble medium. Our 8 and 12 $M_\odot$ models evolve from a first

RSG stage to the blue supergiant stage, and during this stage the RSG shells are completely destroyed, while in the second turn to the RSG stage, these models build up new and more massive shells.

In our models, during their first long lasting RSG stage, the RSG shell forms at a distances ranging from about 1 to 4 pc. The shell masses deducted from our hydro-calculations vary between 0.005 $M_\odot$, 0.01 $M_\odot$ and 1.55 $M_\odot$ which represents a large fraction from the total mass lost during the RSG stage. The mechanism that triggers the Rayleigh-Taylor instabilities in the RSG shell, has a violent impact on the shell's structure and initially fingers of RSG shell material split into clumps which comprise most of the mass ejected during this stage. The temperatures of the RSG shells is maintained to a value of several 10^4 K, while the luminosity of the shells is of the order of $0.2\,L_\odot$. The clumps are eroded away by the the gas from the hot bubble and during this process a large amount of radiation can be emitted.

Second, recent observations of a bow shock shell around α Ori show that the RSG wind has been piled up against the ram pressure from the ISM interaction. While the density of the RSG shell is a few times lower then the ISM density, the discovery of the bow shocks may relate to the possibility of RSG shells as been observable.

The circumstellar material around low and high mass RSGs, is of high importance to understand the bipolar emission nebulae around BSGs and can also affect the supernova evolution.

Additional information

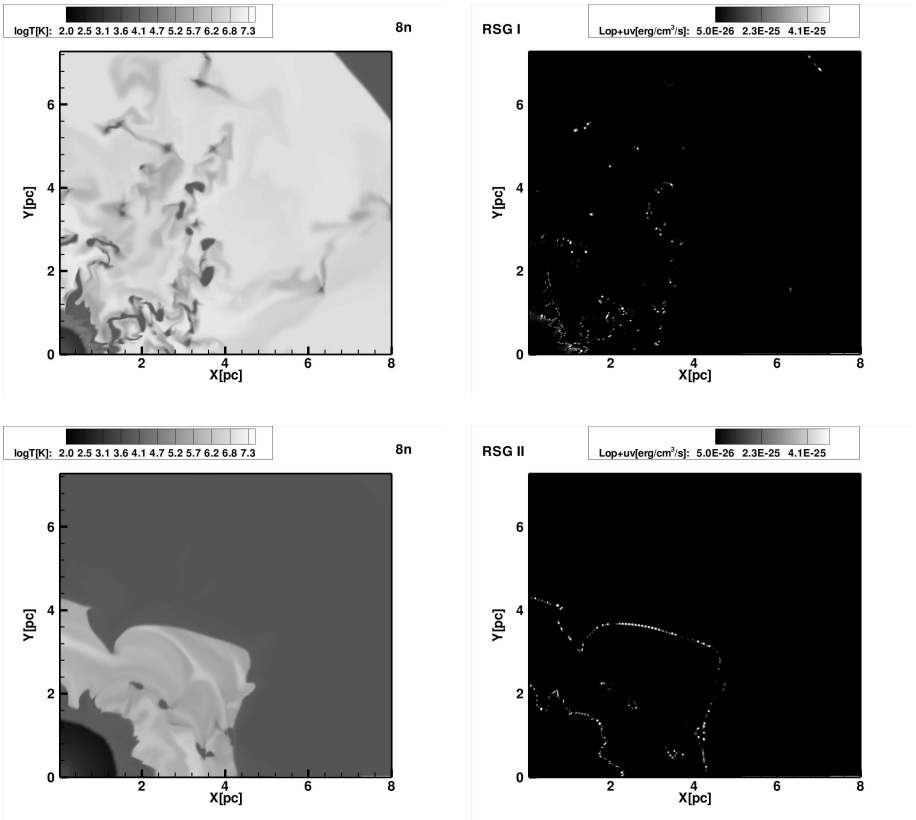

Figure 2.11: Temperature and emissivity as for a circumstellar gas with $10^4 < T < 10^6$ K, emission calculated according to the cooling curve implemented in our hydrodynamical code, for the 8n model with the first RSG stage in the upper panels and the second RSG stage in the lower panels. The time snapshot chosen in the upper panel of this ilustration corresponds to the last panel of Fig. 2.6 and the second panel corresponds to the last panel of Fig. 2.7. The RSG wind nebula is visible before the onset of BSG wind at 1 pc, the second RSG stage gives us a nebula at 2 pc which will interact with the supernova ejecta.

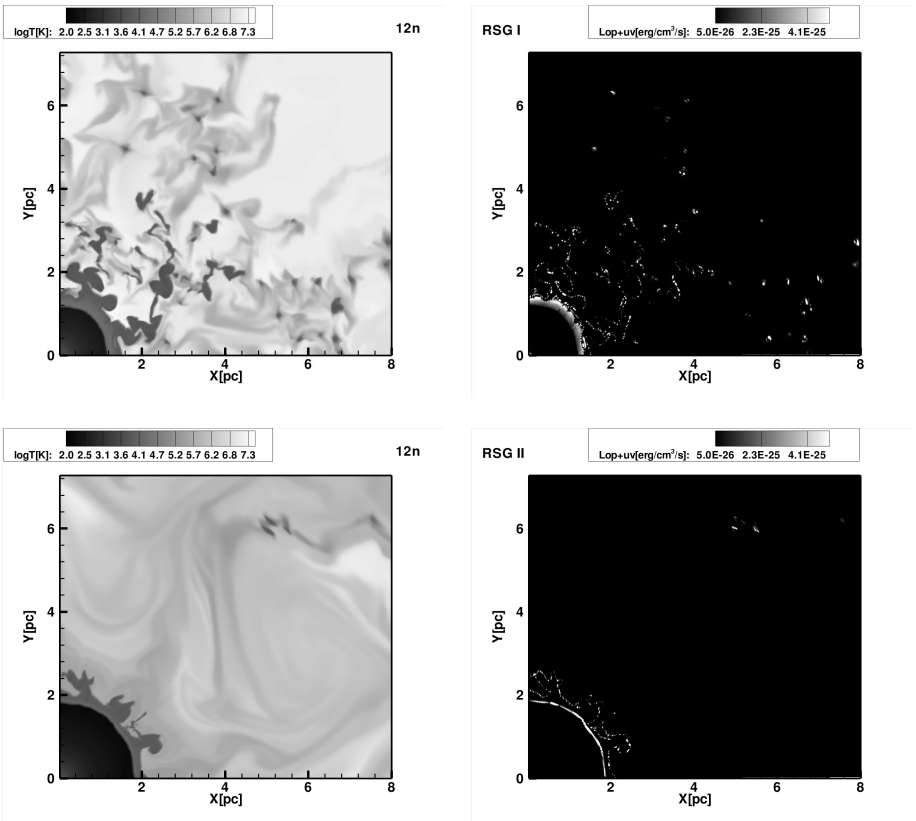

Figure 2.12: Same as Fig. 2.11 but for the 12n model with the first RSG stage in the upper panels and the second RSG stage in the lower panels. The time snapshot chosen in the upper panel of this ilustration corresponds to the last panel of Fig. 2.8 and the second panel corresponds to the last panel of Fig. 2.9. The RSG wind nebula is visible before the onset of BSG wind at 1 pc, the second RSG stage gives us a nebula at 2 pc which will interact with the supernova ejecta.

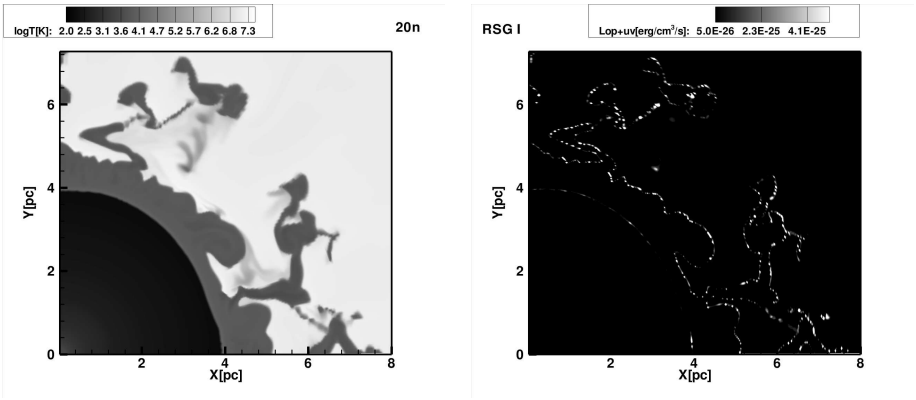

Figure 2.13: Temperature and density emissivity as for a circumstellar gas with $10^4 < T < 10^6$ K, for the 20n model with the RSG time snapshot chosen corresponding to the last panel of Fig. 2.10. The RSG wind nebula is visible before the supernova ejecta at 4 pc.

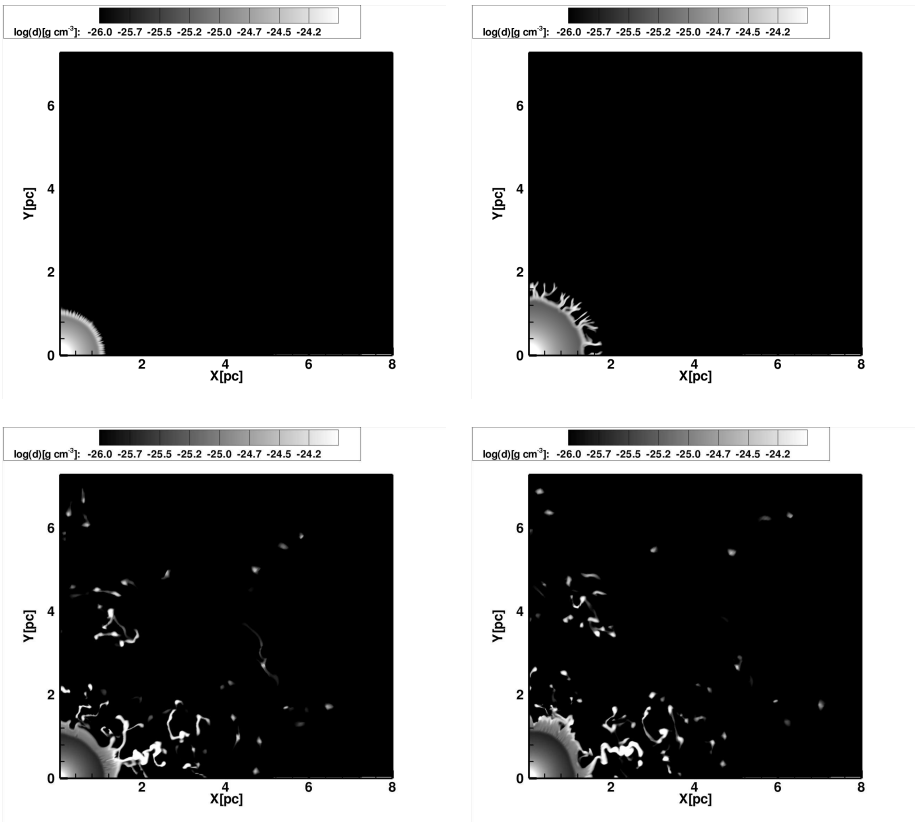

Figure 2.14: Model 12n-MB (see text for details) for the first red supergiant stage. The time frame is the same as in the Fig. 2.8.

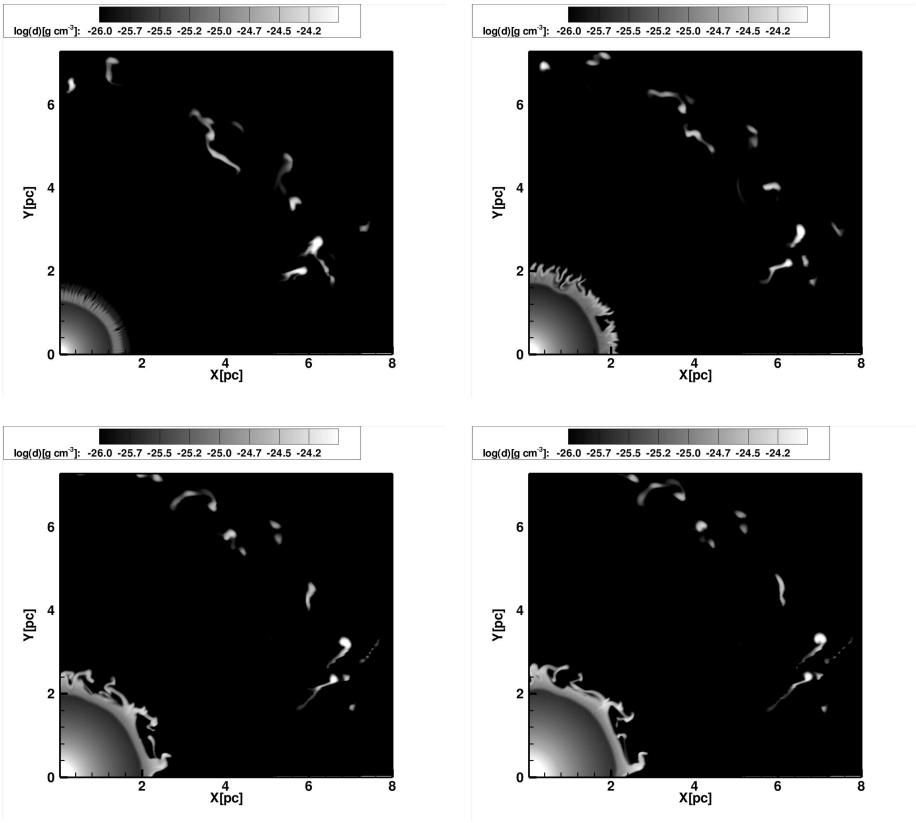

Figure 2.15: Model 12n-MB for the second red supergiant stage. The time frame is the same as in the Fig. 2.9.

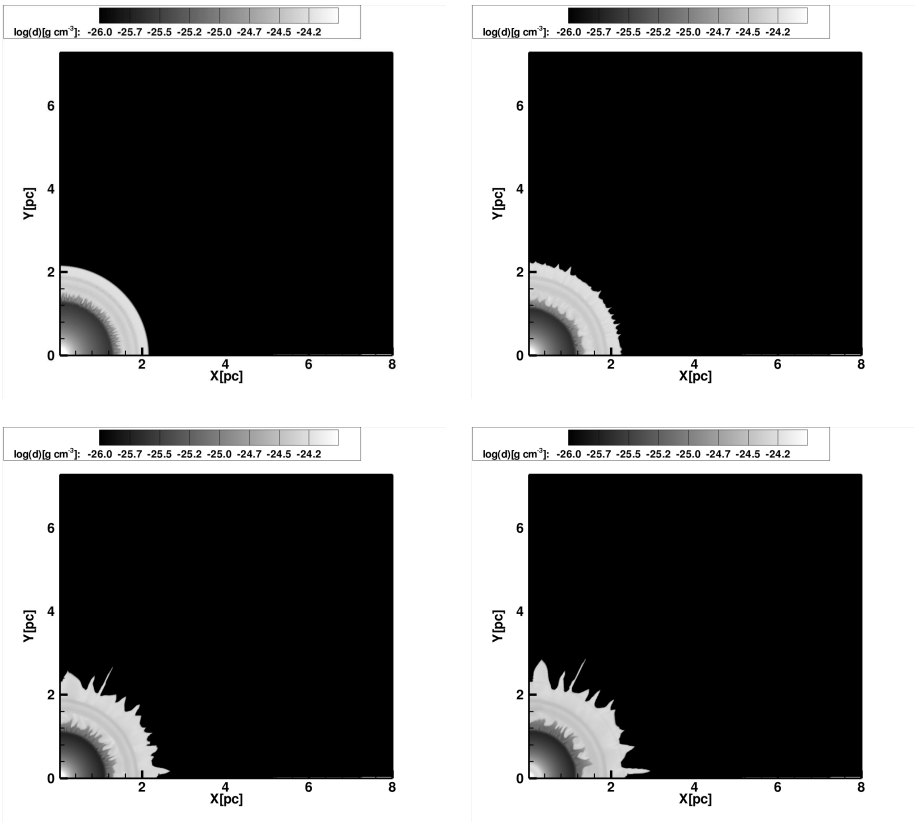

Figure 2.16: Model 12n-RSG (see text for details) for the first red supergiant stage simulation started at the beginning of the RSG stage. The left upper frame is taken 0.3767 Myrs from the start of the 2D simulations. The upper right frame is taken 0.190 Myrs later. The lower frames are depicted 0.381 Myrs and 0.575 Myrs respectively, after the upper left frame.

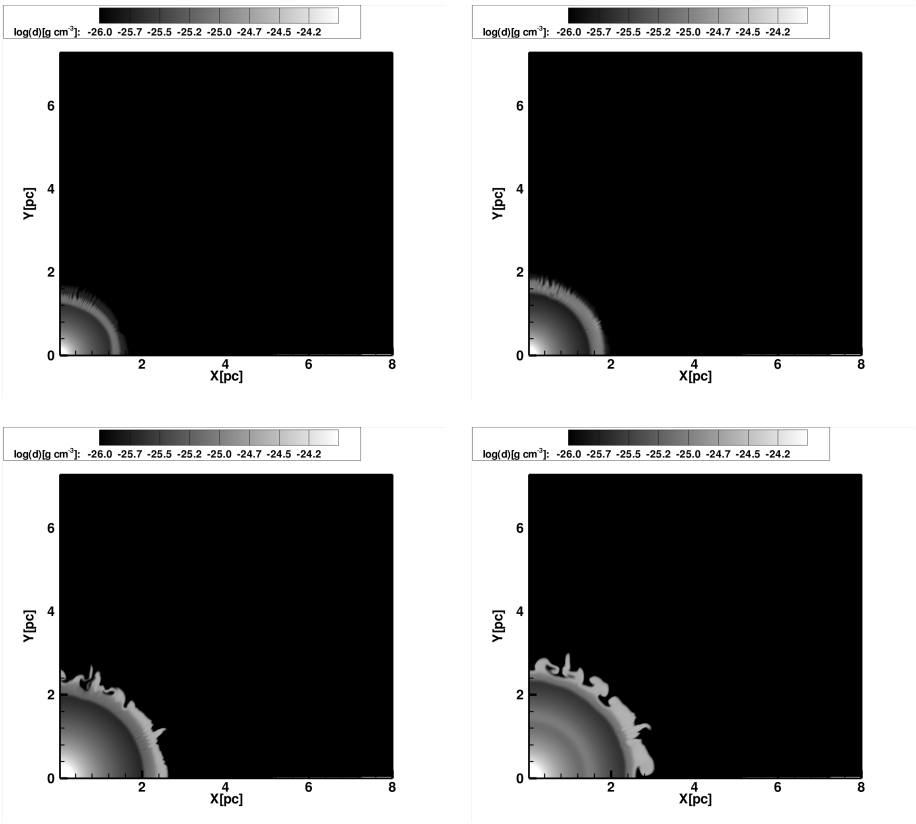

Figure 2.17: Model 12n-RSG for the second red supergiant stage simulation started at the beginning of the RSG stage. The upper left frame is depicted 1.670 Myrs after the start of our 2D simulations. The upper right frame is taken 0.039 yrs later. The lower left frame is taken 0.114 yrs later. The lower right frame is captured before the supernova explosion.

Chapter 3

Multiple ring nebulae around blue supergiants

based on S.M. Chiţă, N. Langer, A. J. van Marle, G. García-Segura, A. Heger 2008, A&A, 488, L37

Abstract

In the course of the life of a massive star, wind-wind interaction can give rise to the formation of circumstellar nebulae which are both predicted and observed in the nature. We present generic model calculations to predict the properties of such nebulae for blue supergiants. From stellar evolution calculations including rotation, we obtain the time dependence of the stellar wind properties and of the stellar radiation field. These are used as input for hydro-calculations of the circumstellar medium throughout the star's life. Here, we present the results for a rapidly rotating $12\,M_{\odot}$ single star. This star undergoes a blue loop during its post main sequence evolution, at the onset of which its contraction spins it up close to critical rotation. Due to the consequent anisotropic mass loss, the blue supergiant wind sweeps up the preceding slow wind into an hour glass structure. Its collision with the previously formed spherical red supergiant wind shell forms a short-lived luminous nebula consisting of two polar caps and a central inner ring. With time, the polar caps evolve into mid-latitude rings which gradually move toward the equatorial plane while the central ring is fading. These structures are reminiscent to the observed nebulae around the blue supergiant Sher 25 and the progenitor of SN 1987A. The simple model of an hour glass colliding with a spherical shell retrieves most of the intriguing nebula geometries discovered around blue supergiants, and suggests them to form an evolutionary sequence. Our results indicate that binarity is not required to obtain them.

Introduction

During the course of their evolution, massive stars have strong winds which eject matter into their surroundings. During their post-main sequence evolution, these stars can move back and forth from the blue to the red side of the Hertzsprung-Russell (HR) diagram and back to the red, with little time spent at intermediate effective temperatures (Langer [1991b]).

Table 3.1: Ejected mass (ΔM), momentum (Δp) and kinetic energy (ΔE) during the various evolutionary phases of our stellar model. The evolutionary phase is identified in the first column: main sequence phase (MS), first red supergiant phase (RSGI), phase of rapid rotation (RR), blue supergiant stage (BSG), and second red supergiant phase (RSGII). The approximate duration of each phase is given in the second column.

Phase	Δt	ΔM	Δp	ΔE
	10^3 yr	$M_\odot$	10^{38} g cm s^{-1}	10^{45} erg
MS	19200	0.43	396	1480
RSG I	825	0.33	71	38
RR	25	0.02	7.2	6.0
BSG	550	0.11	52	68
RSG II	225	0.13	25	12

Hydrodynamic considerations imply that each such transition does produce a circumstellar shell: When the star moves from the blue to the red side of the HR diagram, the slow red supergiant (RSG) wind will be stalled by the high pressure of the previously created hot wind bubble, and will accumulate into a shell at the location where this pressure equals the RSG wind ram pressure (García-Segura et al. [1996b]). We call such a more or less stationary shell the RSG shell. When the star moves from the red to the blue side of the HR diagram, the wind speed increases and the blue supergiant (BSG) wind plows up the preceding RSG wind into a rapidly expanding shell, which we call the BSG shell.

Consequently, we expect a spectacular circumstellar phenomenon for stars undergoing so called blue loops, namely that it triggers the formation of an expanding BSG shell, which will at some point smash into the previously formed stationary RSG shell. While both, the RSG and the BSG shell by itself, may be difficult to observe, their violent interaction may release enough energy to provide an observable nebula.

Despite this simple and intriguing expectation, there are so far only few attempts to obtain quantitative prediction for the outcome of the described shell interaction (see Blondin & Lundqvist [1993], Martin et al. [1995], Podsiadlowski et al. [2005]). Within an effort to describe this phenomenon through generic calculations, which use detailed stellar evolution models as input for the circumstellar hydrodynamic modeling ([Chiţă et al. 2010b]), we focus here on the results for a rotating 12 $M_\odot$ single star.

Computational method

As input for our circumstellar hydrodynamic calculations, we use the results of a stellar evolution calculation for a star of 12 $M_\odot$ and a metallicity of $Z = 0.02$. Specifically, we utilize Model F12B from Heger & Langer [2000b], which has an initial rotational velocity of 328 km s^{-1}. The code used to compute this model includes OPAL opacities, detailed nuclear networks, mass loss according to Nieuwenhuijzen et al. [1990], the physics of rotation for the stellar interior, and rotationally modulated stellar winds, as described in Heger et al. [2000a].

The evolution of the stellar model in the HR diagram is show in Fig. 3.3. At core-H

exhaustion, it moves to the RSG regime where it remains for 825 000 yrs (~60 % of the core-He burning life time), before it undergoes a blue loop. It then stays in the BSG regime of the HR diagram for the remaining part of core helium burning, before it moves back to the RSG regime where it explodes as a Type II supernova.

As shown by Heger & Langer [1998], as the convective envelope retreats during the onset of the blue loop, all its angular momentum is concentrated in a small amount of mass in the top layers of the star by the time convection vanishes. Blue loops therefore provide a natural way to bring the stellar surface to close to critical rotation. This does also happen in our chosen stellar model (Fig. 3.4). The limit of critical rotation is reached during the red-blue transition, which produces a brief period of strong, slow and anisotropic mass loss (Table 1). The strong mass loss then reduces the rotation rate of the stellar surface (Langer [1998]), and the star settles at a rotation velocity of about 50 km s^{-1} in the BSG regime.

To simulate the evolution of the circumstellar matter (CSM) we use the ZEUS 3D code developed by Stone et al. [1992] and Clark [1996]. ZEUS 3D is an explicit non-conservative code that solves the hydrodynamical equations as partial, finite difference equations on a fixed, staggered mesh grid. Radiatively optically-thin cooling is included by solving the energy equation implicitly according to Mac Low et al. [1989], and by using the plasma cooling curve of MacDonald et al. [1981]. We compute the evolution of the CSM during the main sequence and the early RSG stage in 1D, with 4500 grid points over a radius of 45 pc, and we assume an interstellar medium density of 1 cm^{-3}. After 100 000 yr into the first RSG stage, we map the 1D model onto a 2D spherical grid to compute its further evolution. The inflow inner boundary condition is applied at 0.025 pc, and the outer boundary remained at 45 pc. The radial component of the grid is resolved with 1000 grid points, where 900 grid points are used for the inner 5 pc, and 100 grid points for the outer 40 pc. The angular coordinate of 90 degrees is resolved with 200 grid points. The method used here was applied before by García-Segura et al. [1996,a,b] and van Marle et al. [2005, 2007].

We are using the time dependent mass loss rate and the terminal wind speed from the stellar evolution model as input in our central mesh point for the hydrodynamic calculations. The wind speed is obtained from the stellar escape velocity using the scaling proposed by Eldridge et al. [2006]. The wind anisotropy is described using the equations of Bjorkman & Casinelli [1993], as in Langer et al. [1999]. For near-critically rotating stars, this provides a slow and dense equatorial outflow, and a fast wind in polar directions. We note that while the Bjorkman-Cassinelli mechanism has been criticized in the context of line driven winds (Owocki et al. [1996]), it is unclear whether line driving does play a major role in the situation of near-critical rotation.

The effect of photoionization was included in the simulations by calculating the Strömgren radius along each radial grid line as described in García-Segura et al. [1999] and van Marle et al. [2005, 2007, 2008]. The number of ionizing photons is computed according to the effective temperatures and surface gravities of the stellar evolution model, by interpolating in a grid of model atmospheres for massive OB stars of solar metallicity computed with the FASTWIND non-LTE code (Puls et al. [2005]) as described in Lefever et al. [2007].

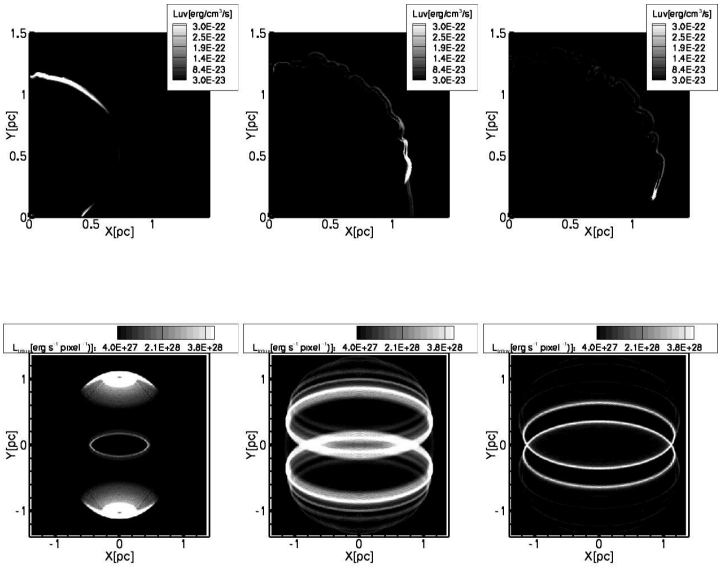

Figure 3.1: Emission structures from our 2D hydro simulation, for the same moments in time as panels 2 to 4 of Fig3.6, i.e., 9000 yr, 15 000 yr, and 18 000 yr after the onset of the BSG wind. **Upper panel**: Emissivity of the gas with $10^4 < T < 10^6$ K, in the simulation plane. **Lower panel**: Projections of the 3D emission obtained by assuming rotational symmetry of the 2D structures of the upper panel, viewed with an inclination angle of 60°, constructed with a resolution of 400×400 pixels.

Results

During its main sequence phase our 12 $M_\odot$ star creates a hot bubble in the interstellar medium which, at core hydrogen exhaustion, is characterized by a radius of 30 pc and an internal energy density of 10^{-12} erg cm^{-3}. Once the star has become a RSG, a slow ($\sim$ 50 km s^{-1}), dense and isotropic wind is injected into the computational domain (Fig. 3.4). This RSG wind accumulates at a distance of $\sim$ 1.5 pc where its ram pressure is balanced by the hot bubble pressure, and forms a RSG shell (cf. García-Segura et al. [1996b]). At the end of the first RSG phase, this shell contains about 0.26 $M_\odot$. It is rather extended ($\Delta r \simeq 1$ pc), and its central parts have condensed due to cooling.

At the onset of the blue loop, the central star reaches close-to-critical rotation, and ejects a dense equatorial disk (Heger & Langer [1998]). While mass and time scales differ, this phenomenon occurs quite analogous to the simulation of the outburst of η Carinae by Langer et al. [1999]. Like in this case, the ensuing BSG wind sweeps up the preceding slow wind material into an "hour glass" structure (Fig. 3.6). On a time scale of a few 10^4 yr, this hour glass expands into the sphere defined by the RSG shell, with a maximum velocity of $\sim$130 km s^{-1} (Fig. 3.5). The faster polar parts of the hour glass hit the inner edge of the RSG shell first.

The collision creates a hot ($T \simeq 10^5$ K) and dense ($n \simeq 10\,\mathrm{cm}^{-3}$) pair of polar caps. As time proceeds, the collision zone moves to lower latitudes of the RSG shell and becomes more confined in latitude. At the same time, the interaction of the BSG wind with the equatorial disk defines a second, ring shaped collision zone in the equatorial plane, which expands with time with a velocity of 18 $\mathrm{km\,s}^{-1}$.

Figure 3.1 shows snapshots of the emissivity map, according to the employed cooling curve in our hydro simulations, for three slices in time, along with projection maps constructed from rotationally symmetric 3D-structures obtained from the 2D maps. Here, only emission from gas in the temperature range between 10^4 K and 10^6 K is considered, which is the dominant component. Hotter gas, which is formed from the reverse shock of the collision, might be observable in the X-ray regime; the peak luminosity of this component in our model is $10^{33}\,\mathrm{erg\,s}^{-1}$, which is achieved about 50 000 yr after the onset of the collision. At an early interaction stage, the radiation is dominated by two polar caps and one equatorial ring, later on by two mid-latitude rings and one fading smaller equatorial ring, and finally two mid-latitude rings at rather low latitude are visible. Those two rings gradually move to the equatorial plane while fading.

The energy budget for the collision of the polar caps of the hour glass with the RSG shell follows directly from the stellar properties. The polar caps have an emissivity of $l \simeq 10^{-21}\,\mathrm{erg\,cm}^{-3}\,\mathrm{s}^{-1}$ in a volume of $V \simeq 4\pi r^2 \Delta r = 4 \times 10^{54}\,\mathrm{cm}^3$ (with $r = 0.5$ pc and $\Delta r = 0.04$ pc; see Figure 3.1). Thus, they shine with a total luminosity of $4 \times 10^{33}\,\mathrm{erg\,s}^{-1}$, i.e. roughly one solar luminosity, with a time scale of $\tau_{\mathrm{rad}} = l/u \simeq 9000$ yr, where $u = \frac{3}{2}nkT$ is the internal energy of the gas, and $T \simeq 10^5$ K and $n \simeq 13\,\mathrm{cm}^{-3}$ (corresponding to $\rho \simeq 10^{-23}\,\mathrm{g\,cm}^{-3}$; Fig. 3.6). The total radiated energy of the polar caps is about $E_{\mathrm{rad}} \simeq \tau_{\mathrm{rad}} L \simeq 10^{45}$ erg. This corresponds well to the kinetic energy release due to the braking of the polar caps, which reach their maximum velocity of $v \simeq 130\,\mathrm{km\,s}^{-1}$ at the time of collision, where it is reduced to $v \simeq 50\,\mathrm{km\,s}^{-1}$ (Fig. 3.5). That is, $\Delta E_{\mathrm{kin}} = \frac{1}{2}\Delta M \Delta v^2 \simeq 8 \times 10^{44}$ erg, with $\Delta M \simeq 1.2 \times 10^{-2}\,\mathrm{M}_\odot$ and $\Delta v \simeq 80\,\mathrm{km\,s}^{-1}$. This kinetic energy can be compared with the BSG wind kinetic energy, which, for $\dot{M} \simeq 10^{-6.8}\,\mathrm{M}_\odot\,\mathrm{yr}^{-1}$ and $v_{\mathrm{wind}} \simeq 300\,\mathrm{km\,s}^{-1}$ (Fig. 3.4), yields $\sim 1.2 \times 10^{45}$ erg over a time period of 9000 yr. Thus, the polar caps shine because the hour glass shaped BSG shell collides with the spherical RSG shell.

A similar consideration could be made for the inner ring, which is produced by the collision of the BSG wind with the equatorial disk ejected by the central star during the phase of near critical rotation. The disk properties depend on the wind properties of the star during this phase. However, in particular their latitude dependence, can not be expected to be reliably predicted within the current assumptions. The total mass of the disk is determined by the mass loss of the star at critical rotation.

Discussion

Figure 3.2 illustrates a simplified picture of the formation of multiple ring nebulae, according to our model. It contains two kinematic components: a stationary, spherical RSG shell and an expanding hour glass structure. The strongly emitting parts of the structure are the collision surfaces. We believe that both kinematic components are realized by nature in the circum-

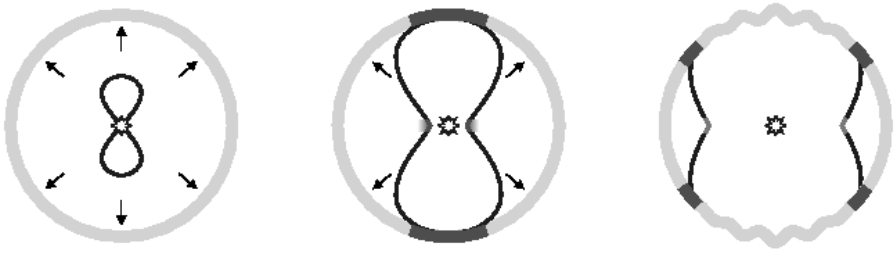

Figure 3.2: Schematic representation of the interaction of the hour glass shaped BSG shell with the RSG shell. The collision regions form the brightest parts of the nebula.

stellar medium of massive stars. RSG shells are unambiguously predicted (García-Segura et al. [2007]) and while they are not yet observationally confirmed, there seems to be no way to avoid their formation. Expanding hour glass structures, on the other hand, are a well documented feature in circumstellar nebulae of low and high mass stars (Nota et al. [1995], Langer et al. [1999]) and are thought to be confined by a circumstellar disk in the equatorial plane of the central star.

A number of predictions emerge from this simple model. First, the collision starts about 10^4 yr after the onset of the blue loop. This timing is set by the expansion speed of the BSG shell and the radius of the RSG shell. Second, the life time of the nebula is determined by the duration of the collision phase, as the emission time scale is shorter than that. In our example, this is about 10^4 yr, or about 1% of the core helium burning life time. This provides an upper limit to the expected number of triple ring nebulae. Third, the rotation rate of the central star during the collision is high for a BSG, since it just about recovers from critical rotation. At the time of maximum brightness of the nebula, the equatorial rotation rate of our central star is about $80\,\mathrm{km\,s^{-1}}$ (Fig. 3.4). Fourth, as all the material in the nebula is ejected after the first dredge-up phase of the central star, the nebula material is nitrogen-rich, here enhanced by a factor of 6.5, and carbon and oxygen depleted by factors of 6.5 and 1.5, respectively. We note that the level of N-enrichment predicted by current stellar evolution models is quite uncertain (see Hunter et al. [2008]), but a RSG phase is still expected to produce some nitrogen enhancement. Due to the assumptions of efficient rotational mixing (Heger & Langer [2000b]), the star and nebula in our model are more enriched than expected from non-rotating stellar models. Fifth, one ingredient of our simple model, namely the RSG shell, is expected for massive stars, but not so for low mass star which produce planetary nebulae. Therefore, while quite analogous expanding hour glass structures are observed for both cases (Langer [2000]), multiple ring nebulae formed through the collision process shown in Fig. 3.2 are expected around massive stars, but not as planetary nebulae. In this sense, the polar caps observed around the blue supergiant Sher 25 might be considered as the first indirect empirical confirmation of a RSG shell.

Previous models of multiple ring nebulae were mostly constructed in the context of the

triple-ring structure observed around SN 1987A (Burrows et al. [1995], Crotts & Heathcote [2000]). While single star models often fail to explain important features (e.g. Martin et al. [1995], Meyer et al. [1997], Woosley et al. [1997]), many invoke rather complex binary phenomena (e.g. Podsiadlowski et al. [1991], Blondin & Lundqvist [1993], Lloyd et al. [1995], Podsiadlowski et al. [2005]). Whereas we do not attempt to reproduce the circumstellar medium of SN 1987A, a single star approach with suitable choices for the major parameters in our model (initial mass, initial rotation rate, metallicity) appears promising and will be pursued in the near future. The current failure of single star models to produce suitable blue loops and blue supergiant pre-supernova models may have to do more with missing physics in stellar evolution models rather than supporting the evidence for a binary progenitor of SN 1987A (Woosley et al. [1997]).

Various multiple ring nebulae around blue supergiants have been observed in the last 20 years (Smith et al. [2007b]). While our generic numerical model was not designed to correspond to any of them, many of the general properties of these nebulae are well reproduced. Most striking is the agreement of the emission geometries. While the nebula around the B1.5 Ia supergiant Sher 25 shows two polar caps and one equatorial ring (e.g. Brandner et al. [1997]) and the other objects discussed by Smith et al. [2007b] rather show narrow rings, including the "twin" of the SN 1987A nebula around HD 168625 (see Smith et al. [2007a]) all these structure occur as an evolutionary sequence in our model. Expansion velocities of the inner ring ($\sim 18\,\mathrm{km\,s^{-1}}$) and the outer collision products ($\sim 50\,\mathrm{km\,s^{-1}}$), the spatial scale of about 1 pc, and the kinematic nebula age agree rather well with empirical values. The rotation velocity of our stellar model fits well to the derived value of $\sim 70\,\mathrm{km\,s^{-1}}$ for Sher 25 (e.g. Hendry et al. [2008]). Central star and nebula of our model are nitrogen enriched, as are most of the observed nebulae.

We note that the emission in our model is caused by compressional heating, which may be in conflict with evidence for photoionization being the dominant process in some observed multiple ring nebulae (see Smith et al. [2007b]). And indeed, looking at the density distributions shown in Fig. 3.6, which might resemble emission geometries in the pure photoionization case, the situation appears more complex. In our simulation, the thick RSG shell ($\Delta r \simeq r \simeq 1\,\mathrm{pc}$) collapses in two parts (at $r \simeq 1.2$ pc and $r \simeq 1.7$) due to a cooling instability. However, this collapse is questionable since it requires a long timescale — our shell has an age of close to 10^6 yr, while in many cases the shell will be much younger at the time of collision —, and since the employed cooling function is uncertain for temperatures below 10 000 K. Without this collapse, its density would be only about $2 \times 10^{-25}\,\mathrm{g\,cm^{-3}}$ (or 0.1 particles/cm^3), which may render it unobservable even if it were photoionized. However, even in the case of the collapsed RSG shell as in our simulation, the collision leads to a clear density enhancement. In panel 2 of Fig. 3.6, we see that in our model, the density enhancement in the polar caps is about a factor 5. This is to be considered a lower limit, as higher resolution models might approach the theoretically expected enhancement factor of about 100, which follows from the (well realized) isothermal shock approximation and a Mach number of about 10. The lower panels of Fig. 3.6 show that in order to represent the rings of SN 1987A, further refinements are required, which, as we think, might be achieved by altering the properties of the RSG shell. For this particular case, this may indeed be justified, as the life time of the final RSG stage of the progenitor of SN 1987A might have been

quite short (e.g. Woosley [1988], Langer [1991a]).

Despite that our model does not fit any of the observed cases in detail, the approximate agreement with most general properties of this class of objects encourages to produce tailored models for individual nebulae as next step. Our results indicate that stars with multiple ring nebulae might just have left the RSG branch — as stellar evolution models argued for the case of SN 1987A (e.g. Woosley [1988], Langer [1991a])and furthermore, that binarity may not be required to obtain multiple ring emission geometries.

Additional information

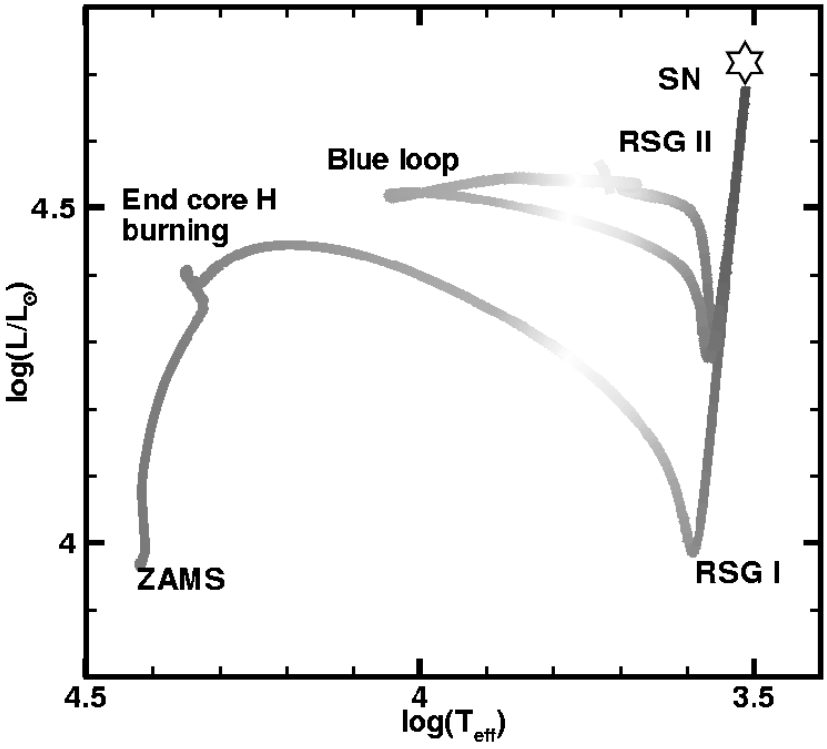

Figure 3.3: Evolution of our rotating 12 $M_\odot$ stellar evolution model in the Hertzsprung-Russell diagram, from the zero age main sequence to the pre-supernova stage. The initial metallicity of the model is $Z = 0.02$, and the initial equatorial rotation velocity is 328 km s^{-1}.

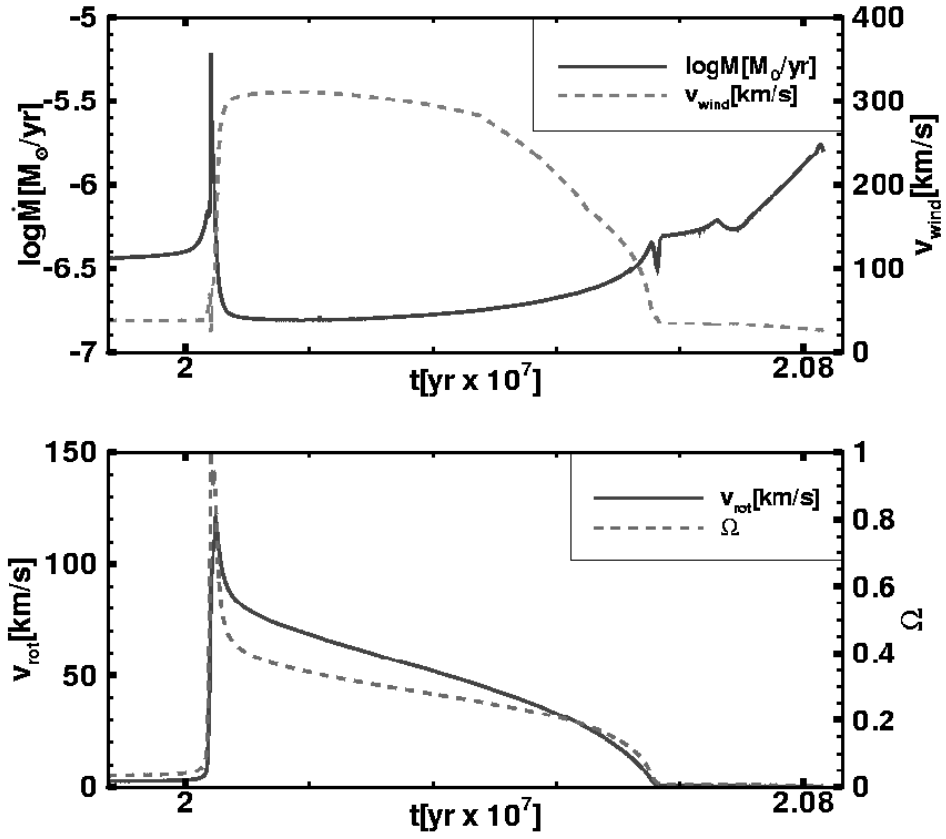

Figure 3.4: Time dependence of various quantities of the employed 12 $M_\odot$ model, for about the final one million before core collapse. The upper panel shows stellar mass loss rate and terminal wind velocity. The lower panel depicts stellar rotational velocity, and the ratio of stellar and critical rotation rate, Ω.

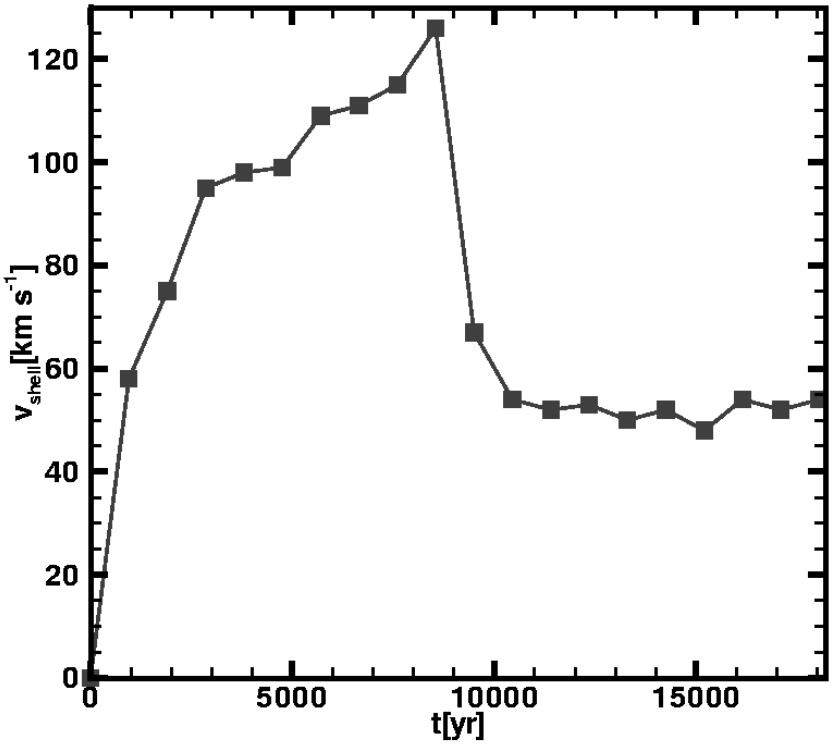

Figure 3.5: Blue supergiant shell velocity, covering a timespan of 18 000 yrs, from its formation ($t = 0$), until its collision with the red supergiant shell. The time between two squares corresponds to 950 yrs. The time zero point corresponds to ~ 9000 yrs before the time of the first snapshot in Fig.3.1.

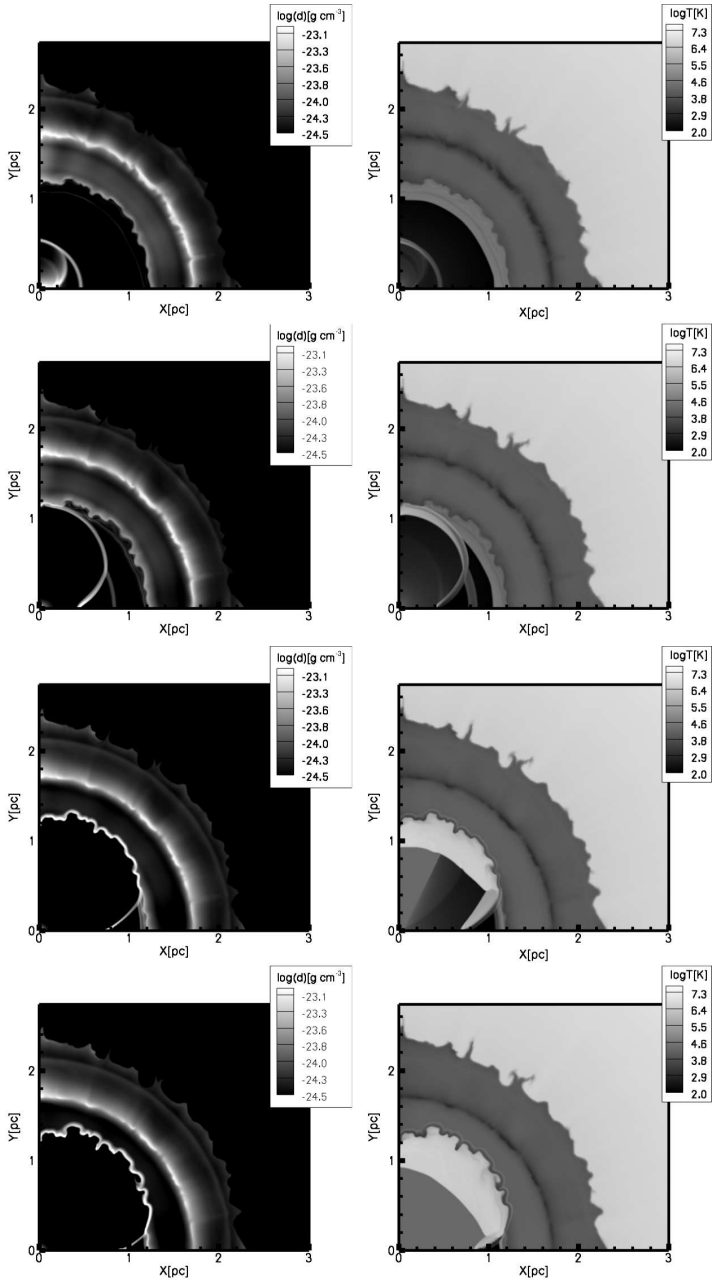

Figure 3.6: Snapshots of the density (left figures) and temperature (right figures) distributions of the circumstellar material around our 12 $M_{\odot}$ model after its first red supergiant stage. The first panel corresponds to beginning of the blue supergiant stage. The spherical red supergiant shell is situated between 1 pc and 2.2 pc. The hourglass shaped blue supergiant shell occupies the inner 0.4-0.5 pc. The second panel depicts the situation 4500 yr later, when the polar parts of the BSG shell collide with the RSG shell. Panels 3 and 4 show the density and temperature distributions 10 700 yr and 13 600 yr after the first time of Panel 1.

Chapter 4

The circumstellar medium of massive stars. II. Models for blue supergiants

based on S. M. Chiţă, B. van Veelen, N. Langer, A. J. van Marle, G. García-Segura 2010, submitted to A&A

Abstract

Massive stars emit strong winds throughout their lives, which shape their surounding medium and can give rise to the formation of circumstellar cavities and nebulae. We present calculations that predict the properties of the circumstellar medium for blue supergiants. The interaction of their winds with the outside medium is followed through all stages of stellar evolution, from main sequence to the pre-supernova stage, for stellar models with masses of 10, 12 and 18 $M_{\odot}$. From stellar evolution models with rotation we use the time-dependent stellar wind parameters, as an input for 1D and 2D hydrodynamical simulation of the circumstellar medium. We compute the entire evolution of the circumstellar medium in 1D and the post-main-sequence stages also in 2D. We present the results for rapidly rotating and slowly rotating blue supergiants. In the case of a rapidly rotating central star, the collision of an hour-glass shaped shell with a stationary red supergiant shell forms a highly structured rotationally symmetric nebula. For slow stellar rotation, a spherical nebula may form. The clumpyness of the red supergiant shell may induce a patchyness of the nebula. Short-lived luminous and highly structured nebulae are formed by wind-wind interaction around blue supergiants just after their return from the red supergiant stage. The obtained nebula properties are reminiscent of observed nebulae around blue supergiants. We predict that about 1% of all blue supergiants should posess such nebulae.

Introduction

Massive stars spend almost their entire life in the main sequence stage and have different post-main sequence phases. During their evolution, the stars can have strong winds which eject material that interacts with the surrounding gas. During the post-main-sequence evolution the central star can move back and forth between the red and the blue side of the Hertzsprung-Russell diagram, making a so called blue-loop (e.g. Langer [1991b], Schaller et al. [1992]).

When the star becomes a red supergiant (RSG) the ejected wind stalls at the point where the thermal pressure in the hot bubble formed by the previous (main sequence) wind equals the ram pressure of the RSG wind (e.g. García-Segura et al. [1996b]). When the star moves to the blue supergiant stage (BSG), the wind velocity increases, and the preceding wind material is swept up into an expanding shell. Massive stars are often rotating rapidly such that their winds may by highly anisotropic, which can give rise to structured, rotationally symmetric circumstellar shells and nebula (e.g. Langer et al. [1999], Chiţă et al. [2008], hereafter Paper I).

In the past decades, observations of massive stars in the Wolf-Rayet (WR) or Luminous Blue Variable (LBV) stages with ring nebulae (e.g. Marston et al. [1994]) and multiple ring nebulae around BSGs (e.g. Smith et al. [2007b]) have been made. For instance: models of the circumstellar material around single massive stars have been constructed by Martin et al. [1995], García-Segura et al. [1996a], Meyer et al. [1997] and Woosley et al. [1997]. Burrows et al. [1995] and Crotts & Heathcote [2000] have presented models of triple-ring nebulae as have been seen around SN 1987A. Complex binary phenomena were invoked by Podsiadlowski et al. [1991], Blondin & Lundqvist [1993], Lloyd et al. [1995] and Podsiadlowski et al. [2005] as responsible for the complex triple-ring structures.

The previous circumstellar medium modeling for massive stars either concentrated on stars above ~ 30 $M_\odot$ (e.g. Perez-Rendon et al. [2009]), which become WR stars or LBVs, or on individual cases, in particular the triple ring system around Supernova 1987A. In this Paper, we follow a generic approach for stars in the mass range of typical Type II supernova progenitors, i.e. the mass range 10...20 $M_\odot$. We use stellar evolution models from Heger & Langer [2000b] and Woosley (priv.com.) for this mass range, and perform hydrodynamic calculations for the circumstellar medium around these stars using the time-dependent wind and radiation characteristics of the stellar evolution models as input. While the analysis of the RSG of these models is presented in Chiţă et al. [2010a], (hereafter Paper II), we focus here on the formation of structure in the circumstellar medium structures during the BSG stages.

The structure of the Paper is as follows: in Sect. 2 we give a brief description of our stellar models used. In Sect. 3 we explain our numerical method used to simulate interactions of the circumstellar medium. In Sect. 4 and 5 we present our results, while in Sect. 6 we make a few predictions for our observed structures. In Sect. 7 we summarize our main conclusions.

Stellar models

Massive stars eject strong winds into the interstellar medium during their life time. In this paper we consider the effect of these winds on the circumstellar environment using hydrodynamic calculations. As input for our circumstellar hydrodynamic calculations, we use the results of a stellar evolution calculation for stars of 10, 12 and 18 $M_\odot$ with a metallicity of $Z = 0.02$. Specifically, we utilize Model E10 (hereafter as 10n), G12B (hereafter as 12n) and F12B (hereafter as 12r) from Heger & Langer [2000b], and Model 18sw from Woosley (priv.com.) that describe stars with an initial rotational velocities of 208 $\mathrm{km\,s^{-1}}$, 99 $\mathrm{km\,s^{-1}}$, 328 $\mathrm{km\,s^{-1}}$ and 380 $\mathrm{km\,s^{-1}}$, respectively. The evolution of 10n, 12n, 12r and 18sw models in the Hertzprung-Russell diagram (HRD) is shown in Fig. 4.1. The code used

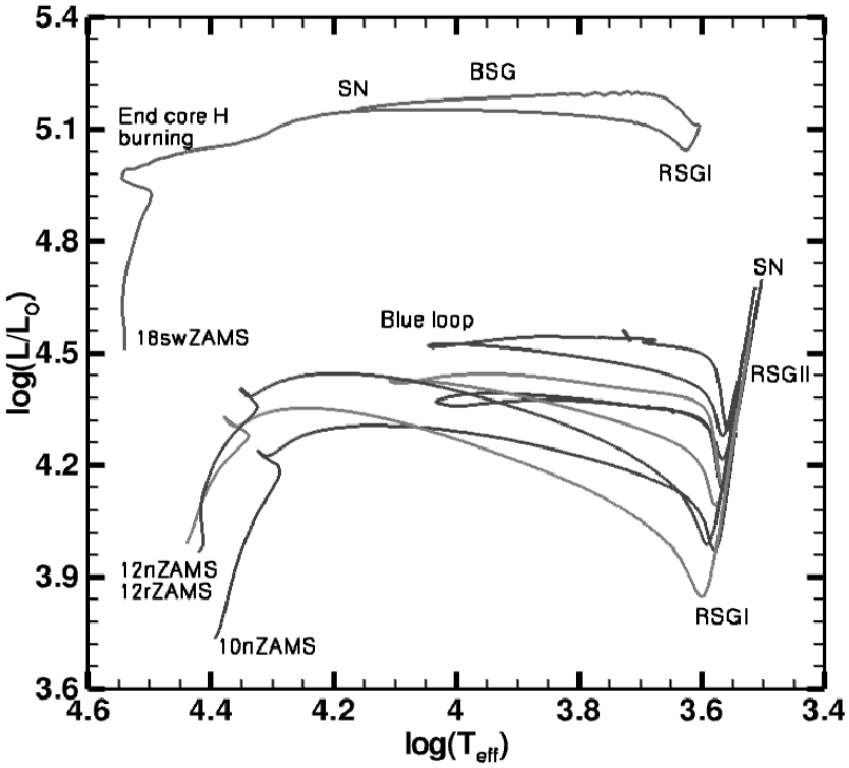

Figure 4.1: Evolution of the adopted stellar evolution models in the Hertzprung-Russell diagram from the zero age main sequence to the pre-supernova stage for Model 10n, 12n 12r and 18sw. The initial metallicity of all models is $Z = 0.02$, and the initial equatorial rotation velocity is 208 km s^{-1}, 99 km s^{-1}, 328 km s^{-1} and 380 km s^{-1}, respectively.

to compute this model includes OPAL opacities, detailed nuclear networks, a mass-loss description according to Nieuwenhuijzen et al. [1990], the physics of rotation for the stellar interior, and rotationally modulated stellar winds, as described in Heger et al. [2000a].

The 10 $M_\odot$ and 12 $M_\odot$ models evolve into RSG right after core hydrogen exhaustion, and they undergo so called blue loops during core helium burning. This means that, after spending a considerable fraction of their core helium burning life time as RSG (cf. Table 1), they evolve into the blue part of the HR diagram, where they remain until they return to the RSG regime at core helium exhaustion. The movement in the HR diagram is reflected in the time evolution of the stellar wind properties, as shown in Fig. 4.2.

As shown by Heger & Langer [1998], rapid rotators may be forced to near critical rotation

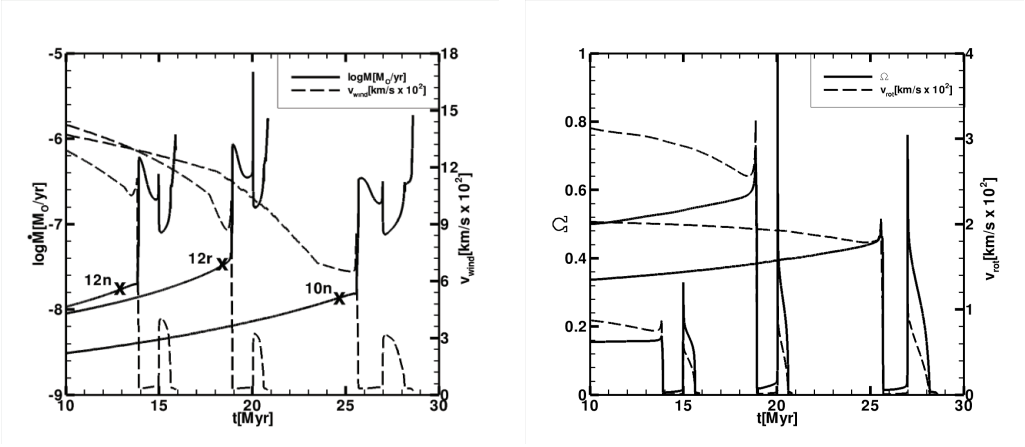

Figure 4.2: Various quantities of our employed models. The left panel shows the time dependence of stellar mass-loss rate(solid line) and terminal wind velocity (dashed line) for Models 10n, 12n and 12r during the main sequence until the pre-supernova stage. The right panel shows, the stellar rotational velocity (with dashed line) and the ratio of stellar and critical rotation rate, Ω (solid line). In this plot we start the time axis at 10 Myrs to focus on the post-main sequence wind parameters used in our computations. The symbols mark the starting point of our 2D simulations.

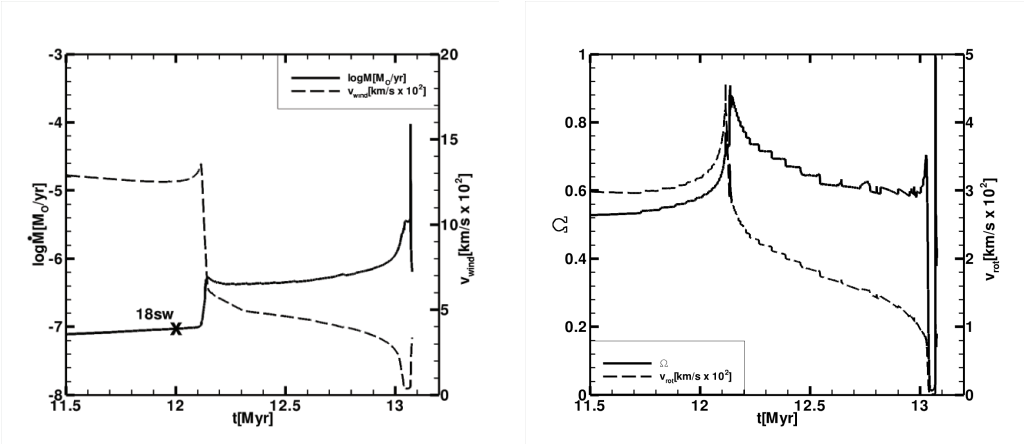

Figure 4.3: Same as Fig. 4.2 but for Model 18sw with the symbol representing the 2D hydro-calculations starting point. We have cut from the time axis 11.5 Myrs for enhancing the later stage of evolution. The time dependence of stellar mass-loss rate(solid line) and terminal wind velocity (dashed line) from the zero age main sequence until the pre-supernova stage is shown in the left panel. The stellar rotational velocity (with dashed line) and the ratio of stellar and critical rotation rate, Ω (solid line) are illustrated in the right panel.

Table 4.1: Ejected mass (ΔM), momentum (Δp) and kinetic energy (ΔE) during the various evolutionary phases of our stellar models. The evolutionary phase is identified in the first column: main sequence phase (MS), first red supergiant phase (RSG I), second red supergiant stage (RSG II), first blue supergiant stage (BSG I), and second blue supergiant stage (BSG II) . The approximate duration of each phase is given in the third column.

Model	Phase	Δt	ΔM	Δp	ΔE
		Myr	$M_\odot$	10^{38} g cm s^{-1}	10^{45} erg
10n	MS	25.69	0.14	193.07	719.84
	RSG I	1.29	0.33	68.25	35.85
	BSG I	1.20	0.14	60.57	71.97
	RSG II	0.43	0.17	31.61	14.82
12n	MS	13.90	0.13	206.37	869.53
	RSG I	1.07	0.35	76.29	42.26
	BSG I	0.65	0.07	39.85	63.32
	RSG II	0.26	0.13	26.27	13.09
12r	MS	18.93	0.23	356.86	1459.78
	RSG I	1.09	0.53	109.29	56.23
	BSG I	0.59	0.14	61.22	74.59
	RSG II	0.21	0.17	30.08	13.73
18sw	MS	12.15	0.42	1277.19	9941.67
	BSG I	0.90	0.54	412.28	878.38
	RSG I	0.03	0.10	7.11	1.31
	BSG II	0.01	0.03	7.30	6.77
12sy	MS	10	0.10	290	2104
	BSG I	0.55	0.23	555	3343

during the red-blue transition, which leads to enhanced and anisotropic mass and angular momentum loss, e.g. Langer [1998]. This situation does apply to Model 12r (see Fig. 4.2, second panel) and corresponds to the highest peak in the mass-loss rate of this model shown in Fig. 4.2 (first panel).

The original 18 $M_\odot$ model from Woosley (priv.com.) did not reach critical rotation during the final red-blue transition. For the purpose of computing the wind properties of Model 18sw, we have assumed a slight increase of the rotational velocity of the star for the entire stellar evolution such that 99 % of critical rotation is reached during the final red-blue transition (Fig. 4.2, second panel).

The stellar evolution models do not provide us with the terminal wind velocity needed for our hydrodynamical calculations. Thus we follow Cherchneff et al. [1994] and assume that the winds are radiation driven, with a wind terminal speed v_∞ proportional to the escape speed from the stellar surface,

$$v_\infty = \sqrt{\frac{2\beta GM}{R}(1-\Gamma_E)}, \tag{4.1}$$

where $\Gamma_E = L/L_E$ is the ratio between stellar luminosity and Eddington luminosity. The proportionality constant β as function of the surface temperature of the star is taken from Eldridge et al. [Eldridge et al. 2006].

In our models the limit of critical rotation is reached only during the red-blue transition, which produces a brief period of dense, slow and anisotropic mass-loss (Table 4.1). Rotating stars have a latitude-dependent mass-loss, but if the rotation is well below critical, as it happens with our 10n and 12n models (Fig. 4.2), this effect is negligible. However, if the star rotates fast enough (see 12r and 18sw models) and its rotational velocity increases (Fig. 4.2 and Fig. 4.3), the wind becomes aspherical. To describe this latitudinal dependence of mass-loss we use the equations found by Bjorkman & Casinelli [1993], as used by Langer et al. [1999] and by van Marle et al. [2008]. This model assumes that for a rapidly rotating star, the wind will be denser at the equator than at the poles and faster in polar directions. Given the wind velocity:

$$v_\infty(\theta) = \sqrt{\frac{2A\beta GM(1-\Gamma_E)}{R}}\,(1-\Omega\sin\theta)^\gamma, \tag{4.2}$$

and the wind density:

$$\rho(\theta) = \frac{(\alpha/2)B\,\dot{M}(1-\Omega\sin\theta)^\xi}{4\pi R^2\, v_\infty(\theta)}, \tag{4.3}$$

the parameters defined in Bjorkman & Cassinelli are set to $\gamma = 0.35$ and $\xi = -0.43$ and Ω is defined as $\Omega = v_{rot}/v_{crit}$. The quantity α is defined as:

$$\alpha = \left[\cos\phi' + \cot^2\theta\left(1+\gamma\frac{\Omega\sin\theta}{1-\Omega\sin\theta}\right)\phi'\sin\phi'\right]^{-1}, \tag{4.4}$$

with $\phi' = \Omega\sin\theta\, v_{crit}/[2\sqrt{2}\, v_\infty(\theta)]$ and Ω set to $\Omega \leq 0.99$. The factors A and B, are correction factors for the stellar mass-loss and wind velocity, to assure that these parameters remain the same as in the 1D approximation, and they are calculated by integrating the Eqs. (4.2) and (4.3) over the surface of the star and normalizing to unity. We will adopt this scaling of wind parameters (wind velocity, wind anisotropy) in the numerical calculations presented below. The mechanism of Bjorkman & Cassinelli has been criticized in the past in the context of line-driven winds [Owocki et al. 1996], but it is not clear still if the line driving mechanism plays a role in the situation of near-critical rotation. While the model of Bjorkman & Cassinelli results in a fast outflow in the polar direction with a dense and slow outflow at the equator, the model of Owocki et al. predicts a wind enhanced in the polar direction with both a high density and a high velocity. We demonstrate below that a slow and dense equatorial outflow appears to be required by the observed BSG nebula structures.

We also computed the circumstellar material evolution for a hypothetical 12 $M_\odot$ star which, after the main sequence evolution, settles in the BSG stage. For this Model 12sy we assume an MS stage of 10 Myrs duration followed by a BSG phase of 0.55 Myrs. We used time-independent wind parameters, i.e. a mass-loss rate of 9×10^{-9} $M_\odot$ during the MS phase and 4×10^{-7} $M_\odot$ during the BSG phase. The adopted averaged wind velocity for the MS stage is 1430 $km\,s^{-1}$ and the adopted effective temperature is 25 000 K. For the BSG stage, the averaged wind velocity is 500 $km\,s^{-1}$ and the adopted effective temperature is 12 000 K.

Numerical method

To simulate the evolution of the circumstellar matter we use the ZEUS 3D code developed by Stone et al. [1992] and Clark [1996]. ZEUS 3D is a three-dimensional, ideal (non-resistive, non-viscous, adiabatic), non-relativistic, magnetohydrodynamical, Eulerian explicit code which solves the coupled partial differential equations as function of time and space on a fully staggered grid. Radiatively optically-thin cooling is included by solving the energy equation implicitly according to Mac Low et al. [1989] and employing the plasma cooling curve of Smith et al. [2008].

The evolution of the circumstellar material for all our models is computed in 1D from the main sequence until the pre-supernova stage, with 1000 grid points over a radius of 45 pc, were the interstellar medium (ISM) density is assumed to be 20 cm^{-3}. At the end of main sequence, we map the 1D model onto a 2D spherical grid to compute its further evolution. The inflow inner boundary condition is applied at 0.025 pc, and the outer boundary is at 45 pc. The radial direction in the grid is resolved with 500 grid points for 45 pc, where 400 grid points are used for the inner 10 pc, and 100 grid points for the outer 35 pc. The angular coordinate of 90 degrees is resolved with 200 grid points for both the latitude plane (for 12r and 18sw, the rotating models) and the alt-azimuth plane (for 10n and 12n the non-rotating models). The mapping method was applied before by García-Segura et al. [1996,a,b] and van Marle et al. [2005, 2007] and Papers I, II. All models have been computed both in 1D and in 2D except for 12sy model (which has been computed only in 1D).

The effect of photoionization was included in the simulations by calculating the Strömgren radius along each radial grid line as described in García-Segura et al. [1999], van Marle et al. [2005, 2007, 2008] and Papers I, II. The number of ionizing photons is computed according to the effective temperatures and surface gravities provided by the stellar evolution model, by interpolating in a grid of model atmospheres for massive OB stars of solar metallicity computed with the FASTWIND non-LTE code (Puls et al. [2005]) as described in Lefever et al. [2007] and Papers I, II.

1D results

Stars lose mass by ejecting winds into the ISM. The MS wind moves at supersonic velocities and at the collision with the ISM creates a shock. At this moment the wind starts sweeping up matter from the ISM, forming a shell which expands outward inflating a hot bubble. Massive stars emit also high-energy photons that create a photo-ionized H II region, with an outer radius given by the Strömgren radius. The main sequence wind will now be sweeping up this H II region instead of the cold ISM. At the end of the main sequence stage the number of high-energy photons decreases and the region of photo-ionized wind eventually starts to recombine.

In the post-main-sequence stages, depending on the surface temperature, the star can produce high-energy photons. During the same period, the wind parameters change as the mass-loss rate and wind velocity vary with time. In the circumstellar medium of stars with a blue loop, four wind interactions take place: firstly, an interaction between the fast MS wind

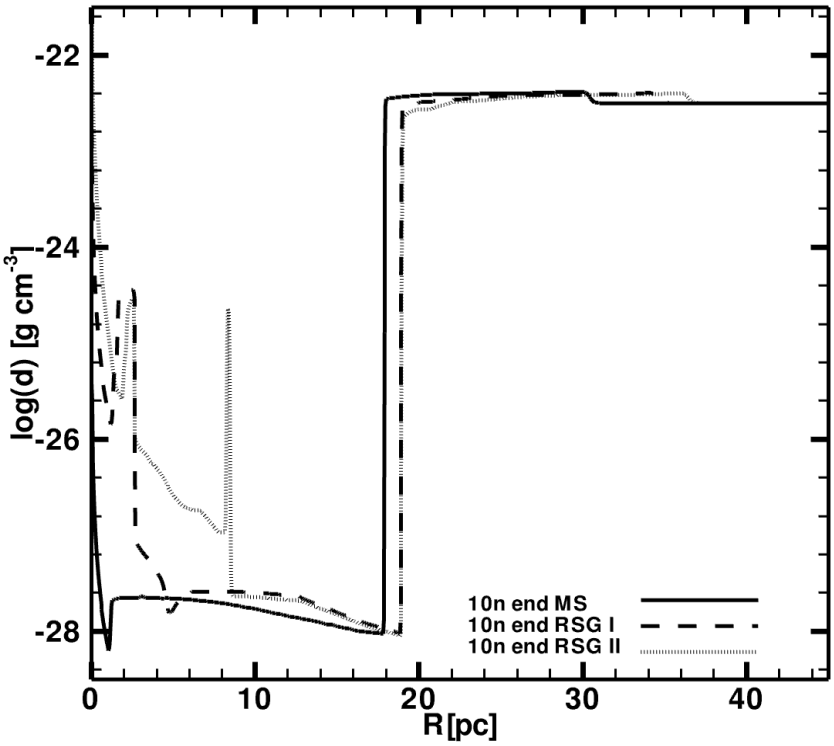

Figure 4.4: The density distribution of the circumstellar medium around the 10n model, as function of distance from the central star for three time snapshots: the end of MS (solid line) is used to start the 2D simulation, the end of first red supergiant stage (with dashed line) and the pre-supernova stage (dotted line). The main sequence wind has swept up ISM material to form a shell, which has kept its location at $\simeq 18$ pc. The first red supergiant shell forms at 2 and 3 pc. The following stellar evolution stages are captured by the wind-wind interaction: a blue-red supergiant shell at 8 pc and a pre-supernova shell at 2.5 pc.

and the ISM; secondly, an interaction between the high density, slow RSG wind and the hot bubble created by the MS wind; thirdly, an interaction between the fast high density BSG wind and the previous RSG wind; fourthly, as all our models end their evolution as RSGs, an interaction between the last high density slow RSG wind and the hot bubble created by the MS wind. The interaction of a fast wind with a slow preceding wind, but also that of a slow wind with the hot bubble created by a fast preceding wind, give rise to the formation of circumstellar shells. Because of high surface temperature of the BSG usually a large

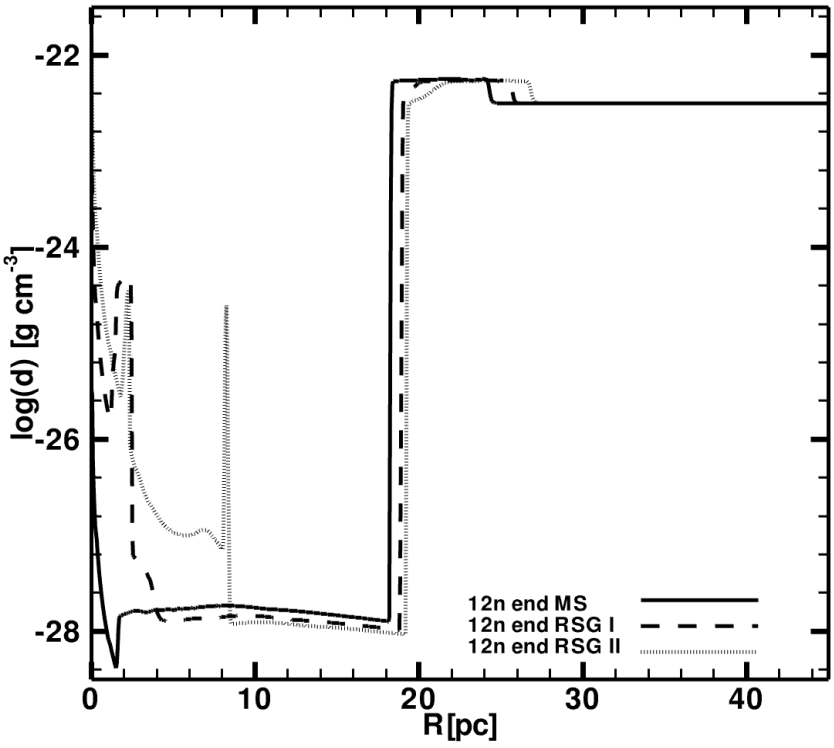

Figure 4.5: Same as Fig. 4.4 but for Model 12n. Also in this case the main sequence swept up shell has maintained its location, at 18 pc, the first red supergiant shell is visible at 2 pc (dashed line), while in the pre-supernova stage, in the hot bubble, the blue-red supergiant shell is visible at 8 pc and the last swept up red supergiant shell can be seen at 2 pc. The end of MS point in time is used to start the 2D simulations for this model.

number of high energy photons is produced. However, the photons can be ”trapped” in the immediate surroundings of high-density circumstellar shells. Thus, the Strömgren radius of a BSG depends on the distribution of the circumstellar material.

In the case of our Model 10n, which has a life time of 25.59 Myr, the main sequence wind sweeps up matter from the ISM to form a shell situated at 18 pc, as seen in Fig. 4.4. The main-sequence shell, with a density almost equal to the density of the ISM, remains stationary during the entire evolution. The MS hot bubble with a constant density, has expanded up to 18 pc. In the transition phases between MS and RSG as in our Models 10n, 12n and 12r, the ram pressure of the wind is reduced, as the mass-loss rate increases and the wind

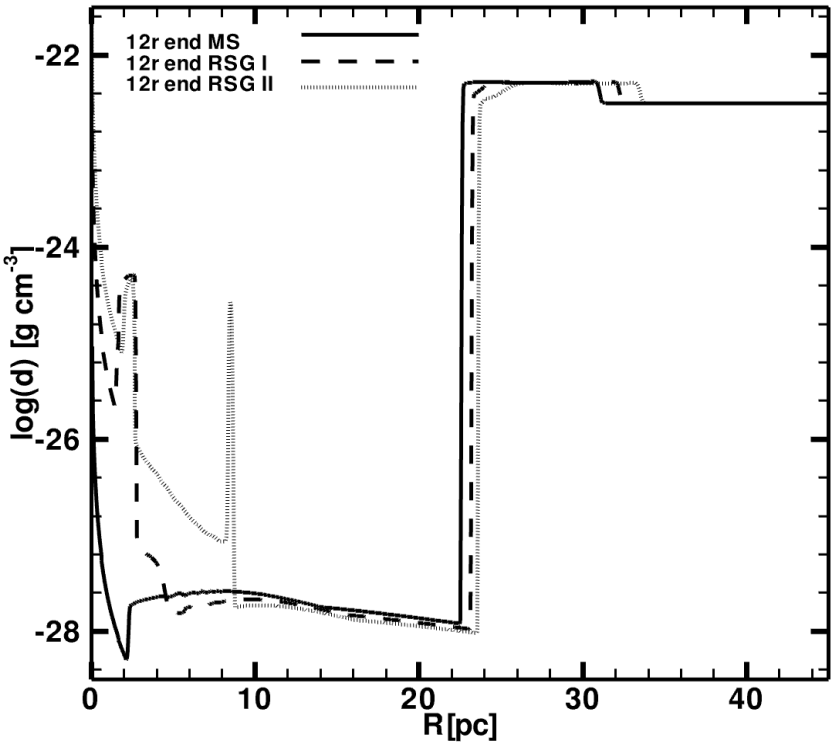

Figure 4.6: Same as Fig. 4.4 but for Model 12r. The MS shell remains at 22 pc until the pre-supernova stage (solid line); in the hot bubble, the first red supergiant shell can be seen between 2 and 3 pc (dashed line), the blue-red supergiant shell at 8 pc and the pre-supernova shell at 3 pc (dotted line). Also the solid line represent the starting point in time used for our 2D simulations.

velocity decreases. The wind termination shock moves inward and oscillates until it finds a new location, basically the radius where the ram pressure equals the thermal pressure of the hot bubble. At this location a RSG shell starts to form, as shown by García-Segura et al. [1996b]. This shell, represented in Fig. 4.4 by the dashed line, keeps its location for 1 Myr, and shortly after, the free streaming BSG wind sweeps up RSG wind material to form a BSG shell. As a consequence of free streaming BSG wind high speed, the BSG shell collides with the previous RSG shell and completely destroys the previous RSG shell. In 1D this process is shown by the high density peak at 8 pc. Before the supernova stage the star will eject a second RSG wind and form a shell with a radius of about 2 pc (Fig. 4.4).

With a total life time of 15.87 Myr, the Model 12n has a similar distribution of the cir-

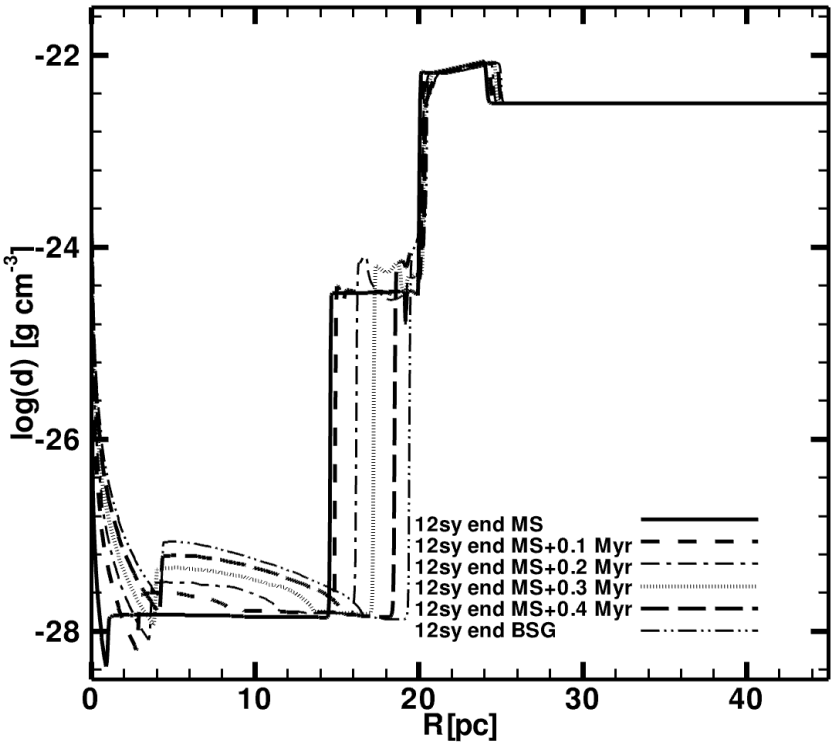

Figure 4.7: Density distribution of the circumstellar medium as function of radius for various times, for 12sy model, starting from the end of main sequence. The time difference between profiles is 0.1 Myr and the outward movement of the CSM is shown at each of these snapshots with different lines. During the evolution, the main sequence shell has maintained its original location from 20 pc, while the HII region visible at the end of main sequence (solid line) from 14 up to 20 pc, has decreased its radius, by the time the star has reached the blue supergiant phase. In the hot bubble, after the main sequence, the blue supergiant free streaming wind does not sweep up shocked wind material to form a shell. The end of the blue supergiant phase and the end of this simulation are illustrated by the dashed double-dot line.

cumstellar matter as 10n model. The main sequence shell radius, with a density of 50 cm^{-3}, has remained almost constant during this time, while in the hot MS bubble the blue supergiant shell has interacted with the RSG shell at 8 pc, as seen in Fig. 4.5. The last RSG wind forms a pre-supernova shell at 2 pc. With a density distribution not very different from the previous models, our 12r model with a total life time of 20.82 Myr, ejects wind into the ISM, sweeping up material from the ISM to form a MS shell situated at 22 pc as seen in Fig. 4.6. The BSG wind sweeps up the RSG wind to form a shell which will smash into the previous

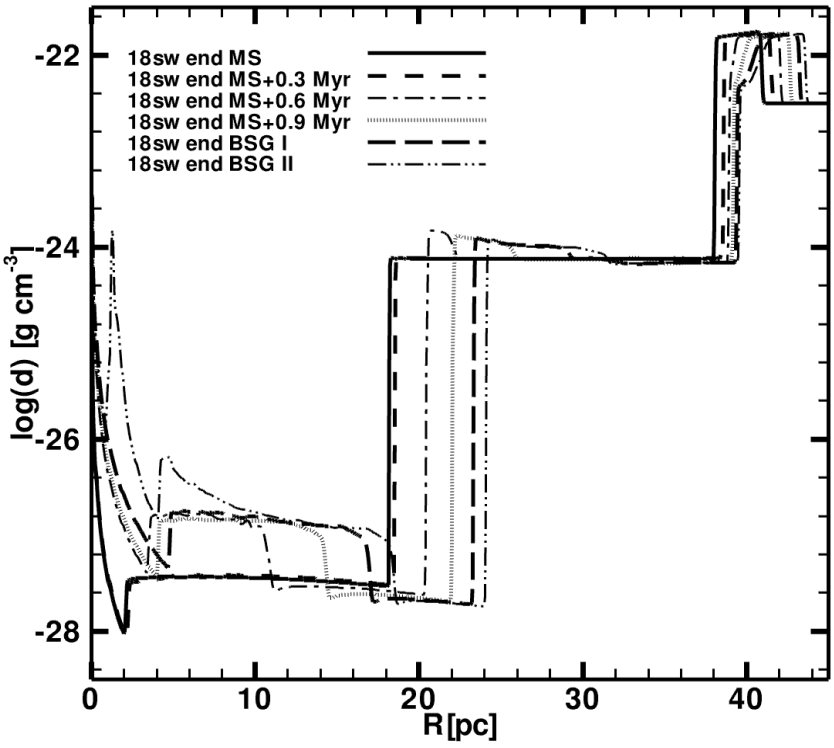

Figure 4.8: Same as Fig. 4.7 but for 18sw model. The time difference between the moving outwards density profiles and represented by different lines is 0.3 Myr. The main sequence shell remains almost constant during this time at 38 pc. The end of main sequence is represented here by the solid line. This moment in time has been used to start up the 2D simulations. A very large HII region is pushed from 18 pc and inside the hot bubble the free streaming wind has swept up to form a pre-supernova shell situated at 2 pc. The last evolutionary stage is captured by the dashed double-dot line and shows formation of a shell at 2 pc.

RSG shell, giving a density peak structure located at 8 pc. The second red supergiant wind forms a pre-supernova shell at 2 pc from the star.

The circumstellar material for stars which, after their MS stage, settle in the blue part of the HRD to burn helium in their core without becoming RSG first (as for Models 12sy and 18sw), forms a different distribution. The MS wind sweeps up matter from the ISM to form a MS shell. Also, during this stage, an HII region is created during the MS evolution. Later as the number of high energy photons drops slightly due to the lower surface temperature of the

BSG star, the radius of the photoionized region decreases, and it is found between 18 pc and 20 pc for Model 12sy at the end of the BSG stage, as seen in the Fig. 4.7. During the BSG stage the wind ram pressure is increasing slowly due to the increase in mass-loss. The wind termination shock is moving outwards into the hot bubble. The BSG wind forms a thick shell which slowly spreads inside the hot bubble interior.

For Model 18sw model, the MS shell is located at 38 pc (solid line in Fig. 4.8). The evolution of the circumstellar material during the first BSG stage, which lasts for 0.90 Myrs, is represented in the same illustration by three successive density profiles. During the first BSG stage, the BSG wind forms a thick shell which expands with time, as in the case of the Model 12sy. During the ensuing short (0.03 Myrs) RSG stage the slow wind material is accumulating close to the central star and is pushed to a radius of about 1.5 pc by the final BSG wind.

2D results

At the end of the MS stage of Models 10n, 12n, 12r and 18sw, represented by the solid line in Fig. 4.4, 4.5, 4.6 and 4.8, we start our 2D simulations. For Models 10n and 12n, where no significant effects of rotation are to be expected, we neglect any latitudinal dependence of the stellar winds and we use the $r - \phi-$plane for our simulations. Any non-sphericity in these models is due to hydrodynamic instabilities. Models 12r and 18sw reach near break-up rotation and are simulated in the $r - \theta-$plane using spherical coordinates.

While we calculate the entire post MS phase evolution of the mentioned models in 2D, we present here the results obtained during the various BSG stages. By the end of their main sequence evolution, all models have developed hot main sequence bubbles of about 20 pc in radius (cf. Sect. 4). While our 2D runs maintain a large grid with a radius of 45 pc, most of the structures created during the post-main sequence evolution are located close to the center of the hot bubble. Our analysis thus focuses on the inner few parsecs around the central star. Models 10n, 12n and 12r develop into red supergiants right after core hydrogen exhaustion. The formation of the Rayleigh-Taylor unstable red supergiant shells has been described in detail in Paper II.

Model 10n

By the time Model 10n leaves the main sequence, its hot constant density main sequence bubble extends to about 18 pc. The first RSG stage lasts for 1.29 Myrs (cf. Table 4.1) and produces an unstable RSG shell with a radius of about 1.5 pc, together with numerous clumps of RSG wind material further out (cf. Paper II). This is the situation at the onset of the BSG wind, which is depicted in the upper left panel of Fig. 4.9.

The BSG wind sweeps-up the previous RSG wind to form a spherical shell, as seen in the upper right panel of Fig. 4.9. Over a period of 19 000 yr this shell moves outwards into the hot bubble (middle left panel of Fig. 4.9), until it collides with the fragmented RSG shell at 1.5 pc. During the collision between the two shells a region of hot and dense gas forms, which gives rise to a luminous circumstellar nebula whose properties are discussed in the

next section. Due to the collision a reverse shock forms which moves inward and creates a hot low-density region between the collided shells and the blue supergiant wind termination shock (which is identical with the reverse shock). Further on, the red supergiant shell is disrupted, and pre-existing clumps in the red supergiant wind material are condensed and heated when they are hit by the faster material coming from smaller radii.

Figure 4.9 encompasses only a few 10 000 yr. After that time, the main interaction is over, and the clumps get distributed all over the hot bubble and disperse. Therefore, for most of the BSG stage of Model 10n, which lasts about 1.20 Myrs, no marked circumstellar structures are expected near the central star.

Model 12n

Model 12n undergoes a similar evolution as Model 10n. After 13.90 Myrs in the MS stage, Model 12n spends 1.07 Myrs in its first RSG stage, when the RSG shell develops instabilities (Paper II). These instabilities lead to clumps which move into the hot bubble and are found up to a radius of 18 pc. Here we show the evolution of the circumstellar material after the first RSG stage, during the BSG phase.

The upper left panel of Fig. 4.10 corresponds to the lower right panel of Fig. 8 in Paper II, which is taken just at the beginning of the BSG stage. The upper right panel of Fig. 4.10 shows how the BSG wind has swept up RSG wind material and formed a spherical BSG shell at 0.6 pc. Over a period of 12 500 yr, the spherical BSG shell moves outwards until it collides with the RSG shell. The moment of collision is captured in the middle right panel of Fig. 4.10. As for Model 10n, due to the collision a bright nebula is formed which will be discussed below. Also the further evolution is similar to that of Model 10n; during the remaining blue supergiant life time of 0.59 Myr, the clumps and fragments spread throughout the hot bubble and disperse.

Model 12r

While the wind input for Model 12r is based on a different stellar evolution model than that for Model 12n — the star is more long-lived and luminous —, the circumstellar medium evolution proceeds in principle similar to that of Model 12n. A marked difference arises, however, from the fact that the the central star in Model 12r reaches near-critical rotation during the red-blue transition, and accordingly the blue supergiant wind shell has an hourglass shape (Fig. 4.11, right upper and middle frames).

Due to the non-sphericity of the blue supergiant wind shell, its collision with the red supergiant shell occurs first in the polar direction. At this stage, a hot dense pair of polar caps forms at about 1.8 pc as seen in the middle right panel of Fig. 4.11. As the collision progresses the interaction region moves consecutively to lower latitudes. The equatorial parts collide with the RSG shell about 13 300 yr after the formation of the polar cap. This effect has been described by Paper I for a similar model, and can lead to complex emission structures, such as triple ring nebulae.

Model 12r is based on the same stellar evolution model and stellar wind assumptions as the one previously presented in Paper I. However, the red supergiant shell in Model 12r is

significantly more unstable. While one difference between both models is that here we have updated the employed cooling curve (cf. Sect. 3), the main difference is due to the fact that our 2D calculations in Model 12r start before the end of the main sequence evolution and thus include the highly variable transition phase between main sequence and red supergiant stage. The 2D models of Paper I were initiated 100 000 yr after the onset of the red supergiant phase from a spherically symmetric 1D model, and the corresponding red supergiant shell is thus less unstable (see the corresponding discussion in Paper II).

Model 18sw

Model 18sw is interesting in the context of the triple-ring nebula observed around SN 1987A and for the formation of nebulae around BSG. After 12.15 Myrs spent in the MS stage, the circumstellar matter around the Model 18sw contains a hot bubble from 2 to 38 pc with a large photo-ionized region from 18 to 38 pc. This surrounding gas is the material with which the post-main-sequence wind interacts. In a post-main-sequence period of 0.94 Myrs the wind mass-loss and terminal velocity change dramatically. The onset of the first BSG wind as seen also in our 1D results (Fig 4.8) has not formed any high density peak structure, thus no BSG shell as in the previous models. The BSG wind material is maintained in a thick shell that spreads out into the hot bubble. A very short time (0.03 Myrs) is spent by this model in the RSG stage and no RSG shell is formed during this stage. The model reaches critical rotation during the final red-blue transition (Fig. 4.3) and emits an anisotropic wind. This wind sweeps up the previous red supergiant wind, and an expanding anisotropic blue supergiant shell is formed (Fig. 4.12). The second BSG stage lasts for 0.01 Myrs before the central star explodes as a supernova.

While our model does develop an equatorial ring structure, it is not suited to develop a triple ring structure due to the mechanism discussed by Paper I as it does not form a red supergiant shell. We leave it to future investigations to see whether a triple ring structure as found around Supernova 1987A can be achieved through a plausible variation of the stellar input parameters.

Discussion of BSG nebulae properties and comparison with observations

Nebulae from slowly rotating stars

In Paper II we discuss in detail the two RSG stages of Model 8n. In this case, although the star passes through the BSG stage, the BSG wind is brief and does not sweep up the previous RSG wind to form a shell. However, for consistency, we mention a few relevant quantities in Table 4.2.

Models 10n and 12n lose about 0.64 $M_\odot$ and 0.55 $M_\odot$ respectively during their post-main sequence evolution (Table 4.1). In Table 4.2 we estimate the amount of mass involved in the collison between the blue and the red supergiant shell. For the moment of the collision,

Table 4.2: Various nebular quantities as calculated for models 8n, 10n, 12n, 12r, 18sw. Δr, as nebular width, mass, as integrated for Δr, temperature, emissivity, total luminosity as calculated for a gas with $10^4 < T < 10^6$ K.

Model	Nebula mass $M_\odot$	Δr pc	log T K	$\epsilon_{(op+uv)}$ 10^{-23} erg cm^{-3} s^{-1}	L_{total} 10^{32} erg s^{-1}
8n	0.007	0.9...1.2	4.7	0.282	1.531
10n	0.021	2...2.2	4.93	2.255	3.772
12n	0.016	1.4...1.5	4.97	3.457	9.846
12r	0.012	2...2.3	5.19	5.290	27.547
18sw	0.006	0.7...0.8	5.6	2360	22.191

we list the radius interval which contains the collided shells, and the mass contained in this interval. We see typical values are of the order of 0.01...0.02 $M_\odot$.

A region of hot dense gas forms during the collision between the RSG shell and the BSG shell. This gas dominates the emission from the circumstellar medium. Figure 4.13 shows the emissivity for Model 10n (in the upper panel) at the time of maximum brightness, and reveals a fragmented spherical nebula with a temperature of $T = 10^{4.93} K$ and an emissivity of $\epsilon_{(op+uv)} = 2.255 \times 10^{-23}$ erg cm^{-3} s^{-1}. The total luminosity of this nebula is about 10 % of the solar luminosity. Model 12n forms a more intact spherically symmetric nebula, with a temperature of $T = 10^{4.97} K$ and an emissivity of $\epsilon_{(op+uv)} = 3.457 \times 10^{-23}$ erg cm^{-3} s^{-1} as seen in Fig. 4.13 lower panels. Its maximum luminosity is about 30 % of the solar luminosity.

The collision nebulae produced by Models 10n and 12n are bright for periods of $\simeq$ 40 000 *yr* and $\simeq$ 28 000 *yr*, respectively. This can be seen from the light curves shown in Figs. 4.15 and 4.16 (upper right panel). For these nearly spherically symmetric collisions, the duration of the bright phase of the nebula is determined by the cooling time. The expansion velocities of the nebulae at the time of the maximum brightness is 77 km s^{-1} for Model 10n, and 81 km s^{-1} for Model 12n.

The reverse shock of the collision forms a region of hot gas (a few 10^6 K) in between the bright nebula shell and the free streaming BSG wind (see Fig. 4.13). This region dominates the X-ray emission from the central 5 pc of our grid during the bright nebula phase for Models 10n and 12n (cf. Figs. 4.15 and 4.16, lower right panel; respectively). However, the X-ray luminosity is only of the order of a promille of the solar luminosity. The total X-ray emission is generally dominated by emission from the entire CSM sphere of 45 pc, which includes the hot MS bubble, as seen in the lower left panels of Fig. 4.15 and Fig. 4.16.

Figures 4.15 and 4.16 also give the kinetic wind energy inflow into the grid as function of time (first panels). During the post MS stages, for Model 10n and 12n, we can see big contributions from the BSG stage, most of which is transfered into thermal energy of the hot bubble.

Nebulae from rapidly rotating stars

In Paper I we described the BSG hour-glass shaped shell based on the same stellar evolution model as Model 12r in this paper. This shell expands into a spherical RSG shell that contains 0.26 $M_\odot$, reaching a velocity of $\simeq$ 130 km s^{-1}. Over a period of 10 000 yr, the collision between the two shells occurred first in the polar region, creating a hot (T$\simeq 10^5 K$) dense ($n \simeq$ 10 cm^{-3}) pair of polar caps. The emissivity of these polar caps was $\epsilon_{(\mathrm{op+uv})} \simeq 10^{-21}$ erg cm^{-3} s^{-1}, while their total luminosity was $L_{\mathrm{total}} \simeq 4 \times 10^{33}$ erg s^{-1}. The hotter gas formed due to the reverse shock of the collision observable in the X-ray regime, showed a peak luminosity of 10^{33} erg s^{-1}.

In our Model 12r, before the collision with the BSG shell, the RSG shell accumulates 0.37 $M_\odot$. The hour-glass structure expands into the RSG shell with a velocity of 88 km s^{-1} over a period of 13 320 yr, and collides first in the polar region, forming polar caps of hot dense gas. As Fig. 4.14 shows (upper left panel), the temperature of this polar caps is T$\simeq 10^{5.19} K$, and they accumulate a total mass of 0.12 $M_\odot$. Their emissivity is $\epsilon_{(\mathrm{op+uv})} \simeq 5.3\times 10^{-23}$ erg cm^{-3} s^{-1} (Fig. 4.14, upper right panel), and their total luminosity is $L_{\mathrm{total}} = 1.2 \times 10^{33}$ erg s^{-1}. The collision phase lasts for 35 520 yr, and the peak in luminosity $L_{\mathrm{total}} = 3 \times 10^{33}$ erg s^{-1} (upper right panel of Fig. 4.17) is reached 8880 yr after its onset. Compared to our previous results, when multiple ring collision zones were formed, here we find less confinement in the nebula structure.

With 0.67 $M_\odot$ lost in the post-main-sequence stages, the hour-glass BSG nebulae of Model 18sw, contains 0.06 $M_\odot$. At the time of the supernova explosion, the temperature of the nebula region is T$\simeq 10^{5.6} K$ and the emissivity is $\epsilon_{(\mathrm{op+uv})} = 2360 \times 10^{-23}$ erg cm^{-3} s^{-1}, as seen in Fig. 4.14 (lower left and right panels). The nebula has a peak in luminosity of $L_{\mathrm{total}} = 19 \times 10^{32}$ erg s^{-1}, seen in the upper right panel of Fig.4.18.

Comparison with observations

For low-mass stars, which evolve from the Asymptotic Giant Branch towards the white dwarf stage, as well as for very massive stars, which become WR stars after a RSG or LBV stage, it is well established that the corresponding red-blue transition in the HR diagram leads to the formation of well defined circumstellar nebulae. Our models show that nebulae are also to be expected around blue supergiants which have just undergone a red-blue transition in the HR diagram in the frame of their blue loop evolution.

Compared to Planetary Nebulae (PNe) and Wolf-Rayet Nebulae (WRNe), the nebulae around blue supergiants are fainter, due to two main reasons. Firstly, the amount of mass involved in our BSG nebulae is of the order of 0.01 $M_\odot$, which is a factor 10 to 100 less than the amount of mass in PNe and WRNe. Secondly, the effective temperatures of our BSG models are significantly lower than those of central stars of planetary nebulae or of WR stars. Indeed, photoionization plays a minor role in our models as the ionizing fluxes of our BSG central stars are small (except perhaps for Model 18sw). Nevertheless, they can appear as nebulae with luminosities of up to one solar luminosity for a period of several 10^4 yr, due to the collision of the BSG and the RSG shells. For rapidly rotating central stars, non-spherical geometries are predicted, in particular single and triple ring structures.

Whether any such nebulae have been observed so far is unclear. Nebulae around blue supergiants (other than LBVs) have been found in a few cases. Most prominent are the rings found around SN 1987A, which occurred from an exploding blue supergiant in the Large Magellanic Cloud. The SN 1987A nebula was only discovered since the photoionisation from the supernova increased its brightness sharply. Similar nebulae have been found around HD 168625 (the so called "twin" of the progenitor of SN 1987A) and SBW 1 (e.g. Smith et al. [2007b]), and around the Galactic B supergiant Sher 25 (Brandner et al. [1997]), which shows a central ring and two polar caps.

Although none of our models fits any particular object in detail, and while there is no evidence for shock excitation in any of the observed cases, many of the general characteristic of the observed BSG nebulae are well represented by our models. Paper I has shown that their 12 $M_\odot$ model reproduces the general properties of the nebulae observed around Sher 25: the emission geometry with two polar caps and one inner ring, as well as the expansion velocity of the inner ring ($\sim$ 18 $\mathrm{km\,s^{-1}}$) and the velocity of polar caps ($\sim$ 50 $\mathrm{km\,s^{-1}}$). The rotational velocity of the central star in our model corresponds to the value of $\sim$ 70 $\mathrm{km\,s^{-1}}$ found for Sher 25, (see Hendry et al. [2008]) and, as most observed nebulae, the star and nebula are nitrogen enriched as predicted. Also for the other cases, geometrical distances and shapes, and expansion velocities fit rather well to our models.

Our models predict life times of BSG nebulae of the order of some 10^4 yr. This, compared to a BSG life time of about 10^6 yr (cf., Table 4.1) implies that about a few per cent of the BSG should be surrounded by a nebula — assuming that the majority of them are on a blue loop excursion. Given the relative faintness of the predicted nebulae, this number seems not incompatible with the fact that only very few BSG nebulae have been found so far. Finally we conclude that in order to obtain geometries similar to those observed around BSGs, a slow and dense equatorial outflow density, the brief phase of rapid rotation at the onset of the blue loop (Heger & Langer [1998]) as we assumed in our models (cf. Sect. 2) is required. Altough we did not compute models assuming an enhanced polar rather than equatorial mass loss during this phase, the resulting nebula geometries would clearly be very different.

Summary and Conclusions

In this Paper we have described the evolution of circumstellar matter for stellar models with initial masses of 10, 12 and 18 $M_\odot$. We computed the entire evolution of the circumstellar medium starting from the zero-age main sequence until the supernova explosion in 1D, while 2D computations were performed for the post-main-sequence stages. While Paper I focused on the RSG stage of our models, this study analyzes the surrounding medium of our models during the BSG stage.

Our stars spend most of their life time in the main sequence stage. In their post-main-sequence phases, the stars with 10 and 12 $M_\odot$ undergo a blue-loop after a first red supergiant stage. Before they explode as supernova, the stars go back for a second time to the red supergiant stage. We also analyze an 18 $M_\odot$ model with an evolution presumably resembling that of the progenitor of SN 1987A, which explodes as a blue supergiant after evolving through a short red supergiant stage.

During the post-main-sequence stages, the wind properties shape the distribution of the circumstellar matter. BSG nebulae are formed during the red-blue transition from the first RSG stage to the BSG stage, a so called blue loop. The BSG wind sweeps up the RSG wind material to form a shell, which then collides with the previously formed unstable RSG shell. The nebulae produced in these wind-wind collisions have lifetime of some 10^4 yr and luminosities up to one solar luminosity. For slowly rotating central stars, their shape is spherical but possibly fragmented. Rapidly rotating central stars give rise to triple ring emission geometries similar to the observed features around BSG. The properties of these structures are determined by the wind properties, such as mass loss rate, wind velocity and anisotropy, which due to rotation of the star, produce a dense equatorial ring and a fast polar wind. If most of the stars in the considered mass range undergo a blue loop evolution, a few per cent of all blue supergiants are expected to show a nebula of the kind described here.

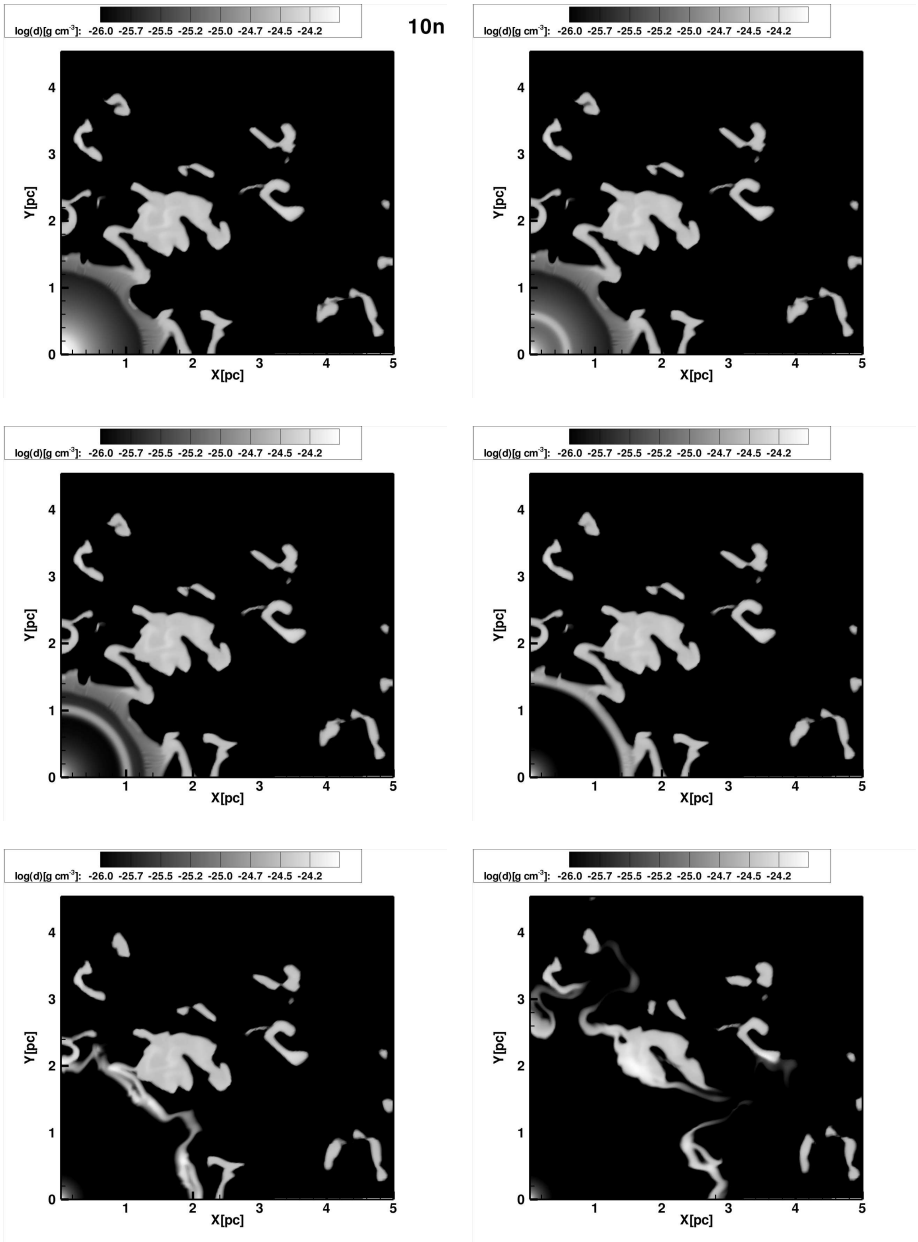

Figure 4.9: Snapshots of the density distribution of circumstellar medium, showing the inner 5 pc of a 2D run on a grid with a radius of 45 pc grid, at the onset of the blue supergiant stage, for our 10n model. The upper left frame is taken 1.5 Myr after the end of main sequence (starting point of our 2D simulations) and shows the onset of the blue supergiant wind and a stationary red supergiant shell at around 1.4 pc. The blue supergiant wind sweeps up the preceding red supergiant wind to form a spherically symmetric shell. This shell, situated at 0.6 pc initially as seen in the upper right panel, expands in time and collides with the previous red supergiant shell situated at 1.4 pc visible in all upper and middle frames with a time difference of 6342 yr. The left lower panel shows the circumstellar distribution after 31710 yrs from the upper left panel and the last snapshot is taken 25367 yrs later.

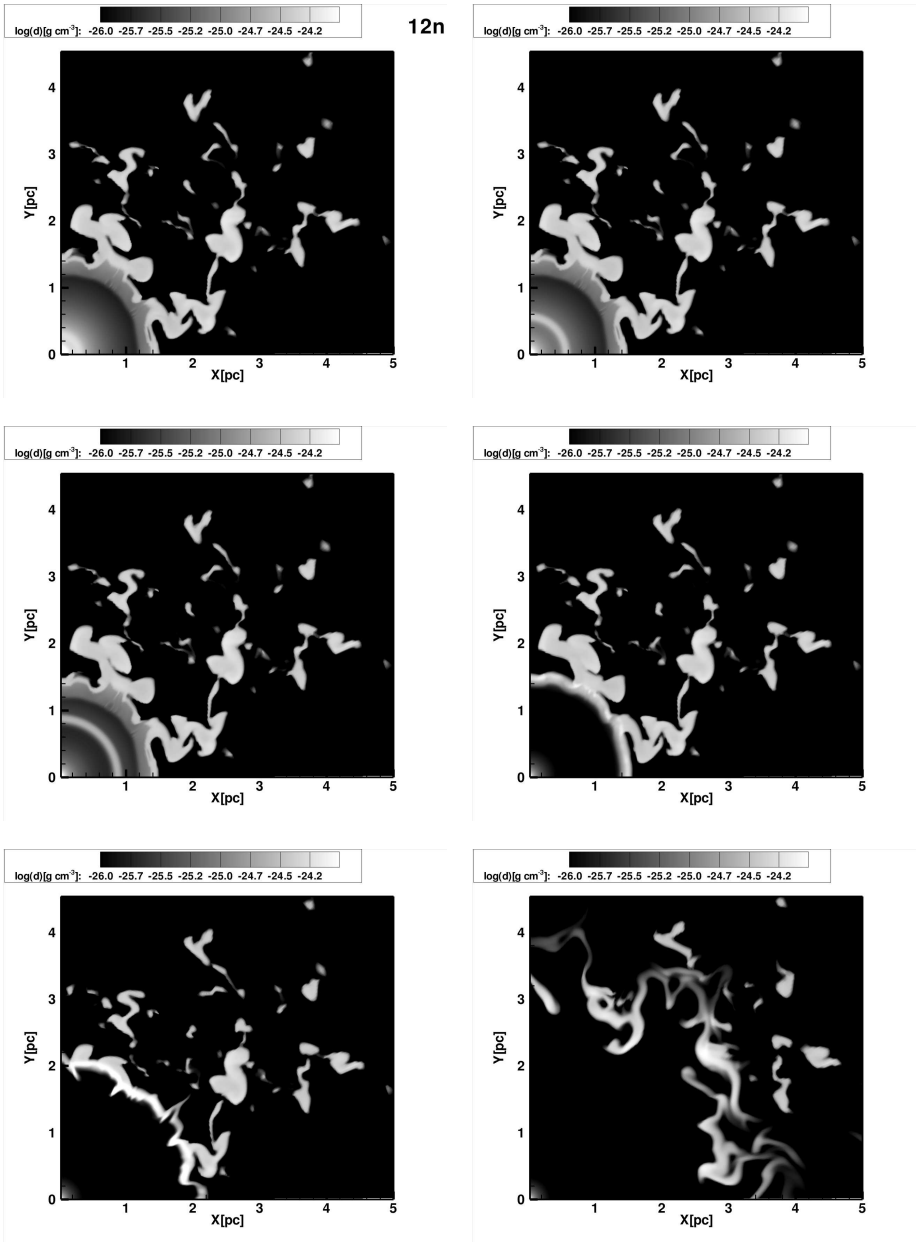

Figure 4.10: Same as Fig. 4.9 but for 12n model. The upper left panel is taken 1.185 Myr after the end of main sequence and shows again the inner 5 pc from the entire 45 pc radius of CSM distribution. The upper right frame showing a blue supergiant shell at 0.5 pc is depicted 4186 yr after the upper left frame. The spherical blue supergiant shell, as seen in the middle left panel situated at 0.8 pc, 8372 yrs from the upper left frame, will be moving outwards and collide, 8371 yrs later, with the red supergiant shell situated at 1.4 pc, situation captured in the middle right panel. Same as in the previous case, the remnant structures of the collision between the blue and the red supergiant shell, are moving outwards into the hot bubble, situation represented in the lower panels, 12557 yrs and 54414 yrs after the collision(middle right panel).

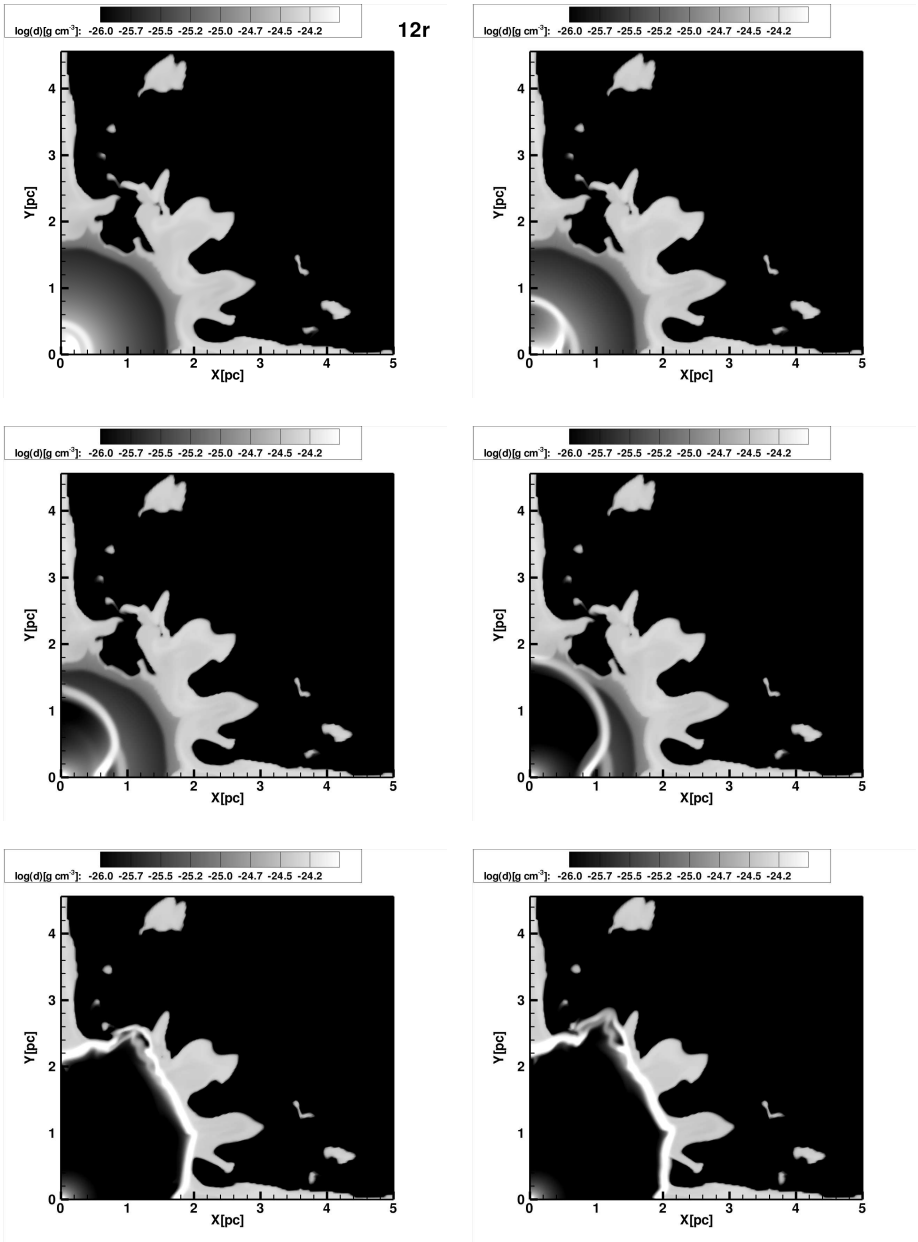

Figure 4.11: Same as Fig. 4.9 but for model 12r. The upper left panel shows the inner 5 pc CSM distribution 1.40 Myr after the end of main sequence, at the onset of the blue supergiant stage. The upper right panel depicts an hour-glass blue supergiant shell, 4440 yr after the upper left frame. As it ages, the hourglass shell expands outwards, as seen in the middle left panel 4440 yrs after the upper right panel, until it collides with the red supergiant shell, situation captured in the middle right panel, 4440 yrs after the previous frame. The lower left and right panels are depicted 8880 and 13200 yrs after the middle right panel. The blue supergiant shell has smashed into the stationary red supergiant shell breaking it apart, and forcing the remnants of both shells to move outwards in the hot bubble.

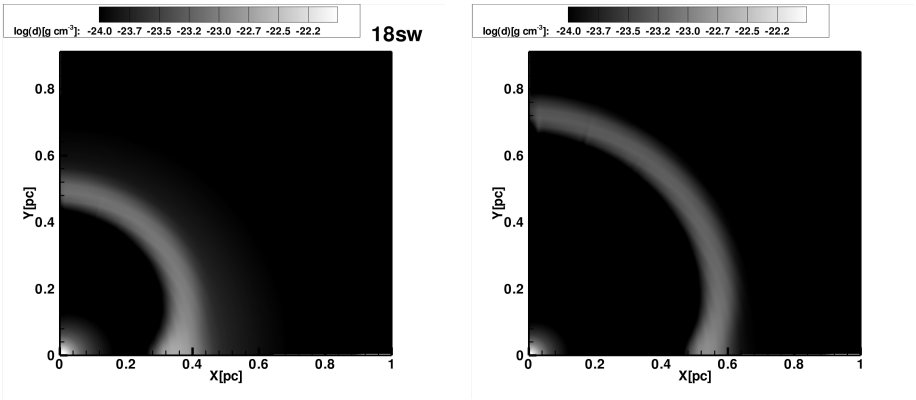

Figure 4.12: Same as Fig. 4.11 capturing the blue supergiant stage which occurs 1 Myrs after the end of main sequence for the model 18sw in the left frame, and 2220 yrs later in the upper right frame. An hour-glass shaped blue supergiant shell has formed at the wind termination shock, when the blue supergiant wind has swept up the preceding red supergiant wind.

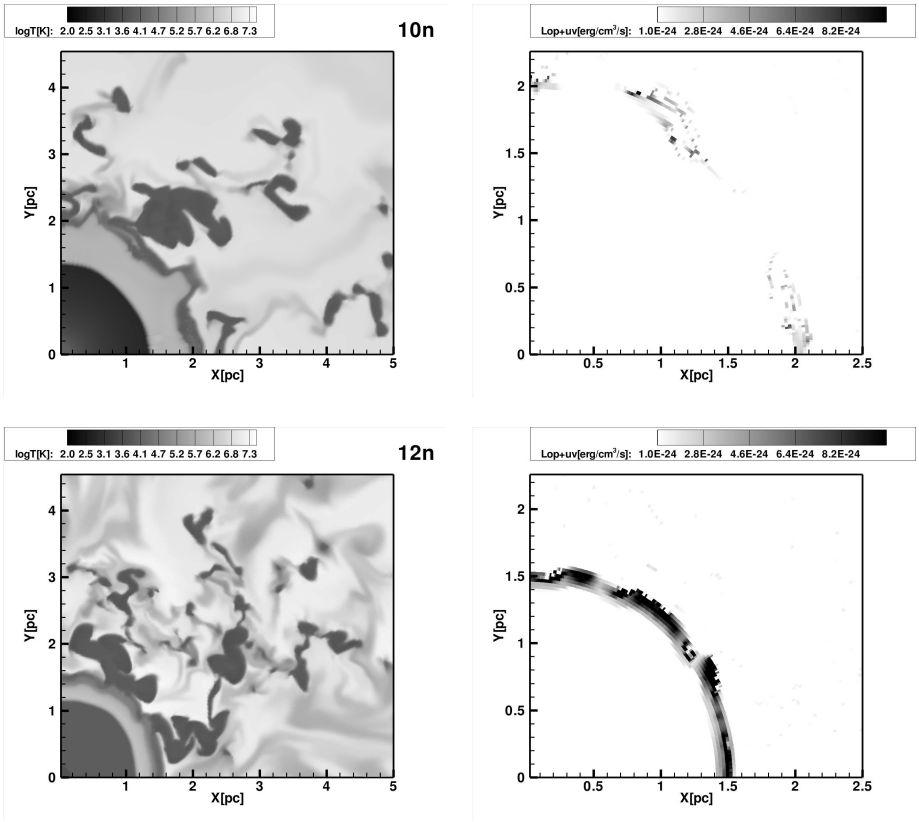

Figure 4.13: Temperature and density emissivity for the non-rotating models, 10n model in the upper panels and 12n for the lower panels. The time snapshot chosen for each model is the collision between the blue and red supergiant shell, when, because of gas density enhancement and temperature rise, the collision zone emits at maximum as for a circumstellar gas with $10^4 < T < 10^6$ K, emission calculated according to the cooling curve implemented in our hydrodynamical code. For the upper panel, 10n model, this happens as shown in Fig. 4.9 lower left panel. The lower panels, 12n model, present the same situation of maximum emission due to collision between the blue and red supergiant shells, captured by the middle right frame in Fig.4.10. A more pronounced spherical wind nebula is visible in this case at about 1.4 – 1.6 pc.

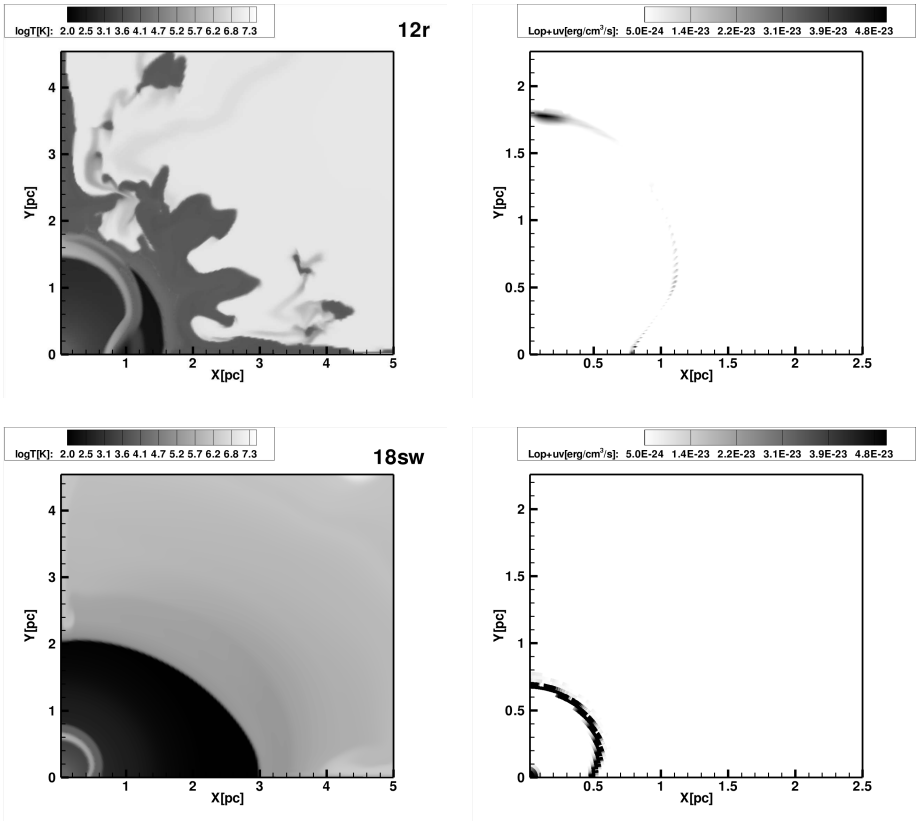

Figure 4.14: Same as Fig. 4.13 temperature and maximum of density emissivity for the density distribution of the circumstellar gas with $10^4 < T < 10^6$ K, as calculated according to the cooling curve implemented in our hydrodynamical code. The upper left panel shows in the temperature and corresponding of maximum emissivity for middle right panel of the Fig. 4.11 for model 12r and the last two snapshots correspond to the 18sw model peaked as maximum of emissivity from the upper right panel of Fig. 4.12.

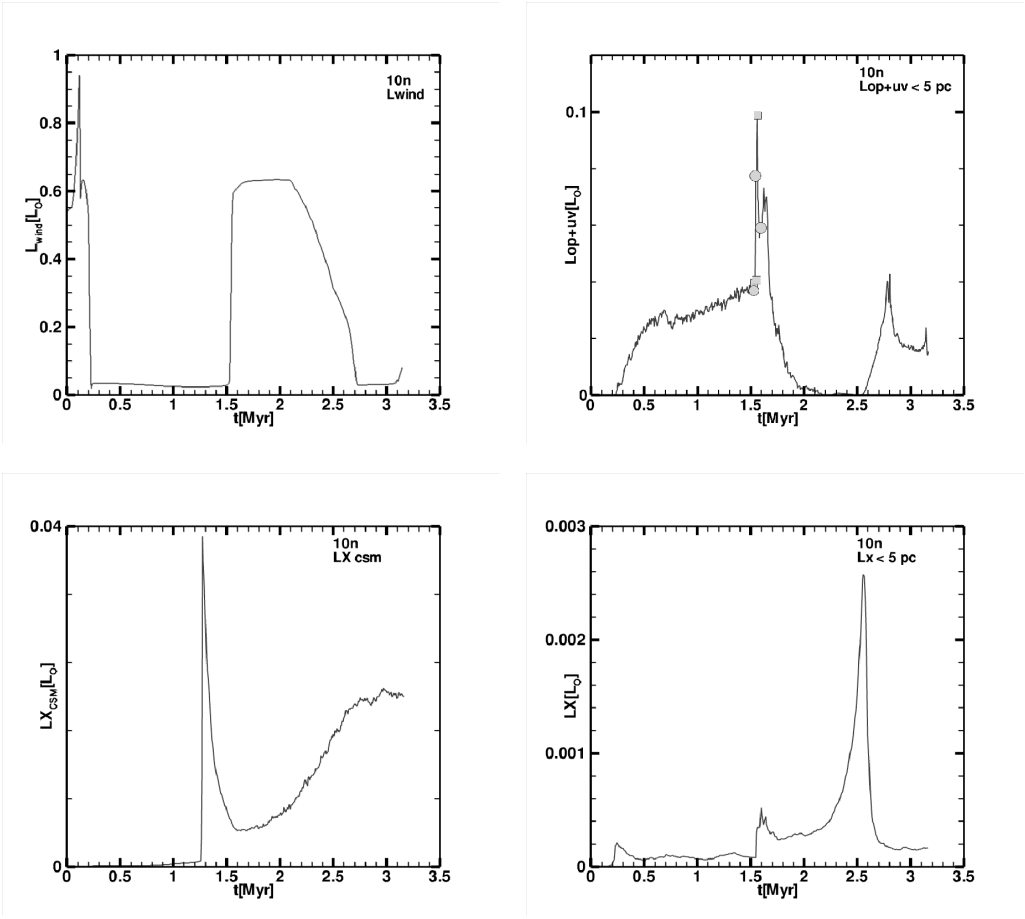

Figure 4.15: A comparison of various quantities as calculated from the 2D simulations of 10n model. The upper left panel shows the time dependent mechanical luminosity calculated from the stellar evolution model with the point zero as the start of our 2D simulations. The upper right panel shows the total luminosity as for a gas with $10^4 < T < 10^6$ K. Here only the blue supergiant nebula (the inner 5 pc from a sphere with 45 pc radius) is shown. The lower left panel shows the total luminosity as for a gas with $10^6 < T < 10^9$ K for the entire 45 pc sphere. The lower right panel shows the same quantity but for the blue supergiant nebula (inner 5 pc). The squares and circles represent consecutively, where in time each of the six panels of Fig. 4.9 correspond to.

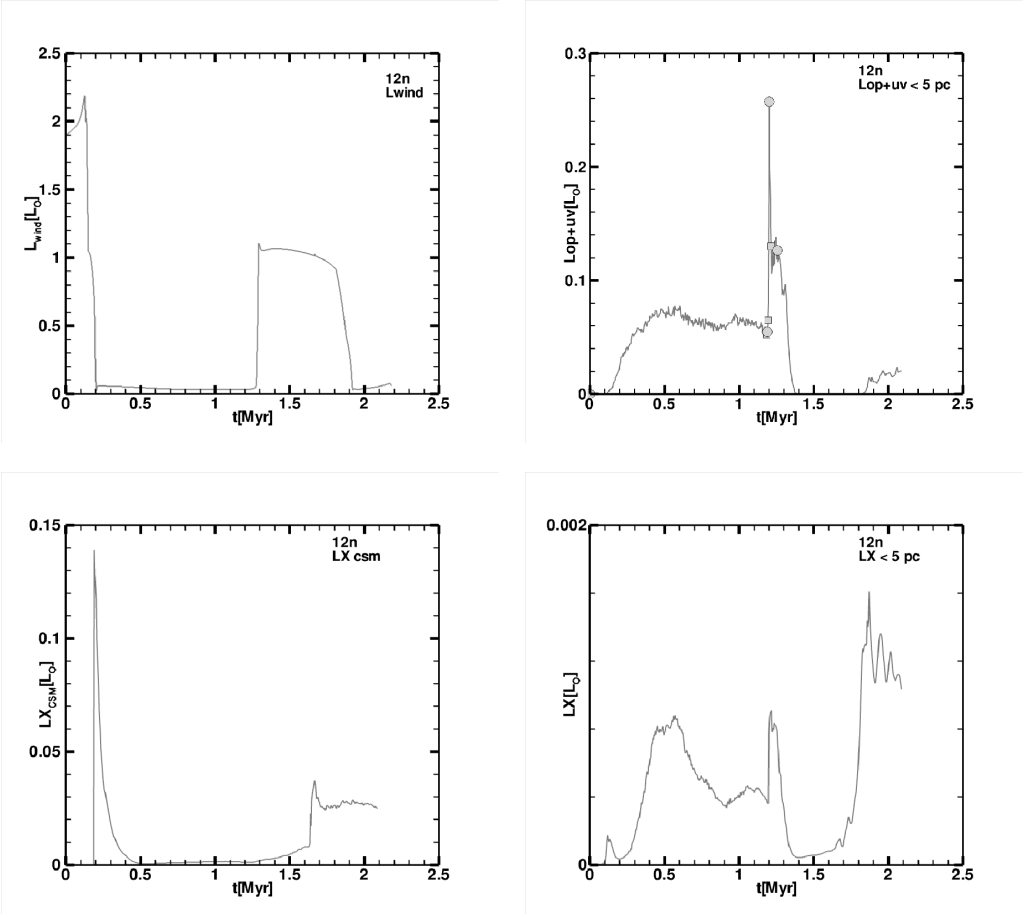

Figure 4.16: Same as Fig. 4.15 but for model 12n. The symbols show each of the panels of Fig. 4.10.

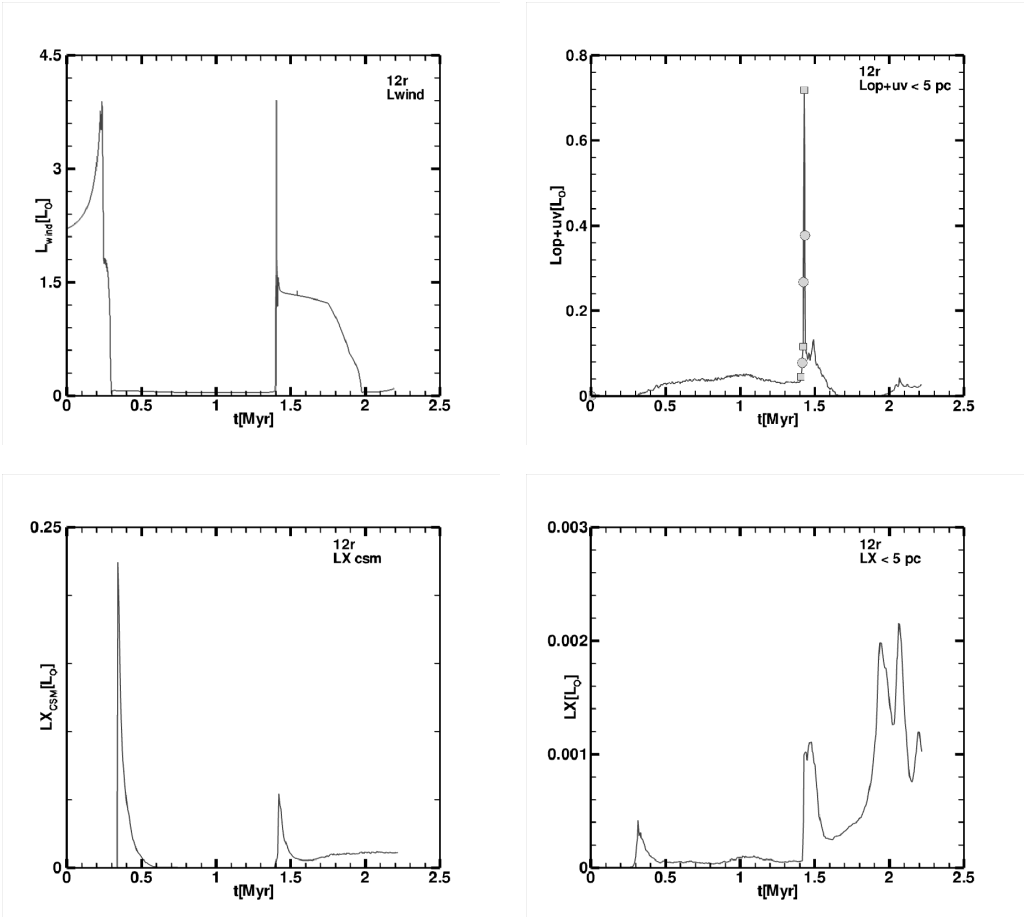

Figure 4.17: Same as Fig. 4.15 but for model 12r. The squares and the circles (in a consecutive order) represent each of the panels from Fig. 4.11.

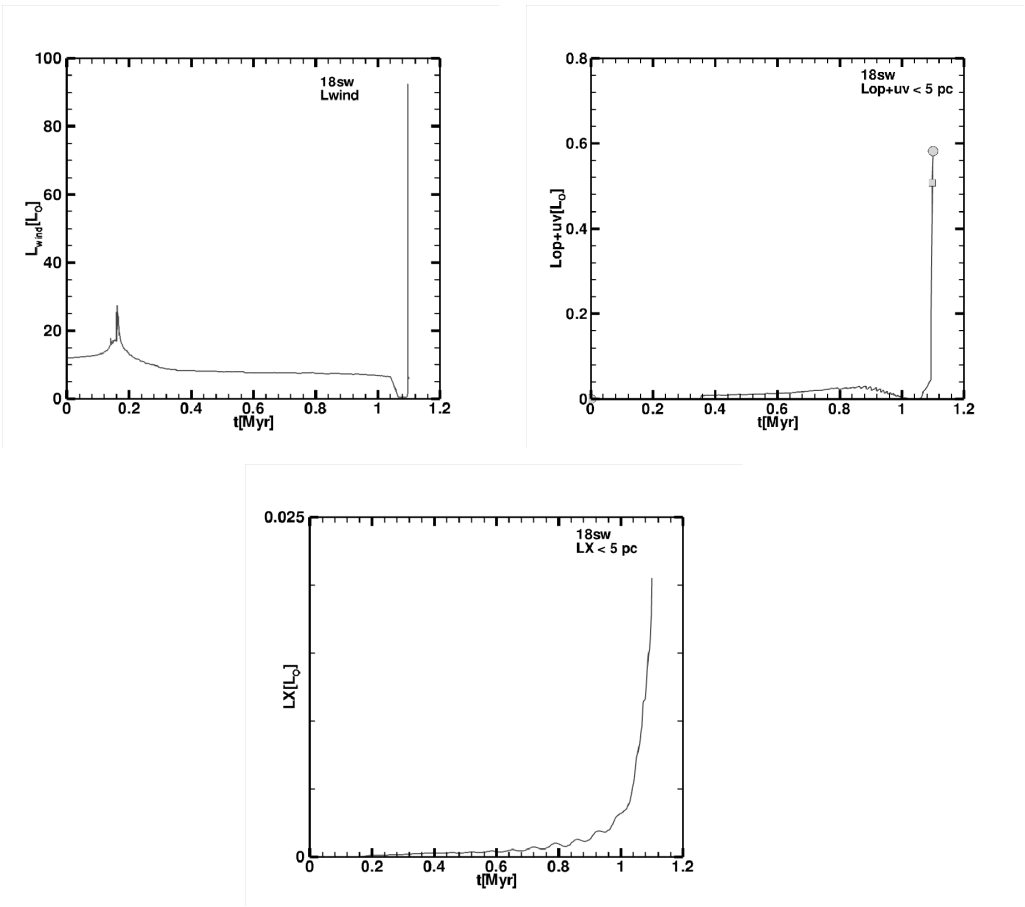

Figure 4.18: Same as Fig. 4.15 but for model 18sw. The X-ray emission from the lower panel is only calculated as for the BSG nebula. The square represents the left panel of Fig. 4.12 while the circle shows the right panel.

Chapter 5

A new mechanism to form mid-latitude circumstellar rings

Abstract

Massive stars eject winds throughout their life time. The interaction between the winds produced during various evolutionary stages can form circumstellar nebulae that are observed in nature. We seek to investigate possible mechanisms for the formation of the outer rings observed around SN 1987A nebula through wind-wind interaction from a rotating single star. From stellar evolution calculations, including rotation, we obtain the time dependence of the stellar wind properties and of the stellar radiation field. These are used as input for hydrodynamic calculations for the development of the circumstellar medium throughout the star's life. We present the results of models derived from the evolutionary model of a rotating single star of 18 $M_{\odot}$. At the end of the main sequence stage, this star first enters a blue supergiant post-main sequence stage, where it rotates close-to-critical for an extended period. Later, towards the end of core helium burning, it becomes a red supergiant. Before exploding as supernova, the star becomes a blue supergiant for a second time. We find a new mechanism capable of producing mid-latitude circumstellar rings, relating to the anisotropic wind ejected during the first blue supergiant stage. During the red supergiant stage the slower red supergiant wind is accumulated in a shell around the central star. Due to the previously accumulated non-spherical blue supergiant wind, this shell is broken into two parts, with a high-density, ring-shaped intersection at mid-latitudes, which has some similarity to the outer circumstellar rings of SN 1987A. While our models are far from corresponding to the SN 1987A ring system quantitatively, we conclude that the formation of mid-latitude rings from single stars may be possible. A detailed reproduction of the SN 1987A rings requires further studies.

Introduction

During their life massive stars have strong winds ejecting material into their surroundings. In their post-main sequence stages stars can make several blue loops in the Hertzsprung-Russell (HR) diagram, spending a very short period in the red-to-blue transition, Langer [1991b]. Each of these specific stages produces a circumstellar shell (Chiţă et al. [2010a], Chiţă et al. [2010b]) (hereafter Paper II and III respectively). In the transition from the main

sequence to the red side of HR diagram, a red supergiant (RSG) wind accumulates in a shell at the point where the the thermal pressure of the previously emitted and shocked main-sequence wind material and the ram pressure of the RSG wind are equal (García-Segura et al. [1996b]). When the star moves from the red to the blue side of the HR diagram, a blue supergiant (BSG) wind is produced that sweeps up the preceding RSG wind into an expanding shell.

The interaction between winds in the circumstellar material around the stars that go through these particular stages can be observed since it produces visible nebulae. The observation of SN 1987A in the Large Magellanic Cloud presented a major astronomical surprise. The progenitor star was a blue supergiant and its pre-supernova circumstellar medium formed a highly structured triple ring nebula.

Theoretical models attribute the circumstellar rings to binary mergers of massive stars, (Podsiadlowski et al. [1991], Lloyd et al. [1995], Podsiadlowski et al. [2005]). Alternative models using single star wind-wind interactions were constructed as an explanation of the triple ring nebula around SN 1987A (Burrows et al. [1995], Crotts & Heathcote [2000], Martin et al. [1995], Meyer et al. [1997], Woosley et al. [1997]). Chiţă et al. [2008] (hereafter Paper I) showed that single stars, which have just left the RSG branch, can produce multiple ring nebulae. However, while emission geometries similar to those found in the SN 1987A ring system were found in this paper, these models failed to produce triple-ring *density* structures — which is required to reproduce the SN 1987A rings since due to the supernova outburst, all dense circumstellar material was ionized and radiates.

Using a similar approach as presented in Paper I, here we present two CSM models which are derived from an 18 $M_\odot$ stellar evolution calculation (cf., Paper III). The details of the stellar evolution model, including its mass, its initial chemical composition, and its evolution in the HR diagram, represent well what is thought to correspond to the progenitor of Supernova 1987A.

Stellar models and computational technique

For our hydrodynamical calculations, we use input from the stellar evolution sequence Model 18sw (Woosley, priv. com.), where the initial rotation rate is scaled to 380 $\mathrm{km\,s^{-1}}$ (cf. Paper III). The BSG nebula formed from this input has also been discussed in Paper III. The central star spends 12.15 Myr in the MS stage, where it expels around 0.42 $M_\odot$. During the post-main sequence stages, the total mass lost sums up to about 0.67 $M_\odot$, but the time the star spends in this stages is relatively short. By modifying the wind output during the last evolutionary phase, we derived two test models from the original wind parameters of Model 18sw.

For the first test model (hereafter Test1), we have only modified the RSG stage by increasing its duration, from 0.0257 Myr to 0.150 Myr (see Fig. 5.2). While with this modification, Model Test1 is no longer self-consistent, the duration of the RSG stage in massive stellar evolution models is quite uncertain. It may thus be justified to consider it as a parameter in our investigation. The mass loss and wind velocity values for this stage, as well as the wind parameters of the first and the second BSG stages, are not changed with respect to the original

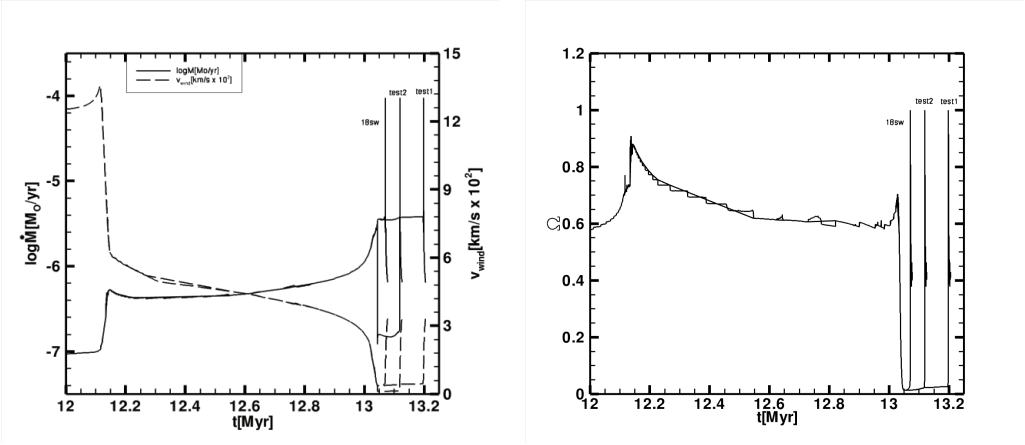

Figure 5.1: Wind parameters of our models during the post-main sequence stages, starting with the end of main sequence evolution. The starting point of the time axis represents the starting point for our 2D simulations. The left panel shows the time dependence of the stellar mass loss rate (solid line) and the terminal wind velocity (dashed line). In the right panel, we represented the time dependence of the ratio of the stellar rotation rate versus its critical rotation rate, Ω, for the post-main sequence stages.

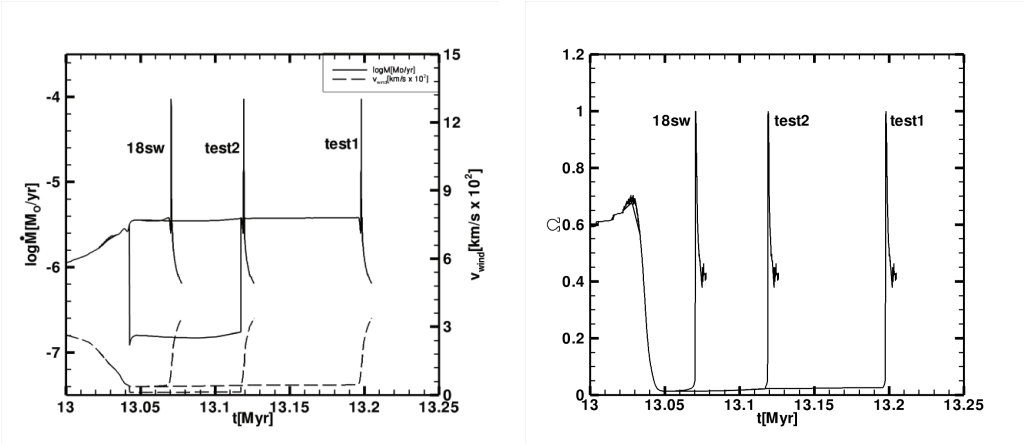

Figure 5.2: As Fig. 5.1 but only for the last two stellar evolution stages, starting at an age of 13 Myr.

Model 18sw.

In the second test model (hereafter Test2), we have modified the wind parameters of the first BSG stage and of the RSG stage of Model 18sw. During the first BSG stage, we smoothened the model values of the wind mass-loss rate as a function of time, rotational velocity and wind velocity by interpolation (see Fig. 1). This has little effect on the hydro-

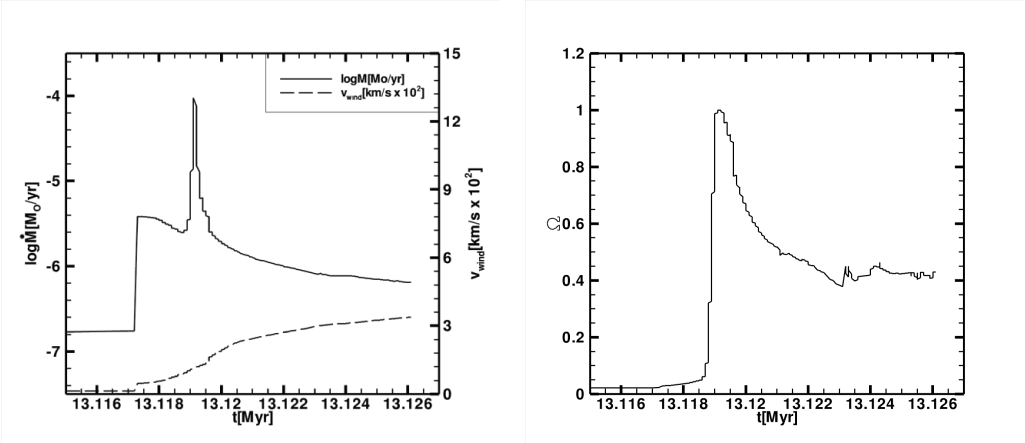

Figure 5.3: Time dependence of wind mass loss, wind velocity (left panel) and ratio of rotation to critical rotation rate (right panel) for Model Test2, for the final BSG stage.

dynamic evolution of the circumstellar medium except that it reduces the numerical noise. The duration of the RSG stage was chosen to be only half of that of Model Test1, the (highly uncertain) mass loss rate during this stage has been decreased by a factor of 1.5, and the RSG wind velocity has been reduced to a fixed value of 10 $\mathrm{km\,s^{-1}}$. The wind parameters for the second BSG stage are identical to those of Model Test1 and Model 18sw.

The ZEUS 3D code developed by Stone et al. [1992] and Clark [1996] was used to perform our computations. This is a three dimensional, ideal (non-resistive, non-viscous, adiabatic), non-relativistic, magneto-hydrodynamical, Eulerian explicit code which solves the coupled partial differential equations as function of time and space on a fully staggered grid. Radiative cooling is included by solving the energy equation implicitly according to Mac Low et al. [1989]. The plasma cooling curve of Smith et al. [2008] is employed in our calculations.

We compute the evolution of the circumstellar material (CSM) in 1D as the star evolves from the main sequence until the pre-supernova stage. We employ 1000 grid points over a radius of 45 pc and we assume an interstellar medium with a density of 20 $\mathrm{cm^{-3}}$. At the end of main sequence, we map the 1D model onto a 2D spherical grid to compute its further evolution. The radial component of the grid is resolved with 1000 grid points for 45 pc, where 900 grid points are used for the inner 5 pc, and 100 grid points for the outer 35 pc. The angular coordinate has 200 grid points over 90 degrees. This method has been used by García-Segura et al. [1996,a,b] and van Marle et al. [2005, 2007] and also Papers I, II, III. The effect of photoionization was included in the simulations by calculating the Strömgren radius along each radial grid line as described in García-Segura et al. [1999], van Marle et al. [2005, 2007, 2008] and Papers I, II, and III. The number of ionizing photons is computed according to the effective temperatures and surface gravities taken from the stellar evolution model, by interpolating in a grid of model atmospheres for massive OB stars of solar metallicity computed with the FASTWIND non-LTE code (Puls et al. [2005]) as described in Lefever et

al. [2007] and Papers I, II, and III.

Results

In Paper III we have discussed the 1D and 2D results obtained for Model 18sw. After 12.15 Myr spent on the MS, the circumstellar matter consists of a hot bubble from 2 to 38 pc with a large photo-ionized region from 18 to 38 pc. During a post-main sequence period of 0.94 Myr, no BSG shell sweeps up, but the BSG wind material remains in the hot bubble. During the short time (0.0257 Myr) spent by Model 18sw in the RSG stage, no RSG shell forms either. The second BSG stage lasts for 0.0089 Myr when Model 18sw reaches critical rotation. A BSG shell forms at ~ 0.5 pc, which moves outwards reaching 0.8 pc before the supernova explosion.

Here we present the 2D results obtained from Models Test1 and Test2. As explained in the previous section, these models differ in the treatment of their wind parameters.

Model Test1

By the time our model has left the main sequence, its circumstellar material consists of the MS shell from 38 to 42 pc and the hot bubble stretching from 2 to 38 pc. We showed in Paper II that, at the onset of the BSG wind, no shell sweeps up material from the hot bubble. Here the situation is identical,as wind material from the first BSG stage is injected into the hot bubble, forming a low density region, with most of the material settled around and somewhat above the equatorial plane. For a long period of time (0.8959 Myr) during the first BSG stage Model Test1 rotates faster than about 60% of critical rotation (see Fig. 5.1). As a consequence the angular distribution of the ejected wind material is aspherical. However, the BSG shell cannot sweep up hot bubble material, but the ejected material remains inside the shocked main sequence wind material.

Towards the end of the first BSG stage, the mass loss increases and the wind velocity decreases. The ram pressure drops compared with the thermal pressure of the hot bubble. A thin dense RSG shell forms at the point when the ram pressure and the thermal pressure become equal. The RSG stage lasts for 0.150 Myr, and produces a dense spherically symmetric shell situated at about 3 pc (see Fig. 5.4), which develops no instabilities. This shell moves outwards over a distance of 2 pc within a timescale of 100,000 yr.

The second BSG stage, which drives the central star again towards critical rotation, lasts for 8900 yr, as seen in Fig. 5.3. Fig. 5.4, which displays the CSM density distribution during the final evolutionary stages of Model Test1. While the original Model 18sw did not produce a shell from the swept-up RSG wind, due to the increases RSG lifetime in Model Test1, such a shell is produced. The lower two subplots of Fig. 5.3 show that an hourglass-shaped shell is swept up by the final BSG wind, visible at 0.2 pc, and later at 0.6 pc. However, while the pre-supernova density distribution shows a mid-latitude kink in the hourglass-shaped shell, this model does not produce ring features at mid-latitudes.

Table 5.1: Circumstellar material properties for the outer and inner rings calculated for model Test2, and measured for SN 1987A (see Pun et al. [2007], Crotts & Heathcote [2000], Lundqvist et al. [1996], Sugerman et al. [2005]): density, radius, velocity and kinematic time scale.

Object / Model		Radius pc	Density 10^{-23} g cm s^{-1}	Velocity km s^{-1}	Time scale yr
SN 1987A	Inner ring	0.2	2000	10	2×10^4
	Outer ring	0.6	100	26	
Test2	"Inner ring"	0.2	7	80	2300
	"Outer ring"	0.3	3.75	130	

Model Test2

Similar to Model Test1 an aspherical region with BSG wind material settles into the hot bubble, during the first BSG stage. At the end of the first BSG stage a RSG shell forms at the point where the ram pressure equals the thermal pressure of the shocked main sequence wind material. The RSG stage of Model Test2 lasts for 0.075 Myr.

Some 1.078 Myr after the beginning of our simulations, the RSG shell begins to move inwards. This motion of the shell is not equally fast in all directions (see Fig. 5.5, middle panels). The pressure in the equatorial region is higher then over the poles, leading to faster movement along the equatorial plane at low latitudes. Two parts of the shell collide at a latitude of ~45 degree. This forms initially a "tail" which becomes more confined (see Fig. 5.5 lower left and right panels) after about 13 000 yr.

The situation is inherently stable: a low density zone (the hot bubble) is pushing a shell into the high density wind. It is a decelerating shell, so it is not found to be Rayleigh-Taylor unstable, and once that tail is formed there is nothing to destroy it. Once it is sitting inside the hot bubble separated from the rest of the shell, the tail is a high-density feature that is compressed on both sides by thermal pressure. Due to its high density it will have a lower temperature than the surrounding material. As a result it is subject to a cooling instability, which keeps the tail compressed and prevents it from expanding and dispersing.

The shell moves inward at supersonic speed (compared to the sound speed in the receiving medium, the free-streaming wind). The "tail" is a density feature left behind by the inward motion. At the base of the shell, where this tail density feature merges with the RSG shell, a high density ring forms, whose properties do resemble to some extent the outer rings observed around SN 1987A.

At the onset of the second BSG stage a BSG shell forms at 0.2 pc. The "tail" together with the asymmetric and confined RSG shell (see Fig. 5.6 middle panels) are wiped out in the collision with the BSG shell.

Comparison to SN 1987A

The nebula around SN 1987A: The circumstellar gas around the SN 1987A nebula progenitor has been ionized by the strong burst of extreme UV and soft X-ray radiation (Blinnikov et

al. [2000], Lundqvist et al. [1996]). This radiation was produced when the shock front of the stellar explosion broke through the surface of the star. The cooling of this gas has produced a ring in emission that has been observed since the SN explosion. Fainter, more complex structures were observed with the Hubble Space Telescope and revealed an equatorial inner ring and two outer thin rings (Burrows [1995], Burrows et al. [1995]). Summarizing, the circumstellar material around the progenitor of the SN 1987A was thus flash-ionized by the SN radiation pulse and remains visible today through recombination cooling.

The geometry of the outer rings is partially controversial because of the inclination of the southern outer ring relatively to the northern outer ring. The increasing X-ray and UV flux from this interaction will reionize parts of the nebular structure that were invisible before, thereby revealing new features (Luo et al. [1994], Crotts et al. [1995]). Light echoes from the SN explosion have lit up most of the circumstellar structure showing an hourglass shaped bipolar nebula.

The outer rings of the SN 1987A have a density of about 10^{-21} g cm^{-3}, while that of the inner ring is about 10^{-20} g cm^{-3} (Pun et al. [2007]). The radius of the outer rings is of 0.6 pc and they move outwards with about 26 km s^{-1} (Crotts & Heathcote [2000]). The planar inner ring is situated at 0.2 pc from the progenitor star, and it expands outwards with a velocity of 10 km s^{-1} (Lundqvist et al. [1996], Sugerman et al. [2005]).

Comparison with our models: Our single stars models, Test1 and Test2 have evolved through multiple transitions during their post-main-sequence stages. The resulting pre-supernova circumstellar material differs from that of SN 1987A in several respects.

We do not obtain high enough densities for the inner ring in the case of Model Test1. The inner ring of our hourglass nebulae has a density of about 3.8×10^{-23} g cm^{-3} which is smaller than the density derived for the inner ring of 2×10^{-20} g cm^{-3}. However, the geometry of the circumstellar material of Model Test2 it is qualitatively closer to the geometry of the triple ring nebula of SN 1987A.

For our Model Test2, the RSG shell (Fig. 5.5) forms a comet-like tail. At the point where this tail merges with the asymmetric RSG shell, a ring of higher density forms at 0.3 pc (see Fig. 5.6 right upper panel), with a density of about 3.75×10^{-23} g cm^{-3}. This can be interpreted as a progenitor for the outer ring nebula (see Table 5.1). The mass in the RSG shell, mostly contained in the high density ring, is about 0.07 $M_\odot$, representing twice the amount calculated for the outer rings of SN 1987A. At the onset of the second BSG wind, a swept up hour-glass shell forms with an inner disk density of 7×10^{-23} g cm^{-3} which travels with about 80 km s^{-1} during 2300 yr.

Discussion

Most previous models for the rings of SN 1987A so far have focussed on the last 20 000 yr of evolution which represents the kinematic timescale of the rings, disregarding the earlier evolution. As a mechanism for the formation of the observed ring structures, many authors have looked into the interaction between a RSG and a BSG wind. Kwok [1982], Balick et al. [1987] present a model that involves an equatorial high-density BSG wind pushing into a previous slow RSG wind. After the interaction a bipolar shaped nebula or wind-blown

bubble is produced (Woosley [1988], Woosley et al. [1988], Weaver et al. [1977], Arnett et al. [1989], Chevalier & Emmering [1989], Fransson et al. [1989], Luo et al. [1994], Wang & Mazzali [1992]). Blondin & Lundqvist [1993] modeled the ring nebula within 2D time-dependent hydrodynamic calculations of interacting stellar winds, assuming reasonable values for mass-loss rate and expansion velocity of stellar winds for RSG and BSG stages as well as an *ad hoc* asymmetry function of the RSG wind. This model uses a simple cooling law and creates images which reproduce the ring geometry only if the outer rings are identified with the limb-brightening along peanut-shaped bubbles. Collins et al. [1999] used the wind compressed model of Bjorkman & Cassinelli to provide the equatorial RSG high density structure. However the central star is required to rotate at 30 % of the break-up rotation rate. To spin up the envelope they invoke a binary merger in which a companion spun up the envelope then merges with the primary's core (Livio & Soker [1988]). However none of these models have given a satisfactory explanation of the outer rings but only modeled the inner ring. As a consequence more complex models involving a binary companion have been suggested (Podsiadlowski et al. [1991], Lloyd et al. [1995]). Many extensive efforts to explain the evolution of the progenitor and the circumstellar surrounding the supernova have been made but they remain speculative.

In Paper I we have shown that a model that uses two kinematic components, an (almost) stationary shell due to a RSG wind and an expanding hour-glass structure due to a BSG wind, can explain the formation of multiple ring-shaped nebulae. There, using a model of a 12 $M_\odot$ single star, we obtained emission density structures similar to the ones observed around objects like Sher 25, with a pair of polar caps and and inner ring. Over a period of 18,000 yr, the polar caps and the inner ring where moving to lower latitudes. However, these rings, in shape similar to the rings of SN 1987A, become visible due to a transient ring-shaped emission, but not due to ring-shaped density structures. While the emission in the model of Paper 1 was triggered by shock ionization due to the collision of two shells, the explosion of SN 1987A has photoionized its surroundings, and in this case the emission and the density structures are identical.

Following the promising idea of the formation of outer rings from this previous paper, we computed Model 18sw, in Paper III (with a mass of 18 $M_\odot$). The stellar evolutionary track in the HR diagram, from the BSG stage to the RSG stage and back to the BSG stage before the supernova explosion, is similar to what has been deduced for the SN 1987A progenitor star. The stellar and wind parameters make this model a possible good test case for obtaining the outer rings as from the collision of the RSG and BSG shell. However the duration of the RSG stage of Model 18sw (only 0.0257 Myr) turned out to be too short, since no RSG shell was formed.

We have increased the duration of the RSG stage in Model Test1. The longer time spent in the RSG stage has indeed allowed a RSG shell to form. However, this shell was so far away from the central star (3 pc) that the BSG hour-glass shell had no time to collide with it before the star exploded as supernova. Without the collision between the two shells we could not obtain a high density region that could give rise to the outer rings.

In addition we constructed Model Test2. During the RSG stage, the duration of which we reduced to half compared to Model Test1, the wind parameters were modified. These modifications are motivated by uncertainties in the mass loss rate and life time of red supergiants

which are still under a large debate (see Paper II). The results we obtained for the RSG shell structure are quite different from the previous model. Due to the reduced RSG wind velocity, the BSG wind material in the hot bubble pushes the RSG shell inwards. This leaves behind a tail of high density at mid-latitudes. The intersection between the RSG shell and the tail forms a high density region which corresponds to a ring in 3D space. The radius of this ring in our 2D computations is at about 0.2 pc, before the BSG wind sweeps up the previous RSG wind material to form an hour-glass shell.

As outlined above, the circumstellar gas around SN 1987A has been photoionized by the supernova outburst. For fully ionized gas, emission scales with the density squared. In Fig. 5.7 we have plotted the particle number density squared for two different times of Model Test2, calculated assuming that all material is hydrogen. In this figure we can distinguish an ”outer ring” (see Fig. 5.6 right upper panel) and an ”inner ring” (see Fig. 5.6 right lower panel). By the time the inner ring of high density material appears (see Fig. 5.7 left panel), the outer ring is almost dissolved (see Fig. 5.7 right panel). The values which we obtain for the density and velocity of the ”inner ring” are qualitatively reasonable but the times when these structures occur does not correspond well to the case of SN 1987A. While this model is still far from representing the circumstellar medium of SN 1987A, its density structure has qualitative similarities. It obtains mid-latitude rings with a high density contrast and with roughly the right dimensions. It also develops an equatorial ring, even though later in time.

Our models show that the circumstellar structures are quite sensitive the the wind parameters during the final evolution, as well as to the duration of the final evolutionary stages. A full scan through the parameter space is beyond the scope of this work, but might reveal models with properties even closer to those of the circumstellar material of SN 1987A. For example, Fig. 5.6 shows that the ring feature visible in the upper two plots reaches the Y-axis (the axis of rotational symmetry) too early, before the star ends emits a fast BSG wind and before it explodes. A model starting a BSG wind at the time corresponding to the right or left plot of Fig. 5.6 could potentially produce mid-latitude winds which survive until the explosion of the central star. In fact, the BSG wind is then expected to compress the ring feature even further, thus enhancing the density contrast between the ring material and the connecting features.

On the other hand, from our models it remains unclear whether the ring structure which occurs in our model is stable. It will require 3D-calculations to show whether this is indeed the case. We conclude that the idea of reproducing SN 1987A’s triple ring nebula from the interacting winds of a rotating single star is well worth pursuing in the future.

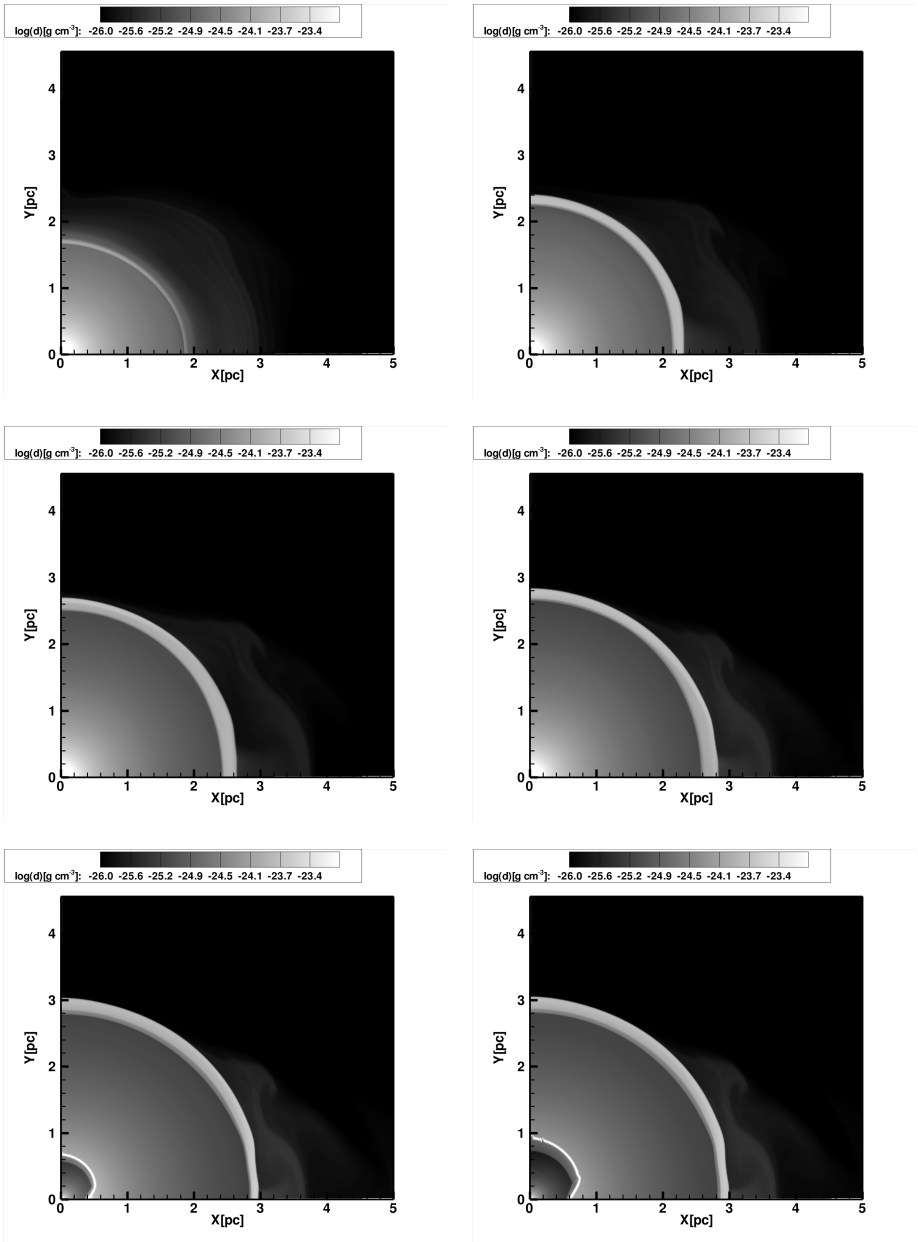

Figure 5.4: Snapshots of the density distribution of the circumstellar medium, showing the inner part of 5 pc from a 2D grid with 45 pc, at the onset of the second BSG stage for Model Test1. The upper left frame is taken 1.07 Myr after the starting point of our 2D simulations and shows the onset of the blue supergiant wind and a spherical symmetric shell at 3 pc. After about 1.15 Myr, the blue supergiant wind sweeps up the preceding red supergiant wind (upper right frame) to form an hour-glass shell (lower left frame), situated at 0.5 pc. The lower right frame is depicted before the supernova explosion.

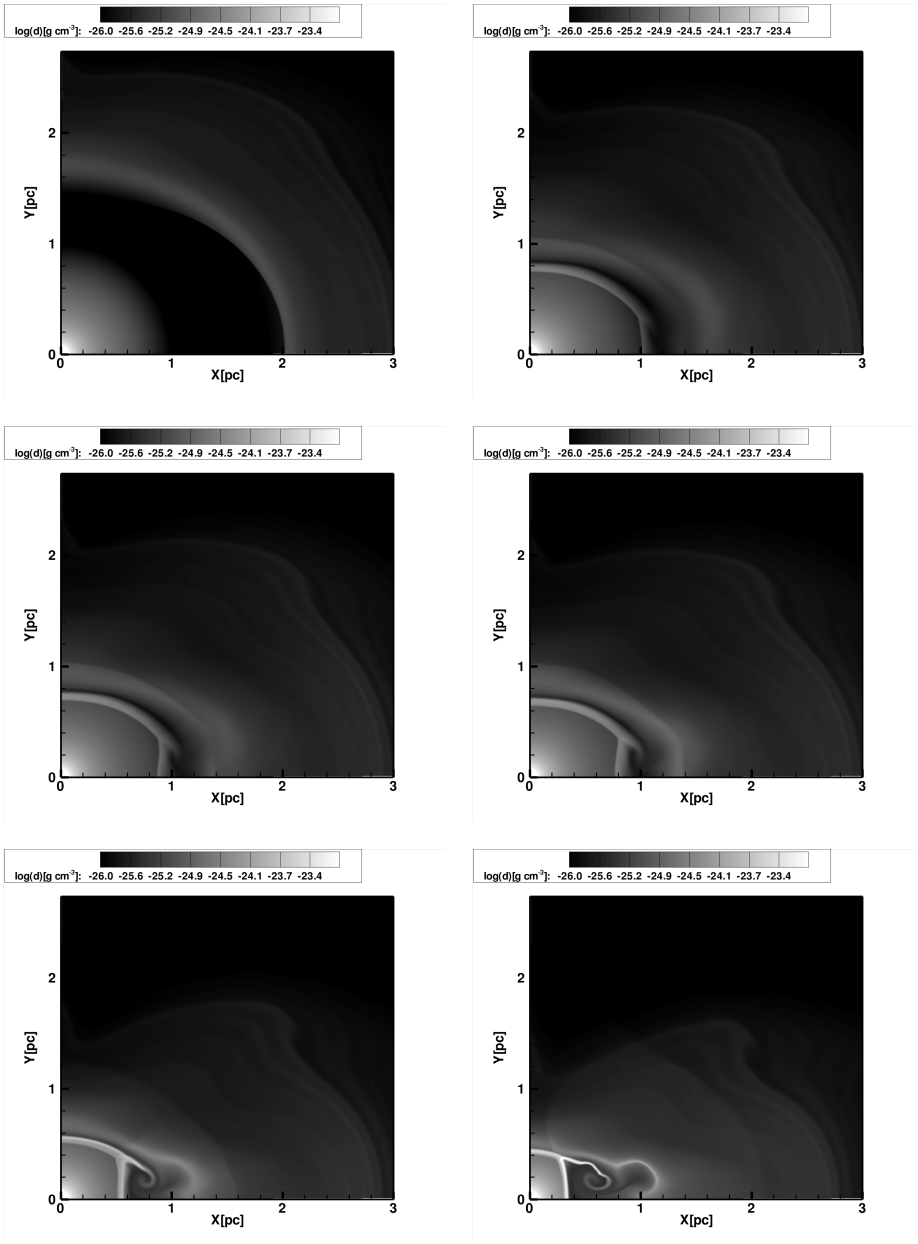

Figure 5.5: Same as Fig. 5.4 but for Model Test2. The upper left frame shows the inner 3 pc CSM distribution, 1.07 Myr after the start of the 2D calculations, at the onset of the red supergiant stage. The previously ejected BSG wind material is aspherical due to close to critical rotation of the central star. This material, during a period of 18,000 yr, pushes against the RSG shell, forming a cometary tail as seen in the right lower panel, 1.095 Myr after the start of te 2D calculations.

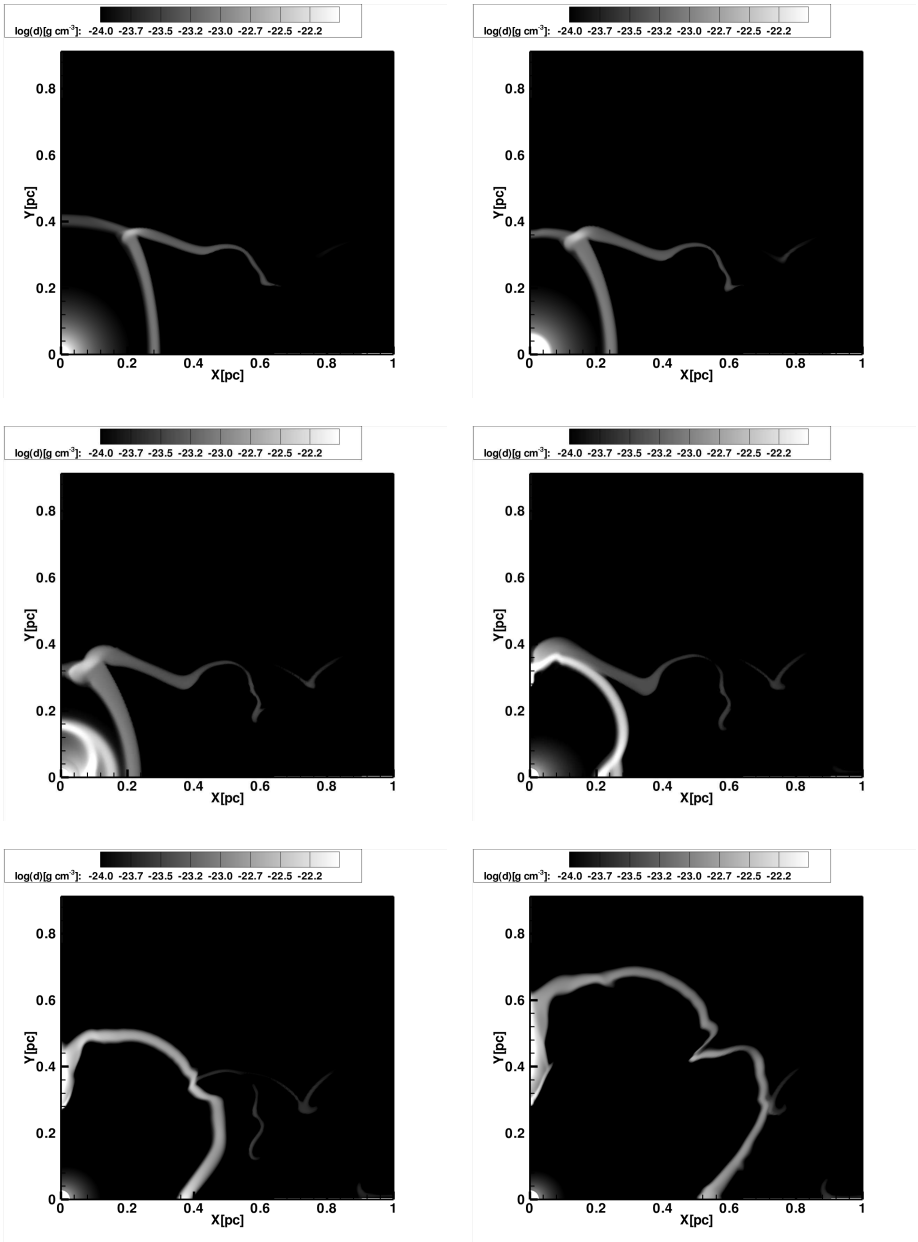

Figure 5.6: Density distribution of the inner 1 pc of Model Test2, 1.096 Myr after the onset of the 2D run. The merger of the cometary tail with the asymmetric RSG shell forms a high density ring, in the upper right panel. Once the hour-glass BSG shell sweeps up RSG wind material, middle left panel 11 Myr after the start of the 2D calculations, and collides with the RSG shell, lower panels, the cometary tail disappears.

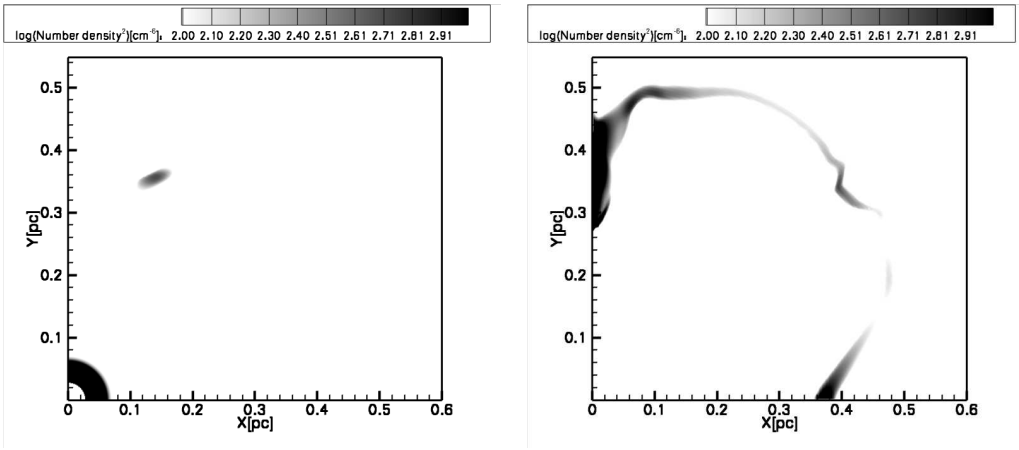

Figure 5.7: Number density squared calculated if all circumstellar material is assumed to be hydrogen. The left and right panels are calculated from the Fig. 5.6 right upper panel and right lower panel respectively.

Chapter 6

Nederlandse Samenvatting

Het leven van zware sterren van geboorte tot dood

Sterren geven licht omdat ze hun eigen energie produceren. Het grootse deel van hun evolutie (de "hoofdreeks") wordt hun energie geleverd door de fusie van waterstof tot helium in hun kern. Deze energie ontsnapt uiteindelijk uit de ster in de vorm van licht en, in veel mindere mate, in de vorm van een sterrenwind bestaande uit deeltjes. Afhankelijk van hun (oorspronkelijke) massa hebben sterren verschillende eigenschappen tijdens hun leven op de hoofdreeks. Hoofdreekssterren zoals onze zon zijn geel, warm (6000 graden) en zij leven ongeveer 10 miljard jaar. Sterren die minder zwaar zijn dan onze zon, zijn koeler en roder en kunnen langer leven, terwijl zwaardere sterren heet (meer dan 25000 graden) en blauw zijn en door hun verkwisting van brandstof slechts een paar miljoen jaar leven. Tijdens het hoofdreeks-stadium blijft de temperatuur van een ster en ook zijn helderheid zo goed als constant. Wanneer het waterstof in de kern opgebrand is aan het eind van dat stadium, kunnen de helderheid en de temperatuur van een ster dramatisch veranderen. De temperatuur loopt op zodat nu helium gefuseerd kan worden. Het lot van een ster na de hoofdreeks wordt bepaald door zijn gewicht bij geboorte. Als de massa minder is dan acht zonsmassa's zal de kern na het verbranden van helium uiteindelijk ineenschrompelen tot een witte dwerg en stoot daarbij zijn buitenste lagen af en vormt zo een zogenaamde planetaire nevel.

Zwaardere sterren kunnen rode superreuzen (RSG voor "red supergiant") worden of lumineuze blauwe variabele sterren (LBV), afhankelijk van hun oorspronkelijke massa. Rode superreuzen zijn relatief koele sterren met een zeer grote diameter (groter dan de baandiameter van de aarde). LBVs zijn extreem heldere blauwe superreuzen. Sterren met een gewicht tussen 8 en 20 zonsmassa's evolueren naar een RSG-stadium en worden blauwe superreuzen (BSG). Na deze zogenaamde "blauwe lus" worden ze voor de tweede keer tijdens hun leven een RSG. Als de ster zo zwaar is als 20 tot 30 zonsmassa's betekent het RSG-stadium het einde van hun evolutie. Nog zwaardere sterren met een massa tussen 30 en 50 zonsmassa kunnen worden Wolf-Rayet (WR) sterren en verliezen dan razendsnel massa in de vorm van sterrenwind (rond 10^{-5} zonsmassa's per jaar). De allerzwaarste sterren met een massa van meer dan 50 zonsmassa's worden LBV-sterren. Deze zwaarste sterren in het universum branden alle elementen op totdat ze een ijzer-nikkel-kern vormen. Het fuseren van ijzer in zware elementen in de kern kost energie in plaats van dat het energie oplevert. Nu de ster echt al zijn brandstof heeft uitgeput kan hij zijn eigen gewicht niet meer in balans houden. Middels een enorme supernova-explosie stort de kern van zulke sterren dan ineen en vormt een neu-

tronenster of een zwart gat. De lagen buiten de kern worden bij deze explosie uitstoten en vormen een supernova-rest.

De meeste sterren (zo niet alle) draaien om hun as. Als een ster snel genoeg roteert kan dat de evolutie van de ster significant beïnvloeden. Een snel roterende ster heeft in het algemeen een grotere helium-kern en is helderder dan een langzaam roterende ster met dezelfde massa. Als zo'n snel roterende ster explodeert als een supernova, dan kan deze explosie waargenomen worden als een "gamma-flits". Met zulke explosies gaan gigantische energie-uitstoten gepaard ($E \geq 10^{51}$ erg).

Waneer een ster deel uitmaakt van een dubbelstersysteem doorloopt deze in het algemeen een andere evolutie dan een enkele ster. In veel gevallen wordt massa overgedragen van de grootste naar de kleinste van de twee sterren. Op deze manier verandert de evolutie van beide sterren en worden hun temperatuur en helderheid gewijzigd.

Vingerafdrukken van de sterevolutie: circumstellair materiaal

Figure 6.1: Dit beeld toont een gebied in de Carina-nevel met sterren in allerlei stadia van geboorte tot dood. De nevel bevat tientallen heldere sterren met 50 tot 100 keer de massa van onze zon. Credit: NASA, ESA, N. Smith (University of California, Berkeley), and The Hubble Heritage Team (STScI/AURA)

Tijdens hun leven verliezen de meeste sterren massa door het uitstoten van een stroom van deeltjes ("sterrenwinden") in het interstellaire medium (ISM). Deze stroom van materiaal verlaat het oppervlakte van de ster en bereikt na een zekere afstand afgelegd te hebben een supersonische snelheid ten opzichte van het ISM. Op dit punt ontstaat een schok en veegt de sterrenwind materiaal uit het ISM op in een bolvormige schil. Tijdens het hoofdreeksstadium van een ster beweegt breidt de schil zich steeds verder uit en zo blaast de ster een

bel met een relatief constante dichtheid en (thermische) druk. Gezien vanuit het centrum kan de morfologie van de hoofdreeks-bel in verschillende stukken onderverdeeld worden. Het eerste stuk is de vrijelijk stromende sterrenwind die een constante snelheid heeft en een dichtheid proportioneel met de afstand tot de ster in het kwadraat. Het volgende deel van de circumstellaire bel bestaat uit geschokt wind-materiaal. Aan de buitenkant van de warme bubbel, kunnen wij de bewegende schil van geschokt interstellair materiaal vinden. Deze schil wordt bijeen geveegd en opgedreven door de hoge thermische druk van de sterrenwind in de hete bel.

Zware sterren zenden ultraviolet licht uit met hoge energie en kunnen zo het waterstof in hun omgeving ioniseren en een "H *II*-regio" creëren. Een ster kan niet al het materiaal rond zichzelf ioniseren en omdat de recombinatie van de gecreëerde ionen constant is in het gas, worden de fotonen van de ster continu geabsorbeerd. De maximale straal tot waar een ster gas kan ioniseren heet de Strömgren-straal, die die rand van de zogenaamde Strömgren-bol definieert. Als de Strömgren-bol zich verder uitstrekt dan de wind-bel, dan veegt de wind geïoniseerd gas op in plaats van koud, neutraal interstellair medium. Als de wind niet sterk genoeg is, kan de snelheid van de schil dan subsonisch worden en lost deze op. Maar bij een sterke wind (zoals in het geval van sterren die LBVs worden) is de thermische druk van de H *II*-regio onvoldoende om de snelle schil tegen te houden. De morfologie van de hoofdreeks-bel wordt zo gestructureerd in een regio met een binnenkant bestaand uit geschokt wind-materiaal, terwijl de buitenkant bestaat uit foto-geïoniseerd ISM.

Als een ster de verschillende stadia van zijn evolutie doorloopt, zal de sterrenwind en de resulterende circumstellaire nevel telkens verschillend van aard zijn. Een circumstellaire nevel bevat zo informatie over de evolutie van de centrale ster. In eerste instantie heeft de sterrenwind enkel interactie met het interstellaire medium. Nevels uit ISM verschillen van de nevels die materiaal bevatten uit de opeenvolgende stadia van de sterrenwind die materiaal bevatten die zich in eerst in de ster bevond. Circumstellaire nevels vormen de directe omgeving van zware sterren op het moment van hun explosie als supernova. De structuur (massa, grootte) van circumstellaire nevels beïnvloedt zo de evolutie van de supernova-resten die overblijven nadat de ster in de explosie is verdwenen.

Zoals eerder genoemd kan bij het einde van hoofdreeks-stadium een zware ster kan een RSG, BSG of een LBV worden. Wanneer de ster de hoofdreeks verlaat, verandert niet alleen de binnenkant van de ster, maar ook de eigenschappen van zijn sterrenwind: de hoeveelheid massa-verlies gaat omhoog terwijl de windsnelheid omlaag gaat. Dit proces beïnvloedt de vorm van de circumstellaire nevel die de ster vormt. Een nieuwe schil van post-hoofdreeks wind-materiaal wordt gevormd als een gevolg van de veranderde wind-eigenschappen. Ook de hoeveelheid van hoge-energie fotonen gaat omlaag aangezien de oppervlaktetemperatuur van de centrale ster omlaag gaat. De regio buiten het geschokte wind-materiaal is nu dus niet meer foto-geïoniseerd. De thermische druk gaat ook omlaag en de schil begint langzaam op te lossen. De regio van geschokt wind-materiaal begint nu een nieuwe schil in de oude H *II*-regio te ploegen. Als vervolgens de ster een sneller roterende BSG wordt, dan gaat de windsnelheid omhoog en wordt al het bestaande materiaal in de nevel opgeveegd in een snel uitbreidende schil. Omdat een BSG erg snel roteert is zijn wind sterk anisotroop, oftewel niet bolvormig. Dit zorgt ervoor dat een BSG sterk gestructureerde nevels maakt met een rotatiesymmetrie. Deze nevels kunnen bijvoorbeeld ringen of polaire kappen bevatten.

Circumstellaire nevels kunnen ons dus vele interessante dingen leren over het leven en de dood van de zwaarste sterren in ons universum.

Dit proefschrift

Dit proefschrift vormt de eerste generieke studie van de structuur van nevels rond zware sterren: sterren met massa van meer dan acht keer dan die van onze Zon. Het werk in dit proefschrift legt de nadruk op de hydrodynamische modellering van de nevels rond enkelvoudige, massieve sterren, van hun geboorte tot hun supernova-explosie. Met onze modellen wij kunnen een voorspeling maken over de massa en de temperatuur van de nevel, zijn morfologie en de chemische elementen die erin aanwezig zijn.

Het proefschift bevat de volgende resultaten:

- **Hoofdstuk 2:**

In dit proefschrift, en in het bijzonder in hoofdstuk 2, modelleren wij de circumstellaire nevel van sterren met een massa van 8, 12, and 20 zonsmassa's, gedurende hun hele leven. De nadruk wordt gelegd op de RSG-stadia van deze sterren. Tijdens post-hoofdreeks stadia kunnen sterren evolueren door meerdere blauwe en rode superreus-fasen, afhankelijk van hun massa, compositie en rotatiesnelheid. De evolutie-modellen gepresenteerd in dit hoofdstuk ondergaan langdurende superreus-stadia na de hoofdreks. Tijdens deze fase ontwikkelt de RSG-ster een RSG-schil op het punt waar de vrije sterrenwind de thermische druk ontmoet van de warme hoofdreeks-bel dichtbij de ster. Door turbulentie bevatten RSG-schillen sterke Rayleigh-Taylor instabiliteiten, die plaatsvinde bij de contact-discontinuïteit tussen de RSG-schil en het gescholte hoofdreekswind-materiaal. Tot op moment dat de instabiliteiten niet-lineair kunnen groeien, vormen zich klonten in de RSG-schil en kan het materiaal uit deze schil zich mengen met materiaal uit de warme bel. Later evolueren de rode superreuzen in blauwe superreuzen en worden de RSG-schillen compleet weggevaagd. Vervolgens worden de sterren in de modellen voor de tweede keer een rode superreus nadat de hun helium hebben opgebrand en maken ze nieuwe RSG-schillen met een grotere massa dan in de eerste rode superreus-fase. RSG-schillen zijn dus essentieel om te begrijpen hoe (bipolaire) emissienevels zich kunnen vormen rond blauwe superreuzen.

- **Hoofdstuk 3:**

Dit hoofdstuk presenteert resultaten voor een snel roterende ster met een massa van 12 zonsmassa's. Voor een periode van 10 000 jaar gedurende de RSG-fase breidt een blauwe schil met de vorm van een zandloper zich uit binnen de bolvormige RSG-schil. De snellere delen van de schil die bij de polen van de ster worden uitgestoten raken als de RSG-schil als eerste. De botsing creëert een paar van hete"poolkappen" met een hoge dichtheid. Met verloop van tijd verplaatst de zone van de botsing zich naar beneden langs de RSG-schil en beperkt zich tot de regionen rond het rotatievlak van de ster. Op hetzelfde moment ontstaat er door een interne botsing binnen de BSG-wind een tweede equatoriale ring, die expandeert met een snelheid van zo'n 18 km/s. Deze structuren zijn vergelijkbaar met de nevel die waargenomen is rond de blauwe superreus Sher 25 (zie het beeld op de kaft).

- **Hoofdstuk 4:**

In dit hoofdstuk worden modelberekeningen getoond die de eigenschappen van het circumstellaire materiaal voorspellen voor snel en langzaam roterende blauwe superreuzen. De interactie tussen wind en het interstellaire medium is gemodelleerd voor alle stellaire evolutionaire fasen, van de hoofdreeks tot de supernova explosie voor modelsterren met massa van 10, 12 en 18 zonsmassa's. Onze sterren blijven het grootste deel van hun leven in het hoofdreeks-stadium. In hun post-hoofdreeks-fase maken sterren met een massa van 10 en 12 zonsmassa's een blauwe lus na hun eerste rode superreus-fase. Voor de supernova-explosie worden de sterren voor de tweede keer een rode superreus. Wij kijken ook naar een modelster met 18 zonsmassa's die waarschijnlijk dezelfde evolutie heeft doorgaan als de ster die, na een korte rode en een blauwe superreus-fase, in 1987 supernova is gegaan (SN 1987A). Als deze ster snel roteert vormt de botsing tussen de BSG-wind met een zandloperfiguur en de bolvormige RSG-schil een gestructureerde nevel die opmerkelijke overeenkomsten vertoond met de nevel rond SN 1987A. Als de ster langzaam roteert, dan vormt er zich slechts een bolvormige nevel.

- **Hoofdstuk 5:**

Wij presenteren in dit hoofdstuk voorlopige resultaten van ons onderzoek naar de mogelijke manieren voor de vorming van de ringen in de nevel rond SN 1987A door wind-wind interactie. Bij de einde van de hoofdreeks fase wordt onze modelster een blauwe superreus. Bij het opbranden van helium wordt het een rode superreus. Voor de supernova-explosie als supernova wordt de ster wordt voor de tweede maal een blauwe superreus. Tijdens deze fase neemt de ster een de grootst mogelijke rotatiesnelheid aan. In de fase ervoor heeft de RSG-wind zich opgehoopt in een schil rond de ster, Omdat de wind van de eerste blauwe superreus-fase niet sferisch is, is deze schil is in twee stukken gebroken, met een grote ring van materiaal met een grote dichtheid in het equatoriale vlak. Deze ring is op meerdere vlakken vergelijkbaar met de ring-nevel rond SN 1987A.

Chapter 7

Rezumat in limba română

Viaţa stelelor: geneza, clasificare şi evoluţie

Stelele se formează cu ajutorul gazului molecular. Aceşti nori de gaz molecular, reprezentând o fracţiune minimă in mediul interstelar, pot avea mase de 1000 de ori mai mari decât masa soarelui, in timp ce temperatura lor poate ajunge la valori de 30 K, sau -243,15 C. Un nor molecular este inconjurat de o porţiune de gaz atomic care protejează astfel moleculele din interior de câmpul de radiaţie ultravioletă. Această combinaţie de nor molecular se poate contracta, fragmenta iar aceste fragmente pot forma mai departe proto-stele, in cele din urmă permiţand fuziunii nucleare sa aibă loc şi să dea naştere unui nucleu fierbinte de materie. Dacă masa iniţială este mai mare decât 0.1 $M_{\odot}$, temperatura sa se poate ridica la 10^7 K. In funcţie de masa sa iniţială şi de compoziţie, steaua nou formată poate trăi uneori mai puţin de un milion de ani, alteori un miliard de ani, transformându-se constant pe măsură ce evoluează.

Cea mai indelungată perioadă din viaţa unei stele se numeşte perioada principală. In aceast interval de timp sursa energiei din interiorul nucleului este fuziunea hidrogenului in heliu. Energia degajată este expulzată de la suprafaţa stelei sub formă de radiaţie şi vânt stelar. Dacă stelele aflate in perioada principală sunt ca şi soarele nostru, atunci fac parte din categoria stelelor galbene, calde (6000 K) si pot trăi in jur de 10 miliarde de ani. Stelele care sunt mai puţin masive decât soarele nostru, sunt ”stele reci”, roşii şi pot trăi o vreme mai indelungată, in timp ce stelele enorme pot fi albastre, foarte calde ($\geq$ 25000 K) şi pot trăi pentru doar câteva milioane de ani. In timpul perioadei principale, temperatura si luminozitatea stelei rămân aproape constante. In momentul in care hidrogenul din nucleu este epuizat, la sfârşitul perioadei principale, luminozitatea si temperatura stelei se pot schimba dramatic. Temperatura din nucleu se măreşte iar steaua incepe să fuzioneze heliu. Viitorul unei stele este acum determinat de masa sa iniţială. Dacă masa iniţială a fost mai mică de 8 $M_{\odot}$, in momentul epuizării heliului, nucleul stelei se va contracta intr-o stea pitică albă, aceasta degajând largi porţiuni de materie de la suprafaţă şi formând o nebuloasă planetară. Stele mai masive pot deveni supergigantice roşii sau variabile albastre luminoase, depinzând de masa iniţială a stelei centrale. Stelele supergigantice roşii sunt stele reci cu un diametru foarte mare. Variabilele albastre luminoase sunt stele extrem de luminoase, albastre.

Stele cu mase intre 8 şi 20 $M_{\odot}$ evoluează către stadiul de supergigantică roşie şi pot deveni supergigantice albastre, facând un aşa numit ”drum albastru”, inainte de a se intoarce pentru a doua oară in stadiul de supergigantică roşie şi a exploda ca supernovă. Stelele cu mase in jurul a 20 până la 30 $M_{\odot}$ işi incheie existenţa ca supergigantice roşii inainte de explozia ca

supernovă. Stelele masive cu mase intre 30 şi 50 $M_\odot$ pot deveni stele Wolf-Rayet (WR), pierzând masă sub formă de vânt stelar cu o rată incredibilă (aproape 10^{-5} $M_\odot$ yr^{-1}), in timp ce stele cu masa mai mare de 50 $M_\odot$ devin Variabile Luminoase Albastre. Marea majoritate a stelelor masive continuă existenţa lor trecând prin toate stadiile de ardere nucleară până la formarea unui nucleu de fier. Dar fuziunea nucleului de fier in alte elemente mai grele mai degrabă costă energie decât produce energie aşa că o dată ce sursa de energie din nucleu este epuizată, nucleul işi pierde echilibrul şi implodează intrucât forţele de presiune nu mai pot balansa gravitaţia. Aceste stele işi incheie viaţa ca o stea neutronică sau ca o gaură neagră. Steaua explodează ca supernovă ca o consecinţă a colapsului nucleului, iar invelişul nucleului stelar este expulzat in exterior.

Stelele se rotesc in marea majoritate a cazurilor. Dacă rotaţia este suficient de rapidă, cursul evoluţiei stelare se poate schimba. O stea care se roteşte va dezvolta un nucleu tipic de heliu mai mare, steaua in sine devenind mai luminoasă decât o stea cu aceeaşi masă care nu se roteşte. Dacă steaua care se rotşte rapid explodează ca supernovă, explozia poate fi conectată cu explozia de raze gamma. Aceste fenomene se produc cu eliberarea unor cantităţi masive de energie de ordinul a $E \geq 10^{51}$ erg in doar câteva secunde. Fenomenele de explozie de radiaţie gamma pot apărea şi in cadrul unor anumite tipuri de sisteme binare stelare, formate din obiecte compacte ca de pildă stele neutronice sau găuri negre. Când o stea face parte dintr-un sistem binar, evoluţia sa poate diferi major de cea a unei stele singulare. In sisteme binare inchise, materia stelară poate fi transferată de la steaua masivă la steaua mai puţin masivă. Drept rezultat, evoluţia ambelor stele se schimbă, iar luminozitatea şi temperatura de la suprafaţă sunt alterate.

Amprente lăsate de evoluţia stelară: materia circumstelară

In decursul vieţii lor, marea majoritate a stelelor pierd masă prin ejecţia de vânt stelar in mediul interstelar. Acest jet de materie pleacă de la suprafaţa stelei cu viteze supersonice pâna la o distanţă rezonabilă de steaua centrală. In momentul in care intâlneşte mediul interstelar se crează o undă de şoc. In acest punct, vântul stelar incepe să asimileze gaz din mediul interstelar formând un inveliş foarte dens, ca o "crustă". In timpul perioadei principale, acest inveliş de vânt stelar se indepărtează de steaua centrală in mediul interstelar formând o regiune de gaz fierbinte cu densitate şi presiune termică constantă. Morfologia regiunii de gaz fierbinte din perioada principală pornind de la steaua centrală se poate impărţi după cum urmează: prima parte este alcătuită din vântul stelar liber ejectat cu o viteză constantă in timp, a cărui densitate scade cu raza la pătrat. Următoarea porţiune a regiunii de materie circumstelară conţine material de vânt stelar provenit din unda de şoc. La marginea regiunii de gaz fierbinte se află invelişul de materie al mediului interstelar. Acest inveliş a fost asimilat de vântul stelar şi se indepărtează in exterior datorită presiunii termice foarte mari a regiunii de gaz fierbinte.

Stelele masive emit şi fotoni cu energie mare, creând astfel o regiune fotoionizată de hidrogen atomic H II. O stea nu poate ioniza la infinit o cantitate imensă de materie inconjurător şi din cauza recombinării care are loc permanent in gaz, fotonii sunt absorbiţi continuu. Raza maximă la care steaua poate ioniza gaz se numeşte raza Strömgren, iar aceasta

Figure 7.1: Această imagine reprezintă doar o porţiune din nebuloasa Carina in care se găsesc stele in toate stadiile de evoluţie. Nebuloasa conţine stele cu mase cuprinse intre 50 şi 100 de mase solare. Credit: NASA, ESA, N. Smith (University of California, Berkeley), and The Hubble Heritage Team (STScI/AURA)

defineşte marginea sferei de gaz ionizat ca sferă Strömgren. Dacă sfera Strömgren se extinde dincolo de regiunea de gaz fierbinte formată de vântul stelar, asimilarea de materie se produce cu gaz fotoionizat mai degrabă decât cu mediul rece interstelar. Daca vântul stelar ejectat este puternic, ca in cazul stelelor care devin Variabile Luminoase Albastre, presiunea termică a regiunii de gaz ionizat, H II, poate fi insuficientă pentru a putea opri invelişul rapid de materie. Dacă vântul stelar nu este puternic, viteza invelişului de material poate scădea sub viteza sunetului. Odată ce devine subsonic, invelişul de materie se poate dispersa. Materialul de vânt din şoc şi materialul interstelar ionizat sunt separate de o discontinuitate de contact. Morfologia regiunii de gaz fierbinte din perioada principală este structurată acum ca o regiune cu partea interioară formată din material de vânt din şoc, in timp ce partea exterioară este alcătuită din materie interstelară fotoionizată.

Aşa după cum am menţionat mai inainte, la sfârşitul perioadei principale, o stea masivă poate deveni o supergigantică roşie, o supergigantică albastră sau o Variabilă Luminoasă Albastră. Când steaua părăseşte perioada principală nu numai parametrii din interior se schimbă, dar şi parametrii de vânt stelar: variaţia de masă stelară pierdută se măreşte in timp ce viteza vântului ejectat descreşte. Acest proces influenţează nebuloasa circumstelară. Un nou inveliş de material de vânt stelar se formează ca o consecinţă a variaţiei parametrilor de vânt stelar. Numărul de fotoni cu energie foarte mare poate descreşte o dată ce temperatura de la suprafaţa stelei scade astfel regiunea de material de vânt stelar din şoc nu mai poate fi fotoionizată. Presiunea termică scade iar invelişul de material eventual incepe să se disperseze. Regiunea de material de vânt stelar din şoc incepe să formeze un nou inveliş de material in regiunea fotoionizată.

Nebuloasele care sunt alcătuite din materie interstelară se disting de nebuloasele care

conţin material prezent iniţial in steaua centrală. In decursul vieţii lor, aceste stele ejectează vânt stelar care interacţionează in primă instanţă cu mediul interstelar. In momentul in care steaua centrală trece prin stadii multiple de evoluţie, mediul circumstelar care alcatuieşte astfel nebuloasa circumstelară va conţine informaţii legate de evoluţia trecută a stelei. De asemenea, nebuloasele circumstelare constitue mediul inconjurător la momentul exploziei supernovei. Structura (masa, mărimea) nebuloaselor circumstelare va afecta evoluţia resturilor care rămân după explozia stelei centrale in supernovă.

Această teză

Aici este prezentat un studiu unic al mediului circumstelar pentru precursori de supernove: stele care se nasc cu o masă de opt ori mai mari decât a soarelui nostru. Esenţa acestei lucrări se concentreză pe modelării de nebuloase care se găsesc in jurul stelelor singure, masive, de la geneză şi până la finalul lor ca supernove. Din modelele noastre am fost capabili să prezicem masa, temperatura, structura geometrică şi elementele chimice prezente in nebuloasă.

Structura tezei este următoarea:

- **Capitolul 2:**

In această teză şi in particular in capitolul 2, modelăm mediul circumstelar al stelelor cu 8, 12 şi 20 mase solare, de-lungul vieţii lor, concentrându-ne atenţia pe stadiul de supergigantică roşie. In timpul perioadei post-principală, stelele pot evolua in stadii multiple de supergigantice roşii sau albastre in funcţie de masă, compoziţie şi rata de rotaţie. Modelele incluse in acest capitol petrec o periodă indelungată in stadiul de supergigantica roşie după perioada principală. In această fază, supergiganticele roşii dezvoltă invelişuri de material stelar in atmosfera lor creând astfel ”cruste” in punctul in care vântul stelar liber este oprit de presiunea termică a bulei de gaz fierbinte formată in perioada principală, aproape de steaua centrală. In invelişul de material din jurul supergigantice roşii se crează instabilităţi Rayleigh-Taylor, care apar la nivelul de discontinuitate dintre ”crusta” de material şi vântul stelar fierbinte al bulei de gaz formată in perioada principală. In momentul in care aceste instabilităţi incep să crească neliniar, invelişul de material capătă o structură foarte bine definită formând un grup de materie densă, un pâlc, şi mai mult materia crustei incepe să se amestece cu conţinutul de gaz din bula de gaz fierbinte. Mai târziu stelele evoluează către stadiul de supergigantică albastră, timp in care crusta de material este complet distrusă. Supergiganticele roşii sunt esenţiale pentru a inţelege nebuloasele din jurul supergiganticelor albastre.

- **Capitolul 3:**

Aici sunt prezentate rezultatele obţinute pentru o stea cu masa de $12\,M_{\odot}$. In decursul undei perioade de 10^4 ani, invelişul de vânt stelar sub forma unei clepsidre al unei supergigantice albastre, inaintează, mărindu-şi volumul, către invelişul de vânt in formă de sferă al supergiganticei roşii. Zona polară a clepsidrei ating partea interioară invelişului de vânt stelar al supergiganticei roşii. In urma acestei coliziuni se crează in regiunile polare o porţiune de gaz dens şi fierbinte. In timp, zona de coliziune se va muta in regiunea ecuatorială devenind mai concentrată in latitudine. Structuri similare cu cele obţinute cu modelul acesta sunt observate in jurul supergiganticei albastre Sher 25 (vezi imagine copertă).

- **Capitolul 4:**

In acest capitol sunt prezise o serie de proprietăţi ale mediului circumstelar pentru supergigantice albastre care se rotesc cu diverse viteze de rotaţie. Interacţiunea vânturilor lor stelare cu mediul exterior este urmărită in de-aproape prin toate stadiile de evoluţie stelară, de la perioada principală si până la stadiul de pre-supernovă pentru modele cu masele intre 10, 12 and 18 $M_{\odot}$. Aceste stele petrec cea mai mare parte a vieţii lor in perioada principală. In perioada post-principală, stele cu masa 10 and 12 $M_{\odot}$ trec printr-un stadiu de supergigantică albastră după un prim stadiu de supergigantică roşie. Inainte de a exploda ca supernovă, aceste stele trec printr-un al doilea stadiu de supergigantică roşie. In analiza noastră se găseşte şi un model care ar putea teoretic fi asemenător cu cel al supernovei SN 1987A, care a explodat ca supergigantică albastră după evoluţia rapidă ca supergigantică roşie. In cazul unei stele care se roteşte cu o viteză foarte mare, o nebuloasă cu o structură foarte bine definită se poate forma. Dacă steaua centrală se roteşte cu o viteză mică, se poate forma o nebuloasă sferică.

- **Capitolul 5:**

In acest capitol, sunt prezentate rezultate preliminare conţinând posibile modalităţi de formare a inelelelor observate in nebuloasa din jurul supernovei SN 1987A prin interacţia vânt-vânt. La sfârşitul perioadei principale, modelul nostru trece printr-un prim stadiu de supergigantică albastră devenind după arderea He in nucleu, o supergigantică roşie. Inainte de a exploda ca supernovă, steaua centrală devine pentru a doua oară o supergigantică albastră. In această perioadă, steaua centrală atinge o viteză de rotaţie critică. Datorită vântului asferic al primului stadiu de supergigantică albastră, invelişul de vânt stelar este impărţit in două părţi cu o densitate ridicată sub forma unui inel, care este oarecum similar cu mediul circumstelar din jurul SN 1987A.

Bibliography

Arnett, W.D., Bahcall, J.N. & Kirshner, R.P. 1989, ARA&A, 27, 629 (cited on page 94)

Balick, B., Preston, H.L. & Icke, V. 1987, AJ, 94, 164 (cited on page 93)

Bjorkman, J.E. & Casinelli, J.P. 1993, ApJ, 409, 429 (cited on pages 5, 47, and 62)

Blinnikov, S.I., Lundqvist, P., Bartunov, O.S.et al. 2000 ApJ, 532, 1132 (cited on page 92)

Blondin, J.M. & Lundqvist, P. 1993, ApJ, 405, 337 (cited on pages 10, 46, 51, 58, and 94)

Bodenheimer, P., Tenorio-Tagle, G. & Yorke, H.W. 1979, ApJ, 233, 85B (cited on page 22)

Brandner, W., Grebel, E. K., Chu, Y.H. & Weis, K. 1997, ApJ, 475, L45 (cited on pages 11, 51, and 74)

Brighenti, F. & D'Ercole, A. 1995a, MNRAS, 273, 443 (cited on pages 9 and 18)

Brighenti, F. & D'Ercole, A. 1995b, MNRAS, 277, 53 (cited on pages 9 and 18)

Burrows, C.J. 1995, ApJ, 452, 680 (cited on page 93)

Burrows, C.J., Krist, J., Hester, J. Jeff et al. 1995, ApJ, 452, 680 (cited on pages 10, 51, 58, 88, and 93)

Cherchneff, I & Tiellens, A. G. G. M. 1994, 34th HerstMonceux Conference, Circumstellar Media in the Late Stages of Stellar Evolution, Cambridge History Press, ed. R.E.S. Clegg, P. Meikle & I. Stevens, p. 232 (cited on page 61)

Chevalier, R.A. & Emmering, R.T. 1989, ApJ, 342, L75 (cited on page 94)

Chiosi, C. & Maeder, A. 1986, Ann. Rev. Astr. Ap., 24, 329 (cited on page 5)

Chiţă, S.M., Langer, N., van Marle, A.J., García-Segura,G. & Heger, A. 2008, A&A, 488, L37, (**Paper I**) (cited on pages 10, 18, 58, and 88)

Chiţă, S.M., Langer, N., van Veelen, B., van Marle, A.J. & García-Segura,G. 2010, submitted, (**Paper II**) (cited on pages 58 and 87)

Chiţă, S.M., van Veelen, B., Langer, N., van Marle, A.J. & García-Segura,G., 2010, submitted, (**Paper III**) (cited on pages 18, 46, and 87)

Clark, D.A. 1996 ApJ, 457, 291 (cited on pages 12, 21, 47, 63, and 90)

Collins, T.J.B., Frank, A. Bjorkman, J.E. et al. 1999, ApJ, 512, 322 (cited on page 94)

Crotts, A.P.S., Kunkel, W.E. & Heathcote, S.R. 1995, ApJ, 438, 724 (cited on page 93)

Crotts, A.P.S & Heathcote, S.R. 2000 ApJ, 528, 426 (cited on pages 10, 51, 58, 88, 92, and 93)

Dwarkadas, V.V. 2007, ApJ, 667, 226 (cited on pages 9, 18, 21, 32, and 35)

Eldridge, J.J. & Tout, C.A. 2004, MNRAS, 353, 87 (cited on page 4)

Eldridge, J.J., Genet, F., Daigen, F. & Mochkovitch, R. 2006, MNRAS, 367, 186 (cited on pages 22, 47, and 62)

Fransson, C., Cassatella, A., Gilmozzi, R. et al. 1989, ApJ, 336, 429F (cited on page 94)

García-Segura,G. & Mac Low, M.M. 1995a, ApJ, 455, 145 (cited on pages 8 and 18)

García-Segura,G. & Mac Low, M.M. 1995b, ApJ, 455, 160 (cited on pages 9, 10, and 18)

García-Segura,G. & Franco, J. 1996, ApJ, 469, 171 (cited on pages 13, 21, 22, 24, 47, 63, and 90)

García-Segura,G., Mac Low, M.M. & Langer, N. 1996a, A&A, 305, 229 (cited on pages 9, 10, 13, 18, 21, 47, 58, 63, and 90)

García-Segura,G., Langer, N. & Mac Low, M.M. 1996b, A&A, 316, 133 (cited on pages 9, 10, 13, 18, 21, 24, 25, 31, 32, 46, 47, 48, 58, 63, 66, 88, and 90)

García-Segura,G., Langer, N., Różyczka, M. & Franco, J. 1999, ApJ, 517, 767 (cited on pages 13, 22, 47, 63, and 90)

García-Segura,G. 2007, JKAS, 40, 147 (cited on page 50)

Harper, G., & Brown, A. 2006, ApJ, 646, 1179 (cited on page 36)

Harper, G., Brown, A., & Guinan, E. 2008, AJ, 135, 1430 (cited on pages 10 and 35)

Heger, A., Langer, N. 1998, A&A, 334, 210 (cited on pages 7, 47, 48, 59, and 74)

Heger, A., Langer, N., Woosley, S.E. 2000, ApJ, 528, 368 (cited on pages 13, 18, 19, 46, and 59)

Heger, A., Langer, N. 2000, ApJ, 544, 1016 (cited on pages 7, 13, 18, 19, 46, 50, and 58)

Hendry, M.A., Smartt, S.J., Skillman, E.D. et al. 2008, submitted arXiv:0803.4262 (cited on pages 51 and 74)

Hrivnak, B.J., Kwok, S. & Volk, K.M. 1989, ApJ, 346, 265 (cited on page 36)

Humphreys, R.M., Smith, N., Davidson, K. et al. 1997, AJ, 114, 2278H (cited on pages 10 and 35)

Hunter, I., Brott, I., Lennon, D.J. et al. 2008, ApJL, 676, L29 (cited on page 50)

Iben, I. & Renzini, A. 1983, Ann. Rev. Astr. Ap., 21, 271 (cited on page 5)

Jura, M., Velusamy, T. & Werner, M.W. 2001, ApJ, 556, 408 (cited on pages 10 and 36)

Kastner, J.H. & Weintraub, D.A. 1995, ApJ, 452, 833 (cited on page 36)

de Koter, A. 2008, IAUS, 250, 39D (cited on pages 7 and 34)

Kwok, S.O. 1982, ApJ, 258, 280 (cited on page 93)

Lamers, H.J.G.L.M. & Pauldrach, A.W.A. 1991, A&A, 244, L5 (cited on page 5)

Lamers, H.J.G.L.M. & Cassinelli, J.P. 1999, Introduction to Stellar Winds, Cambridge University Press, ISBN 0 521 59565 7 (cited on pages 5 and 7)

Langer, N. 1991a, A&A, 243, 155 (cited on page 52)

Langer, N. 1991b, A&A, 252, 669 (cited on pages 7, 45, 57, and 87)

Langer, N. 1998, A&A, 329, 551 (cited on pages 7, 47, and 61)

Langer, N. 2000 Science, 287, 2430 (cited on page 50)

Langer, N., García-Segura,G. & Mac Low, M.M. 1999, ApJ, 520L, 49L (cited on pages 10, 47, 48, 50, 58, and 62)

Lefever, K., Puls, J. & Aerts, C. 2007, A&A, 463, 1093 (cited on pages 13, 22, 47, 63, and 90)

Livio, M. & Soker, N. 1988, ApJ, 329, 764 (cited on page 94)

Lloyd, H.M., O'Brien, T.J & Kahn, F.D. 1995, MNRAS, 273, L192 (cited on pages 10, 51, 58, 88, and 94)

Luo, D. McCray, R. & Slavin, J. 1994, ApJ, 430, 264 (cited on pages 93 and 94)

Lundqvist, P. & Fransson, C. 1996, AJ, 464, 924 (cited on pages 92 and 93)

MacDonald, J. & Bailey, M.E. 1981, MNRAS, 197, 995 (**MB**) (cited on pages 12, 13, 21, and 47)

MacFadyen, A.I. & Woosley, S.E. 1999, ApJ, 524, 262 (cited on page 4)

Mac Low, M.-M., McCray, R. & Norman, M.L. 1989, ApJ, 337, 141 (cited on pages 21, 47, 63, and 90)

Marston, A.P., Chu, Y.-H. & García-Segura,G. 1994, ApJS, 93, 229 (cited on page 58)

Martin, C.J. & Arnett, D. 1995, ApJ, 447, 378 (cited on pages 10, 46, 51, 58, and 88)

Martin, C.D., Seibert, M., Neill, J.D. et al. 2007, Nature, 448, 780 (cited on pages 10 and 36)

Meyer, F. 1997, MNRAS, 285, L11 (cited on pages 10, 51, 58, and 88)

Nieuwenhuijzen, H. & de Jager, C. 1990, A&A, 231, 134 (cited on pages 19, 34, 46, and 59)

Noriega-Crespo, A., van Buren, D., Cao, Y. & Dgani, R. 1997, AJ, 114, 837N (cited on pages 10, 18, and 36)

Nota, A., Livio, M., Clampin, M.& Schulte-Ladbeck, R. 1995, ApJ, 448, 788 (cited on page 50)

Owocki, S., Cranmer, S.R. & Gayley, K.G. 1996, ApJL, 472, L115 (cited on pages 47 and 62)

Patel, M., Oudmaijer, R.D., Vink, J.S. et al. 2008, MNRAS, 385, 967 (cited on pages 10 and 36)

Perez-Rendon, B., García-Segura,G. & Langer, N. arXiv:0905.1101v1 (cited on pages 10 and 58)

Podsiadlowski, P., Fabian, A.C. & Stevens, I.R. 1991, Nature, 354, 43 (cited on pages 10, 51, 58, 88, and 94)

Podsiadlowski, P. & Morris, T.S. 2006, ASP, Conf.series, Vol.355, p.259, Stars with B[e] Phenomenon, Eds. M.Kraus & A.S.Miroshnichenko (cited on pages 10, 46, 51, 58, and 88)

Puls, J., Urbaneja, M.A., Venero, R. et al. 2005, A&A, 435, 669 (cited on pages 13, 22, 47, 63, and 90)

Pun, C.J.S. 2007, AIP, 937, 171 (cited on pages 92 and 93)

Reddy, B.E. & Hrivnak, B.J. 1999, AJ, 117, 1834 (cited on pages 10 and 36)

Rigon, L. 2003, MNRAS, 340, 191 (cited on page 4)

Schaller, G., Scharer. D., Meynet, G. & Maeder, A. 1992, A&AS, 96, 269 (cited on pages 3 and 57)

Smith, B., Sigurdsson, S. & Abel, T. 2008, MNRAS, 385, 1443 (**SM**) (cited on pages 12, 21, 34, 63, and 90)

Smith, N., Humphreys, R.M., Davidson, K. et al. 2001, AJ, 121, 1111 (cited on pages 10 and 35)

Smith, N. 2007, AJ, 133, 1034 (cited on page 51)

Smith, N., Bally, J. & Walawender, J 2007, AJ, 134, 846 (cited on pages 11, 51, 58, and 74)

Smith, N., Hinkle, K.H. & Ryde, N. 2009, AJ, 137, 3558 (cited on pages 10, 18, 35, and 36)

Smith, N. 2010, arXiv:1010.3720v1 (cited on page 8)

Sugerman, B.E.K., Crotts, A.P.S., Kunkel, W.E. et al. 2005, ApJS, 159, 60S (cited on pages 92 and 93)

Stone, J.M. & Norman, M.L. 1992, ApJS, 80, 753 (cited on pages 12, 21, 47, 63, and 90)

Ueta, T., Izumiura, H. Yamamura, I. et al. 2008, PASJ, 60, S407 (cited on pages 18 and 36)

van der Veen, W.E.C.J., Habing, H.J., & Geballe, T.R. 1989 A&A, 226, 108 (cited on page 36)

van Loon, J.T., Cioni, M.-R.L., Zijlstra, A.A. & Loup, C. 2005, A&A, 438, 273 (cited on pages 7 and 34)

van Marle, A.J., Langer, N.,García-Segura,G. 2005, A&A, 444, 837 (cited on pages 13, 21, 22, 47, 63, and 90)

van Marle, A.J., Langer, N.,García-Segura,G. 2006, ASP Conference Series, Vol. 355, p.203 (cited on pages 9 and 10)

van Marle, A.J., Langer, N.,García-Segura,G. 2007, A&A, 469, 941 (cited on pages 13, 21, 22, 47, 63, and 90)

van Marle, A.J., Langer, N., Yoon. S.-C.,García-Segura,G. 2008, A&A, 478, 769 (cited on pages 13, 22, 47, 62, 63, and 90)

Wang, L. & Mazzali, P.A. 1992, Nature, 355, 58 (cited on page 94)

Wareing, C.J., Zijlstra, A.A. & O'Brien, T.J 2007, MNRAS, 382, 1233 (cited on pages 10 and 36)

Weaver, R., McCray, R., Castor, J., Shapiro, P.& Moore, R. 1977, ApJ, 218, 377 (cited on pages 6, 8, 18, 22, 24, and 94)

Woosley, S.E. 1988, ApJ, 330, 218 (cited on pages 52 and 94)

Woosley, S.E., Pinto, P.A. & Weaver, T.A. 1988, Pub, ASAu, 7, 355 (cited on page 94)

Woosley, S.E. 1993, ApJ, 405, 273 (cited on page 4)

Woosley, S.E., Heger, A., Weaver, T.A. & Langer, N. 1997, astro-ph/9705146 (cited on pages 10, 51, 58, and 88)

Acknowledgments - Dankwoord - Un cuvânt de mulţumesc

I have had an amazing adventure as a PhD candidate! Not only I did have the opportunity to meet and work in the top astrophysics research group of the Sterrekundig Instituut Utrecht of Utrecht University, but also I was able to travel around the world for several conferences and collaborate with various scientists.

There is quite a lot of people that transformed my experience as PhD here in the Netherlands into an incredible journey through hydrodynamics as applied to massive stars winds and to whom I am very grateful:

My two promotors: Norbert Langer and Bram Achterberg, thank you very much for your scientific and moral support, for teaching and showing me how to tackle a scientific problem from an infinite number of angles and for always being there for me to answer to my “too trivial” questions; it took just a bit longer than expected to perfect this book, but I did it!

My reading committee members: Guillermo Garcia-Segura, Bram Achterberg, Rens Waters and Alex de Koter, thank you very much for your support and efforts in providing your scientific comments to make the best out of this thesis.

Dear Guille, thank you very much for creating the opportunity to visit you at the Institute of Astronomy in Ensenada, Mexico and learn all about the tricks with ZEUS code, but also about the necessity of a siesta. Moreover, thank you for your help with the papers and for the great moral support in the times when things were not so easy for me.

Beste Alex de Koter, hartelijk bedankt voor jouw commentaren op mijn proefschrift, voor de tijd dat wij samen hebben gezeten en over SED hebben gesproken en voor jouw ondersteuning en begrip.

Beste Rens Waters, hartelijk bedankt voor jouw commentaren wat betreft mijn proefschrift en voor het echt interessante gesprek over exoplaneten tijdens de terugreis van “hot and cool stars” conferentie in de VS.

Beste Allard Jan, mijn eerste kamergenoot, dankjewel voor jouw ondersteuning en geduld via mijn “te vaak gestelde vragen”, voor jouw grote hulp met ZEUS en met de artikels en vooral voor jouw immense hydro-kennis van waar ik heb veel geleerd.

Beste Bob, mijn collega van het eind van de SIU gang :-), dankjewel voor jouw hulp met mijn onderzoek, voor jouw ondersteuning en voor alle koffiepauzes waar wij altijd iets hebben gehad om psychoanalytisch te behandelen ;-).

Group meeting people for the stellar evolution and hydrodynamics: Jacco, Arend Jan, Evert, Rob, Selma, Maria, Axel, Onno, Matteo, Ines, Joke, thank you very much for all our interesting scientific discussions and to great times in our institute. To all my previous and new colleagues from SIU and to the ones from my epoch: Klaartje, mijn tweede kamergenoot ;-), bedankt voor grapjes en de leuke tijd in Mexico, Eveline, Ana, Theodora, Sandra, Elisabeth, Peter, Remco, Esteban, Hector, Michiel, Nikola, thank you for the great atmosphere you created in our institute. Our secretaries: Marion and Mariska, and our IT support: Ed and Sake, thank you for making sure things were running smoothly in the background.

And, of course, I enjoyed also the hydrodynamics as applied to life.

There are even more people that I am grateful to:

Dear Christoph, Dear Karen, thank you very much for your amazing support and always warm words, for the great times with delicious dinners and for always interesting discussions.

Dear Axel, hey creature :-) and Dear Catalina, my friend and paranimph, thank you for your moral support, delicious chilean dinners, the wines, the dancing and the cocktails :-).

Dear Dashinka, my east-european counterpart ;-), a “balshoie spasibo” for your friendship, for our numerous cola breaks during which we always talked about achieving the impossible limits of a human being, one way or another :-). I hope you will be happy in France and become a respectable top scientist in their institute, but also that you will keep you passion for extreme sports and things!

Dragă Emilia, iţi mulţumesc pentru că suntem prietene, pentru intâlnirile cu cola şi cioco de la piscină ;-), pentru umărul pe care l-ai avut mereu pe care am putut să mă lamentez, şi mai ales pentru că incă eşti aici in Olanda cu mine :-) Deci mai avem o carte de scris, nu? De data asta o să fie una mai interesantă şi practică ;-)

Dear Catherine, my sister and my paranimph, thank you very much for your support, for always coming over to watch movies, for always being there for me in my happy and less happy moments, for organizing the girls nights with lots of good quality wine, for still being in the Netherlands for a while longer and moreover thank you very much for our great friendship! I hope you will achieve your amazing goals and enjoy ESTEC as much as you can :-)

Mijn schoonfamilie, Jetske, Ger een Bart, een echt ontzettend bedankt voor jullie ondersteuning, voor het altijd lekkere eten met interessante discussies over geschiedenis en cultuur van Nederland en voor de gezelligheid.

Dragii mei mami şi tati, mulţumesc pentru dragostea voastră şi pentru tot ce aţi făcut intotdeuna pentru mine şi pentru Marius. Chiar dacă nu aţi avut posibilităţi imense, visul vostru de a avea o viaţă mai bună s-a realizat prin noi şi desigur cartea asta este dedicată vouă. Dragă Marius, mulţumesc pentru discuţiile filozofice pe care le avem, este mereu o plăcere :-). Iţi urez toate cele bune pentru viitor! Cine ştie, poate intr-o zi vei scrie şi tu o carte ca asta? ;-)

Mijn Frans, ik was nooit terecht tot hier gekomen zonder jouw liefde, ondersteuning en vertrouwen! Jij bent mijn onuitputtelijke steun, altijd daar om mijn gebroken stukjes terug te lijmen en met een zonnige enthousiasme naar de toekomst te kijken. Ik ben meer dan zeer dankbaar voor ons sprookjesleven, voor onze geweldige afgelopen en toekomstige avonturen rond de hele wereld en met de cavia’s en voor veel meer dat ik kan hier uitdrukken...

Curriculum Vitae

I was born on February 26th 1980 in Brăila, Romania. From 1998 until 2003, I attended Faculty of Physics, University of Bucharest where I have received my B.Sc. in physics. With a strong interest in astrophysics and being granted the Socrates-Erasmus Scholarship in 2003, I started working on my Master thesis research at the University of Bonn in Germany.

My passion for combining astrophysics with hydrodynamical modeling materialized in 2005, when I was given the opportunity to be a PhD candidate and began to work under the supervision of Prof. dr. Norbert Langer at the Sterrekundig Instituut Utrecht in the Netherlands. The work performed during my PhD studies has successfully led to this thesis: “Models for circumstellar nebulae around red and blue supergiants ”.